Universidade do Minho
Escola de Ciências

Isabel Soares de Carvalho

Development of antimicrobial multifunctional coatings based on Ag-Ti(C,N)

April, 2014

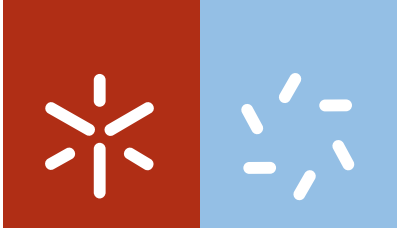

Universidade do Minho
Escola de Ciências

Isabel Soares de Carvalho

Development of antimicrobial multifunctional coatings based on Ag-Ti(C,N)

Thesis for PhD degree in Sciences Specialty in Physics

This work was realized under supervision of:
Supervisor:
Professor Sandra Maria Fernandes Carvalho
Co-supervisor:
Professor Mariana Contente Rangel Henriques

April, 2014

Agradecimentos

A concretização deste trabalho só foi possível devido à colaboração de um conjunto de pessoas e instituições, às quais gostaria de expressar um sincero agradecimento, pois sem essa ajuda não teria chegado até aqui.

Em primeiro lugar quero expressar os meus sinceros agradecimentos às Professoras Doutoras Sandra Carvalho e Mariana Henriques, minhas orientadoras, pela oportunidade que me deram de realizar este trabalho, pela ajuda, disponibilidade, amizade, dedicação, sabedoria e incentivo que demonstraram sempre durante o decorrer do doutoramento.

Quero agradecer ao Professor Doutor Juan Carlos Sánchez-López, Professor Doutor Albano Cavaleiro, Professor Doutor Tomas Polcar, Professor Doutor João Carlos Oliveira (Chapter II), Professor Doutor Ramón Escobar Galindo e Professor Doutor Carlos Palacio (Chapter II e V), pela colaboração e ajuda.

Quero agradecer aos colegas de Braga, a todos, sem exceção, que passaram pelo LMA, agora dividido em LMA I e II. Muito obrigada pelo apoio.

Um obrigado à Doutora Cláudia Sousa por todos os ensinamentos quer práticos, quer teóricos, dedicação e preocupação, durante a minha incursão pelo Mundo dos micróbios.

Um obrigado às Doutoras Rita Costa e Elisa Rodrigues por toda a ajuda, amizade e conhecimento que me transmitiram no Mundo das células animais.

Quero agradecer aos colegas de Guimarães, ao Sebastian Calderón pela amizade e disponibilidade que sempre revelou quando necessitei da sua ajuda. À Mariana Marques, Noora Manninen, Cristiana Alves e Edgar Carneiro pela amizade e todo o apoio.

Um agradecimento muito especial à minha amiga Isabel Ferreri, de outros percursos e agora também deste. “Pelo apoio, ajuda que me dás todos os dias e ainda mais agora na finalização desta etapa, digo-te é um privilégio ter-te como amiga!”

Agradeço também às seguintes entidades:

À Fundação para a Ciência e a Tecnologia pelo financiamento da bolsa de doutoramento SFRH / BD / 67022 / 2009 e pelos projetos PTDC/CTM/102853/2008 - ANTIMICROBCOAT- Desenvolvimento de revestimentos multifuncionais com propriedades antimicrobianas para implantes ortopédicos, PEST-C/FIS/UI607/2011, PEST-C/EME/UI0285/2011 e PEST-OE/EQB/LA0023/2013

Ao FEDER o financiamento através do programa COMPETE – Programa Operacional Fatores de Competitividade

Ao Projeto "BioHealth - Biotechnology and Bioengineering approaches to improve health quality", Ref. NORTE-07-0124-FEDER-000027, co-financiados pelo Programa Operacional Regional do Norte (ON.2 – O Novo Norte), QREN, FEDER.

Ao projeto "Consolidating Research Expertise and Resources on Cellular and Molecular Biotechnology at CEB/IBB", Ref. FCOMP-01-0124-FEDER-027462.

Abstract

The development of new multifunctional coatings to apply on medical biomaterials continues to be required, since materials commonly used in hip prostheses are still presenting failures. Multifunctionality is the result of a synergy, on the nanoscale level, of good corrosion resistance, mechanical and tribological properties. Additionally, a biomaterial must always be biocompatible. Besides these properties, the major challenge would be to get a material with antimicrobial activity. Thus, the aim of this project was the development of advanced materials with the ability to present these properties. Ceramic coatings, based on carbonitrides of transition metals, such as Ti(C,N), which may favour these properties, were used in this study. As innovative approach, silver nanoclusters were added, in order to improve the prevention of microbial adhesion and biofilm formation on these biomaterials, one of the major causes of hip joint failure.

Different Ag-Ti(C,N) thin films were prepared by reactive magnetron sputtering, obtained by varying the density of the current applied to each magnetron and the chemical composition of the mixed Ti + Ag target (silver pellets were placed in the preferential erosion area of one Ti target resulting in a relative Ag sputtering areas of 15 % for atomic ratio Ag/Ti ≤ 0.20 and 37 % for atomic ratio Ag/Ti ≥ 0.37).

The physical, chemical, structural, morphological/topographical, mechanical and tribological properties of these coatings were evaluated, respectively, by ball crater tests, X-ray diffraction (XRD), scanning electron microscopy (SEM)/ atomic force microscopy (AFM), Raman spectroscopy and X-ray photon spectroscopy (XPS). Mechanical properties of the films were studied by nanoindentation and the tribological tests were performed in the presence of Fetal Bovine Serum (FBS), in order to simulate the tribochemical conditions of the use of an artificial implant.

Cytotoxicity of the developed coatings was also determined and assessed by *in vitro* tests using fibroblast cells. Finally, the antibacterial activity was assessed using *Staphylococcus epidermidis*. Bacterial adhesion and biofilm formation on coatings were assessed by the enumeration of the number of viable cells.

XRD, Raman and XPS results showed the crystallization of a fcc-TiC_yN_{1-y} and as the Ag content is increasing in the coatings, the appearance of the soft phases (Ag and CN_x phases) are

evidenced, which become dominant and cause a substantial reduction in the grain size of TiC_yN_{1-y}, decreasing the hardness and the wear resistance.

The incorporation of silver into the coatings to be used in implant and medical devices must be up to 6 at. % to ensure the best tribological and mechanical properties, with hardness of 18 GPa and specific wear rate values in the range of 10^{-6} mm^3/Nm.

Concerning biological properties, all coatings for different Ag content revealed no cytotoxicity. The analysis of the antibacterial activity showed an absence of antibacterial activity. These results were not expected, and therefore the investigation had to be redirected towards finding an explanation for the silver inactivity in these coatings. Hence, phase composition of the surfaces, which are directly related with roughness, can be related with the absence of antimicrobial activity. Additionally, some properties, namely hydrophobicity and surface tension of coatings with silver promoted bacterial adhesion. So, much more should be studied on the lack of silver action in these coatings. So, advanced surface characterization techniques, glow discharge optical emission spectroscopy (GDOES), Rutherford backscattering spectroscopy (RBS) and XPS, were used in order to verify the possible physical and chemical changes that may occur on the surface of Ag-TiCN coatings after its exposure to the culture media used in the microbiological and cytotoxic assays, respectively tryptic soy broth (TSB) and Dulbecco's Modified Eagle's medium (DMEM). The results of GDOES profile, RBS and XPS spectra, of samples immersed in TSB, suggested the formation of a thin layer of carbon, oxygen and nitrogen that could be due to the presence of proteins in TSB. After 24 h of immersion in DMEM, the results also hint the formation of a thin layer of calcium phosphates on surface, since the coatings displayed a greatly oxidized surface in which calcium and phosphorus were detected.

Although there was no great evidence of antibacterial activity against *S. epidermidis* the results showed that the multifunctionality of coatings (good mechanical and tribological performance) was achieved for 6 at. % silver content, concomitantly with the absence of cytotoxicity.

Resumo

O desenvolvimento de novos revestimentos multifuncionais para aplicação em biomateriais é um campo em constante evolução, uma vez que os materiais normalmente utilizados em próteses ortopédicas ainda apresentam falhas. A multifuncionalidade é o resultado de uma sinergia, à escala nanométrica, entre as boas propriedades de corrosão, mecânicas e tribológicas. Adicionalmente, um biomaterial deverá ser sempre biocompatível. Desenvolver um material avançado, com atividade antimicrobiana, sem sacrificar as propriedades já mencionadas, é o grande desafio deste projeto. Os revestimentos cerâmicos que foram utilizados neste estudo são baseados em carbonitretos de metais de transição, tais como Ti(C,N), com o objetivo de atingir estas propriedades. Como abordagem inovadora, foram adicionadas nanopartículas de prata, numa tentativa de inibir a adesão microbiana e consequentemente prevenir a formação de biofilme nestes biomateriais, uma das principais causas de falência das próteses.

Ao longo do estudo foram preparados diferentes filmes de Ag-Ti(C,N), por pulverização catódica reativa, variando a densidade de corrente aplicada a cada magnetrão e a composição química do alvo misto Ti + Ag (pepitas de prata foram colocadas na área de erosão preferencial do alvo de Ti, resultando numa relação de áreas de pulverização da Ag de 15% para a razão atómica de Ag / Ti ≤ 0,20 e 37% para a relação atómica Ag / Ti ≥ 0,37).

As propriedades físicas, estruturais, morfológicas / topográficas e químicas dos revestimentos foram avaliadas, respetivamente, pelos testes da calote, difração de raios-X (XRD), microscopia eletrónica de varrimento / microscopia de força atómica (AFM), espectroscopia de Raman e espectroscopia de fotoeletrões excitados por raios X (XPS). As propriedades mecânicas dos filmes foram estudadas por nanoindentação e os ensaios tribológicos foram realizados na presença de soro fetal de bovino (FBS), a fim de simular as condições triboquímicas durante o uso de um implante artificial. A citotoxicidade dos revestimentos desenvolvidos também foi determinada e avaliada por testes *in vitro* utilizando os fibroblastos como células animais. Finalmente, a atividade antibacteriana foi avaliada utilizando *Staphylococcus epidermidis*. A adesão bacteriana e a formação de biofilme nos revestimentos foram avaliadas pela contagem do número de células viáveis.

Os resultados de XRD, Raman e XPS mostraram a cristalização de uma fase cfc de TiC_yN_{1-y} e com um aumento no teor de Ag nos revestimentos, evidencia-se o aparecimento de fases

macias (fases de Ag e CN_x) que se tornam dominantes e que promovem uma redução do tamanho de grão do TiC_yN_{1-y}, reduzindo também a dureza e a taxa de desgaste. A conjugação dos resultados demonstrou que a incorporação da prata nos revestimentos tem de ser até 6 % at. para assegurar as melhores propriedades tribológicas e mecânicas, com dureza de 18 GPa e com valores de taxa de desgaste específica na ordem de 10^{-6} mm^3/Nm. Em relação às propriedades biológicas, todos os revestimentos com diferentes teores de Ag não revelaram citotoxicidade. A análise da atividade antibacteriana mostrou uma ausência de atividade antibacteriana. Face a estes resultados não esperados, redirecionou-se a investigação com o propósito de encontrar uma explicação para a inatividade da prata nestes revestimentos. Assim, a composição química das superfícies, relacionada com a rugosidade, pode de alguma forma influenciar a inatividade antimicrobiana. Adicionalmente, algumas propriedades tais como a hidrofobicidade e tensão superficial dos revestimentos com prata promoveram a adesão bacteriana. Considerando estes resultados, foi necessário aprofundar o estudo sobre a inatividade da prata nestes revestimentos. Assim, recorreu-se a técnicas de caracterização avançada de superfície, tais como espectroscopia de emissão ótica de descarga luminescente (GDOES), espectroscopia de retrodispersão de Rutherford (RBS) e espectroscopia de fotoeletrões excitados por raios X (XPS), a fim de verificar as alterações físicas e químicas passíveis de ocorrer na superfície dos revestimentos de Ag-TiCN após a sua exposição aos meios de cultura usados nos ensaios microbiológicos e citotóxicos, caldo triptona de soja (TSB) e o Dulbecco's Modified Eagle's medium (DMEM), respetivamente. Para as amostras imersas em TSB, os resultados do perfil GDOES e dos espectros de RBS e XPS, sugeriram a formação de uma fina camada de carbono, oxigénio e azoto, o que pode indiciar a presença de proteínas proveniente do TSB. Após 24 h de imersão em DMEM, os resultados mostraram amostras com uma camada superficial muito oxidada, onde foram detetados cálcio e fósforo, sugerindo a formação de uma fina camada de fosfato de cálcio à superfície.

Apesar de não ter sido observada uma eficaz atividade antibacteriana contra *S. epidermidis,* os resultados mostraram que a multifuncionalidade dos revestimentos (boas propriedades mecânicas e tribológicas) foi conseguida para teores de prata até 6 % at., concomitantemente com a ausência de citotoxicidade.

Contents

Agradecimentos iii

Abstract v

Resumo vii

Contents ix

List of figures xiii

List of tables xvii

Nomenclature xix

Scope of the thesis xxiii

Structure of the thesis xxv

Chapter I – General Introduction

1.1 Hip Joint 3

1.1.1 Structure 3

1.1.2 Tribological properties 4

1.1.3 Mechanical properties 5

1.1.4 Main problems of natural synovial joints 7

1.2 Hip Arthroplasty 8

1.3 Biomaterials for Hip Replacement 9

1.3.1 Inherent Requirements 10

1.3.2 Joint Material Combinations: Tribological Limitations 11

1.4 Surfaces modification 14

1.4.1 Mechanical and tribological properties of coatings 15

1.4.2 Antimicrobial coatings 17

References 21

Chapter II – Coatings characterization

2.1 Introduction 33

2.2 Materials and methods 34

2.2.1 Samples preparation 34

2.2.2 Chemical composition 34
2.2.3 Physical characterization 34
2.2.4 Structural characterization 34
2.2.5 Morphology and topography 35
2.2.6 Chemical bonding characterization by XPS 35
2.2.7 Mechanical characterization: hardness and residual stress 35
2.2.8 Tribological characterization: friction coefficient and wear rate 35
2.3 Results and discussion 38
2.3.1 Chemical analysis 38
2.3.2 Structural analysis 39
2.3.3 Morphology and topography analysis 42
2.3.4 Chemical bonding analysis 45
2.3.5 Mechanical analysis 47
2.3.6 Tribological analysis 49
2.4 Conclusions 52
References 53

Chapter III – Biological characterization

3.1 Introduction 59
3.2 Materials and methods 60
3.2.1 Coatings preparation 60
3.2.2 Cytotoxicity assays 60
3.2.3 Antibacterial assays 60
3.2.4 Surface hydrophobicity characterization 61
3.2.5 Topography characterization 62
3.2.6 Statistical analysis 62
3.3 Results and discussion 62
3.3.1 Cytotoxicity 62
3.3.2 Antibacterial activity 63
3.3.3 Surface hydrophobicity analysis 68
3.4 Conclusions 69

References 70

Chapter IV – Theoretical approach to silver antibacterial inactivity in Ag -TiCN coatings

4.1 Introduction 77

4.2 Surface parameters ruling bacterial adhesion 77

4.2.1 Free energy of interaction 78

4.2.1.1 Thermodynamic approach 78

4.2.1.2 DLVO approach 82

4.2.1.3 Extended DLVO approach 83

4.2.2 Roughness 83

4.2.3 Chemical composition 84

4.3 Control of bacterial adhesion 85

4.3.1 Surface modification 85

4.4 Conclusions 86

References 87

Chapter V - Seeking for an explanation for the antibacterial inactivity of the Ag-TiCN coatings

5.1 Introduction 95

5.2 Materials and method 95

5.2.1 Coatings preparation 95

5.2.2 Chemical and physical analysis 96

5.3 Results and discussion 96

5.3.1 Depth profile characterization 96

5.3.2 Chemical bonding analysis by XPS 101

5.4 Conclusions 105

References 106

Chapter VI – Final conclusions and work perspectives

6.1 Final conclusions 111

6.2 Work perspectives 113

List of figures

Figure 1.1 Hip joint. 3

Figure 1.2 Hip prostheses components: a) the stem femoral of titanium, b) the acetabular component of polyethylene with the cement and c) the stem and head femoral of titanium. 8

Figure 1.3 Stages of biofilm development i) initial attachment of microbial cells to surface; ii) multiplication of the microbial cells forming microcolonies; iii) maturation of the biofilm of cells and production of an extracellular matrix and iv) detachment of some biofilm cells leading to colonization in other parts of surface. 17

Figure 1.4 Biofilm of *Staphylococcus epidermidis.* 18

Figure 2.1 Evolution of the potential on the targets V_{Ti+Ag} and V_{Ti} as a function of the deposition time of the sample a) Ag/Ti = 0.20 and b) Ag/Ti = 0.37. 38

Figure 2.2 XRD patterns of the Ag-TiCN coatings deposited by DC reactive magnetron sputtering on silicon and in the right the deconvolution of peak Ag/Ti = 0.62. 40

Figure 2.3 Phase composition of the samples prepared with Ag/Ti ratios of 0, 0.05, 0.20, 0.37 and 0.62, using silicon substrate. 41

Figure 2.4 Raman spectra of the Ag-TiCN coatings deposited on silicon. 41

Figure 2.5 Cross-sectional SEM micrographs of coatings on silicon: a) Ag/Ti = 0, b) Ag/Ti = 0.20, c) Ag/Ti = 0.37 and d) Ag/Ti = 0.62. The insets show the SEM image from the sample surface on SS 316L where in a) the top of column TiCN is evident and in b), c) and d) BSE image where Ag clusters are visible only in Ag/Ti = 0.37 and Ag/Ti = 0.62. 42

Figure 2.6 AFM images of coatings, a) on silicon with a scan range of 5 × 5 μm^2 and b) on SS 316L with a scan range of 10 × 10 μm^2. Ra is the arithmetic mean of surface roughness of every measurement within the total distance ½ roughness average and Rms is the root mean square roughness. 44

Figure 2.7 XPS spectra of (a) Ti2p, (b) C1s, (c) N1s and (d) Ag3d core levels of the Ag-TiCN coatings deposited by dc reactive magnetron sputtering with different Ag/Ti atomic ratios on silicon. 46

Figure 2.8 Hardness and residual stress values of Ag-TiCN coatings *vs.* the Ag/Ti atomic ratio. 48

Figure 2.9 Variation of the hardness and wear rate properties as a function of the ratio of soft (Ag + CN_x)/hard (TiC_yN_{1-y}) phases. 49

Figure 2.10 Friction coefficients (a) and wear rate (b) values of Ag-TiCN as a function of the Ag/Ti atomic ratio. 49

Figure 2.11 Optical micrograph of the alumina ball after the friction test onto the Ag-TiCN coating with 10 at. % of Ag (a) and corresponding Raman spectra (b) and EDX (c) analysis. 50

Figure 2.12 Optical micrograph of the wear track after the friction test of the Ag-TiCN coating with 10 at. % of Ag (a) and corresponding Raman spectra (b). 51

Figure 3.1 Rate of inhibition of fibroblast cell growth as a function of the Ag/Ti atomic ratio. 62

Figure 3.2 Logarithm of bacterial concentration after 2 h and 24 h contact between Ag-TiCN coatings (with different ratios) and *S. epidermidis* strains: IE186 (a) and 1457 (b). 63

Figure 3.3 SEM micrographs of *S. epidermidis* IE186 adhered to Ag-TiCN coatings after 2 h (column 1) and 24 h (column 2) period of contact: adhesion and biofilm formation to Ag/Ti = 0 (a); to Ag/Ti = 0.37 (b); to Ag/Ti = 0.62 (c). 65

Figure 3.4 SEM micrographs of *S. epidermidis* 1457 adhered to Ag-TiCN coatings after 2 h (column 1) and 24 h (column 2) period of contact: adhesion and biofilm formation to Ag/Ti = 0 (a); to Ag/Ti = 0.37 (b); to Ag/Ti = 0.62 (c). 66

Figure 3.5 Schematic representation of bacterial adhesion (not to scale) (a). AFM section profile of Ag-TiCN coating with zero Ag/Ti atomic ratio (b). 67

Figure 5.1 GDOES depth profile of Ag/Ti = 0. a) control samples, b) samples immersed 24 h in TSB and, c) samples immersed 24 h in DMEM. a), b) and c) extended depth profiles up to 3.5 μm and a_1), b_1) and c_1) the depth profiles near surface (< 700 nm). 97

Figure 5.2 GDOES depth profile of Ag/Ti = 0.20. a) control samples, b) samples immersed 24 h in TSB and, c) samples immersed 24 h in DMEM. a), b) and c) extended depth profiles up to 2.5 μm and a1), b1) and c1) the depth profiles near surface (< 700 nm). 98

Figure 5.3 RBS spectra of: a) Ag/Ti = 0 and b) Ag/Ti = 0.20 of samples immersed in DMEM (top), in TSB (middle) and control (bottom). 100

Figure 5.4 XPS spectra of: a) C 1s, b) N 1s, c) O 1s and d) Ti 2p core levels of Ag/Ti = 0.20 in control samples (top), and samples exposed to 24 h in TSB (middle) and in DMEM (bottom). 102

Figure 5.5 XPS spectra of: a) Ag 3d, b) Ca 2p and c) P 2p core levels of Ag/Ti = 0.20 in control samples (top), and samples exposed to 24 h in TSB (middle) and in DMEM (bottom). 104

List of tables

Table 1.1 Peak pressure in the hip joint during different daily activities 6

Table 1.2 Wear rates and average wear particles size resulting from *in vitro* simulation of several materials pairs 11

Table 1.3 Young's modulus of natural or synthetic materials in joints 14

Table 2.1 Chemical composition, deposition parameters, thickness and deposition rate of deposited coatings 37

Table 3.1 Water (θ_W), formamide (θ_F), and α-bromonaphtalene ($\theta_{\alpha B}$) contact angles, surface energy components (apolar Lifshitz-van der Waals surface free energy component, γ^{LW}, electron acceptor surface free energy component, γ^+, and electron donor surface free energy component, γ^-), and degree of hydrophobicity (ΔG_{sws}) of the Ag-TiCN coatings surface 68

Table 4.1 Surface tension parameters (mJ/m^2) of the liquids commonly used in contact angle measurements 80

Nomenclature

Symbols

at. %. – Atomic per cent

D – Disordered carbon

E – Young's modulus

G – Graphite carbon

H – Hardness

J – Current density

K – Wear rate

L – Width

P – Significance

Ra – Arithmetic mean of surface roughness of every measurement within the total distance ½ roughness average

Rmax – Maximum roughness within the distance measured

Rms – Root mean square roughness

μ – Friction coefficient

σ – Residual stress

Φ – Gas flow

θ_w– Water contact angle

θ_F – Formamide contact angle

$\theta_{\alpha B}$– α-bromonaphtalene contact angle

γ – Surface tension

γ^{TOT} – Total surface tension

γ^{LW} – Apolar Lifshitz-van der Waals surface free energy component

γ_i^+ – Electron acceptor surface free energy component i

γ_i^- – Electron donor surface free energy component i

γ^{AB} – acid–base (AB) component

ΔG_{sws} – Variation of the free energy (ΔG) of interaction between material's surface (s) immersed in water (w)

ΔG_{sws}^{LW} – Free apolar energy of Lifshitz–van der Waals

ΔG_{sws}^{AB} – Free polar energy of Lewis components

ΔG_{adh}^{TOT} – Total free energy of interactions

ΔG^{DL} – Electric double layer free energy of electrostatic interaction

Abbreviations

a.u. – Arbitrary unit

AB – Acid–base

AFM – Atomic force microscopy

BSE – Backscattering electron

CFUs – Colonies forming units

CoC – Ceramic-on-ceramic

CoP – Ceramic-on-polymer

CVD – Chemical vapour deposition

dc – Direct current

DLC's – Diamond-like carbon

DMEM – Dulbecco Modified Eagle medium

DNA – Deoxyribonucleic acid

DR – Deposition rate

EDX – Energy dispersive X-ray analysis

EPMA – Electron probe microanalysis

EPS – extracellular polymeric substances

EPS – Extracellular polymeric substances

FBS – Fetal bovine serum

fcc – Face cubic centred

ICDD – International Centre for Diffraction Data

Jis Z 2801: 2000 – Japanese Industrial Standard Z 2801: 2000

LW – Lifshitz–van der Waals

MeC_x – Transition-metal carbides

MeN_x – Transition-metal nitrides

MoM – Metal-on-metal

MoP – Metal-on-polymer

MTS – 3-(4,5-dimethylthiazol-2-yl)-5-(3-carboxymethoxyphenyl)-2-(4-sulfophenyl)-2H-tetrazolium inner salt

PBS – Phosphate buffer saline

PET – Polyethylene terephthalate

PVD – Physical vapour deposition

RBS – Rutherford backscattering spectroscopy

RNA – Ribonucleic acid

SE – Secondary electron

SEM – Scanning electron microscopy

SS 316L – 316L stainless steels

THA – Total hip arthroplasty

TSA – Tryptic Soy Agar

TSB – Tryptic Soy Broth

UHMWPE – Ultrahigh molecular weight polyethylene

XPS – X-ray photon spectroscopy

XRD – X-ray diffraction

Scope of the thesis

The increase of elderly population observed nowadays leads to a higher incidence of joint diseases such as osteoarthritis, rheumatoid arthritis and osteonecrosis, which in many cases leads to the need for total or partial replacement of the joint by artificial implants. Although, these problems are more often associated with the population with a relatively advanced age, sometimes there are other conditions which lead to the need of joint replacement in young, such as epidemiological factors or situations occurring with trauma caused by accidents. Therefore, the need to adapt the prosthesis to young people is one of the greatest challenges on functionality, particularly hip for long-term use. The surgical technique, which presents as an immediate solution to this problem is hip replacement surgery, named hip arthroplasty, that could be primary or revision. Despite the arthroplasty of the hip to be one of the greatest achievements of orthopaedic surgery in the past decades, different risk factors are associated. The infection is the third most common cause of revision of total hip arthroplasty (THA) after instability/dislocation and mechanical loosening. The materials used in the implants production still require many developments given that their time in service is low. Thus, it is of major importance to overcome this problem, with the development of new coatings which will confer to the usual biomaterials, improved physical, mechanical, tribological and biological properties.

Titanium nitride (TiN) and Diamond–like carbon (DLC) have been used in industrial applications, however the first one shows high friction coefficient and relatively high wear rate and the second one possesses moderate biocompatibility, which can represent a drawback in terms of multifuncionality. Transition-metal carbides, and metal nitrides, proved to be very attractive base materials due to a successful combination of high hardness, good wear and corrosion resistances. The idea is to cover a wide range of mechanical/tribological property outputs (high surface hardness, wear resistant and good lubrication behaviour). Nevertheless, recent results demonstrated that, although biomaterials presented good mechanical properties and low cytotoxicity, they were prone to be colonized by microorganisms, being *Staphylococcus epidermidis* one of the bacteria most commonly found in orthopaedic prosthesis. Infections caused by this microorganism are often associated to implant failure.

Hence, this strengthens the urgent need of the development of new coatings with improved antimicrobial properties.

Several studies have been performed describing the use of silver with antimicrobial property and for biomedical applications. However, they only consider silver antimicrobial action disregarding other important factors, as silver cytotoxicity and materials' mechanical and tribological properties. So, this highlights the importance of gathering all the materials properties, from mechanical and physical to biological properties, in order to develop a new material that is able to last long in patient and is the most harmless possible.

Thus, the main objective of this study consists in the development of antimicrobial multifunctional coatings based on Ag-Ti(C,N). In order to achieve the main goal, three steps were followed. Firstly, it was identified the adequate deposition parameters for the preparation of these coatings, taking in consideration the optimal concentration of silver to be applied on coatings in order to achieve low cytotoxicity and low or no microbial colonization and the best compromises of coatings performance at laboratorial level concerning mechanical and tribological. Secondly, it was studied the influence of processing conditions in the particular film's growth characteristics, in order to correlate the composition, the structural features and the mechanical properties, since these relations are expected to explain/predict the tribological and biological behaviours. Then the last phase included the understanding of the relation of the antimicrobial properties with the amount of silver and/or the rate of silver released.

Structure of the thesis

This dissertation is divided in five chapters.

Chapter I encloses a general introduction, which describes the fundamental points of the natural synovial joint, since, its mechanical and tribological characteristics are the main causes that lead to the necessity of natural joint replacement by an implant. It is also made the contextualization of hip replacement surgery, the biomaterials used in hip replacement surgery with a focus on their mechanical and tribological properties. Finally, it is explained the need of modification of surfaces and the potentiality of TiCN coatings doped with silver for the application concerned.

Chapter II comprises the coatings production, outlining the fundamentals about the methodologies used, its chemical and physical characterization and also its mechanical and tribological behaviour.

Chapter III includes the biological characterization of coatings, analysing its cytotoxicity and its antibacterial activity.

Chapter IV presents a better understanding of hydrophobicity, charge, roughness and chemical composition of surfaces in the effective microorganism's adhesion control. How these microorganisms adhere and how these factors affect adhesion phenomenon and its importance in order to avoid microbial colonization will be also highlighted.

Chapter V presents suggestions about the proteins contribution, characteristic of biological fluids, as well as the surface features of the coating, and the relation between those factors and the absence of antibacterial activity.

Chapter VI offers the major conclusions of the thesis and the suggestions for future work.

Chapter I – General Introduction

The work presented in this chapter was based on the submitted review paper:

- **Carvalho, Isabel**; Henriques, M.; Carvalho, S.

Journal of Biomedical Materials Research: Part B - Applied Biomaterials

Chapter I – General Introduction

The natural synovial joints play an important role in different daily activities and their durability depends on the lubrication mechanisms that are directly related to tribological aspects, such as friction, wear and lubrication. In some cases, the joints degeneration can lead to their substitution.

1.1 Hip Joint

1.1.1 Structure

The hip joint is one of the joints in the human body which is subject to very violent efforts. Its main function is to support the weight, balance the body in static postures (standing) and dynamic (walking or running), protects the reproductive system and the lower part of the digestive system. It is the second most flexible joint in the body, after the shoulder, allowing a greater range of motion. These characteristics result from the configuration of ball-and-socket synovial joint where the roughly spherical femoral head is largely contained within the acetabulum [1–3], as shown in figure 1.1. Both articular surfaces are covered with a layer of strong but lubricated called hyaline cartilage.

Hyaline cartilage is a compact, transparent, elastic and soft substance, located between the contact surfaces of the acetabulum and the head femur, in the majority of the moving joints. This cartilage also acts as a flexible shock absorber to prevent the collision of the bones during movement. Between the layers of hyaline cartilage, synovial membranes secrete synovial fluid to lubricate the joint. Surrounding the hip joint there are many strong ligaments that prevent the joint dislocation. The strong muscles of the hip region also help to hold the hip joint together and to prevent dislocation [3].

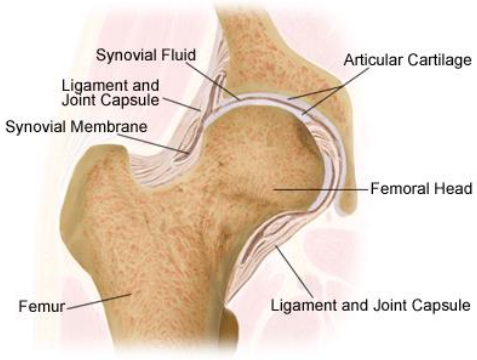

Figure 1.1 Hip joint. Adapted from: http://www.iospak.com/hipjoint.html (02/04/14).

1.1.2 Tribological properties

The synovial joints are remarkable systems as they form the base of movement, allowing the bones to slide against each other with the lowest degree of friction and wear [4,5]. This optimized tribological behaviour is owed to the existence of the joint cartilage. Its thickness and its transparency may vary in the same joint on account of the efforts it is subjected to, fluctuating between the micrometres and even a few millimetres. In the hip joints the average values range between 2 and 4 mm. This cartilage is enriched by its mechanical and physical properties, which confer viscoelastic behaviour to this material, responsible for: protecting the bone against abrasion (wear occurs between surfaces with a different relative hardness), absorbing the transmission/distribution shocks, reducing the contact efforts between opposing bonding surfaces and acting as a lubricating surface, favouring the motion between surfaces and reducing friction [6]. The hyaline cartilage is responsible for these tasks thanks to its highly organized cells and its structural heterogeneity. The cartilage is composed of chondrocytes in lacunae embedded within an extracellular matrix consisting mostly of collagen. Avascular, its nutrition is through the diffusion of substances from the capillaries of fibrous connective tissue that surrounds the cartilage, named perichondrium and from synovial fluid secreted by the synovial membrane [7]. The synovial fluid has an extremely complex chemical composition, formed by an electrolytic solution rich in proteins (mainly albumin), polysaccharides (hyaluronic acid) and other water-solved compounds [8]. Additionally, this synovial fluid acts as a lubricant between articular surfaces, absorbing shocks emerging from the compression of these joints.

Over the years a remarkably high number of concepts and theories have been proposed concerning the lubrication of synovial joints, and this is fundamental to understand and predict friction and wear mechanisms occurring in artificial materials. Synovial joints have an excellent natural lubrication mechanism and display a friction coefficient raging between 0.001 and 0.02 [9]. The friction coefficient is the ratio of the friction force and the normal load. Doubtlessly, the phenomenon responsible for the synovial lubrication is highly complex, and it is obviously very difficult to produce an artificial implant with a similar tribological performance. The viscosity of the synovial fluid is significantly different form the viscosity of the water, and it is believed that the synovial lubrication is explained by the hydrodynamic lubrication theory; the hip joints are completely separated by the synovial fluid [10]. However, the operation mechanism of the hip is extremely complex, insofar as it is subject to several

loads and velocities during the gait cycle [11], during which the thickness of lubricant film experiences fluctuations, as a consequence of its numerous macromolecules reacting to sheer stresses through viscosity, and its rheological properties change [8]. Consequently, the synovial fluid cannot be considered a Newtonian fluid [12], characterized by a linear proportionality between the strain rates and the sheer stresses. Accordingly, the so called "weeping mechanism" is possibly the only type of hydrodynamic lubrication taking place in synovial joints [13], because this mechanism can be compared to a sponge. Owing to its permeability and a natural pumping system taking place during the motion, this fluid is able to lubricate the cartilage during the compression and decompression of the articular cartilage. In this way, when the cartilage is exposed to high loads the fluid is expelled (exudation), lubricating the joints, and, during the decompression, the fluid is absorbed (imbibition) [14,15]. However, this hydrodynamic lubrication is not so clear in certain situations, as when the foot is flat on the floor and the movement of the joint is initiated. In this case, the surfaces of the cartilage are very close to each other and a boundary lubrication takes place, possibly giving way to a direct contact between the cartilage surfaces [16–18]. This type of lubrication is favoured whenever the contact pair is subjected to extremely heavy loads, when the movement is initiated (low sliding speeds), or when the viscosity of the synovial fluid is very low, due to a certain medical condition. In these cases, synovial proteins may be adsorbed into the surface of the cartilage and form a semisolid film that impacts the friction coefficient [17]. Hyaluronic acid and phospholipids can behave in a similar way. According to Saikko *et al.* [19], the phospholipids found in the synovial fluid seem to occupy a significant role in the boundary lubrication of the natural joint, reducing friction and wear.

1.1.3 Mechanical properties

Understanding the efforts applied to the hip joint in different movements and requests to which the joint is subjected, is essential to the knowledge of its functioning and mobility, allowing to realize what causes a major cause of disease of the hip joint - osteoarthritis, as well as to predict potential complications in the development of artificial synovial joint.

Abnormal mechanical stress on joint cartilage is one of the main causes of osteoarthritis. Thus, it becomes crucial to evaluate the distribution of contact pressure and its maximum value along the articular surface [20]. The knowledge of the distribution of the contact pressure during daily activities is an important factor, because it allows predicting the

mechanism of joint degeneration and wear of the joint replacement, providing valid planning of the biomechanical fundamentals before the surgery and rehabilitation. Yoshida *et al.* [20] resorted to methods of computer simulation and finite element analysis to forecast the contact area and pressure on the hip during different daily activities. To this end, it was generated an original three-dimensional surface, based on the assumption that the contact area between the pelvis and the femur is spherical and that the relationship between the femoral head and acetabulum is concentric. The results have shown that during standing up and sitting down and knee bending, the peak pressures were located at the edge of the posterior horn of acetabulum and the magnitude of the peak pressures during sitting down was the highest. For the other daily activities, the peak pressures were located at the acetabulum lateral roof. These results are shown in table 1.1, beyond peak pressure value and location where maximum pressures were observed during different activities of daily living. It is also displayed the percentage of the contact area and the percentage of the cycle that is subject to this pressure.

Table 1.1 Peak pressure in the hip joint during different daily activities [20]

Activities of daily living	Peak pressure (MPa)	Location of maximum pressure	Contact area (% total area)	Activity cycle (%)
Fast walking	3.28	Lateral roof	78.7	12.5
Normal walking	3.26	Lateral roof	76.3	16.5
Slow walking	2.87	Lateral roof	81.2	16.0
Standing up	8.97	Posterior horn	19.7	35.0
Sitting down	9.36	Posterior horn	17.6	50.5
Knee bending	3.65	Posterior horn	51.6	53.0
Up stairs	5.71	Lateral roof	52.1	11.0
Down stairs	3.77	Lateral roof	80.6	55.0

Most models have assumed the hip joint to be a perfect ball and socket joint and have neglected deformation at the interface between bone / cartilage [20,21].

In a more recent study, Anderson *et al.* [22] used methods of finite element analysis with the objective to analyse finite element models of hip cartilage mechanics with varying degrees of

simplified geometry and a model with a rigid bone material assumption to elucidate the effects on predictions of cartilage stress. The results demonstrate that simplifications to the geometry of the bone / cartilage interface, cartilage surface and bone material properties can have a dramatic effect on the predicted magnitude and distribution of cartilage contact pressures in the hip joint.

1.1.4 Main problems of natural synovial joints

Despite human joints present excellent tribological characteristics, these structures have a limited capacity for regeneration. Therefore, the interaction of the femur with the acetabulum may result in damages that originate from hip joint diseases, given the high contact pressures to which they are subject. Since the hip joint is a contact interface between two bone surfaces, it is expected that any diseases that affect cells and bone mass affect also the articulation. The main reasons for total hip replacement derive in most cases of diseases such as rheumatoid arthritis, osteoarthritis, osteonecrosis, post-traumatic arthritis, benign and malignant tumours of the bone, femoral neck fracture [11]. Osteoarthritis, the most cause of failure of the hip joint, is a degenerative joint condition promoted by wear of the cartilage that covers and cushions the interior of joint combined with the decrease of synovial fluid leading to lubrication failure [23]. Understandably, as the bone surfaces are less protected by cartilage the patient will have pain, not only with the support of their weight, but also when it is in motion. Many persons are affected by osteoarthritis after age 60 due to the normal wearing out of cartilage that accompanies the aging body. In an early stage of osteoarthritis, cartilage joint becomes thinner, with a rough texture with fissures on the surface. With its aggravation, the cartilage and underlying bone crack and erode [22]. Depending on the development of this disease, the need to resort to surgery for joint replacement increases, because the joint pain, particularly the hip joint pain, drastically limits the ability to have an active life. This procedure, known for arthroplasty, came to deal the problems caused by various diseases that affect many patients around the world, aged normally between 55 and 65 years. With the increase in average life expectancy, the repair or replacement of the hip joint becomes increasingly common.

1.2 Hip Arthroplasty

Hip arthroplasty is a surgical procedure that consists fundamentally in the functional restoration of the joint through its replacement with an implant, preserving the synovial capsule [11]. The figure 1.2 shows some hip prostheses components.

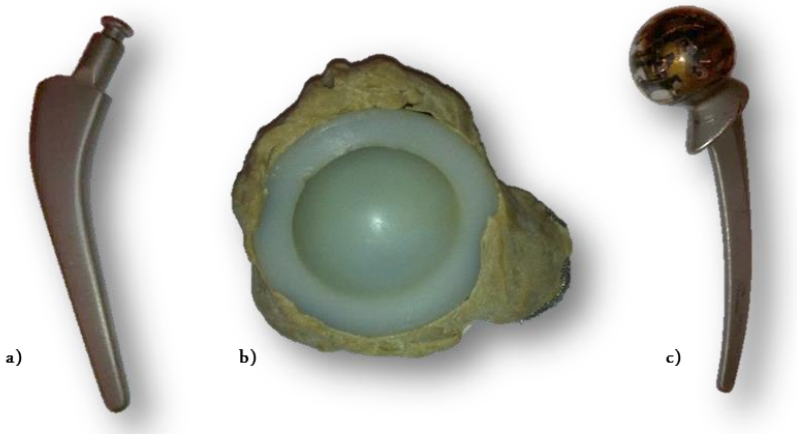

Figure 1.2 Hip prostheses components: a) the stem femoral of titanium, b) the acetabular component of polyethylene with the cement and c) the stem and head femoral of titanium.

This substitution can be done in three ways: (i) only one part of the joint is damaged, with the replacement of the affected component, called hip hemiarthroplasty; (ii) the two parts are affected and the substitution is made at full articulation, named by total hip arthroplasty (THA); (iii) the existent prosthesis is replaced, which is called revision hip arthroplasty.

The hip replacement, beyond knee prosthesis, is the most common used in orthopaedic surgery and it is estimated annually that more than 1 million procedures are undertaken worldwide [24]. Despite the hip arthroplasty be considered one of the greatest achievements of orthopaedic surgery in the last decades, hip implants are not a complete success and still need further developments. This poor performance is reflected in the number of revision arthroplasties realized in the United States surrounding the 20% [25,26]. The materials used in conventional prostheses are designed to perform their duties for a period of at least 15 years [11,27,28]. Another study suggests that the risks of primary revision THA are 5 to 20 % after 10 years [29]. However, these realities for patients younger than 60 years, with an average life expectancy of another 20 to 25 years, are far from satisfactory. Besides, there is the fact that the revision arthroplasties of the hip are significantly more complicated than the

total primary arthrosplasties [30,31]. One of the main reasons for these complications is the loss of bone, in adjacent areas to the primary prosthesis getting thinner and more fragile. This may lead to bone grafts or other materials around the implant replacement to strengthen the bone. These grafts can come from the patient's body itself or from other donor bone if the amount of the patient's bone to remove is large. These complications also may result of prosthesis materials failure, translating in aseptic loosening, instability, wear, and infection of the implant [30,31].

1.3 Biomaterials for Hip Replacement

Currently, the importance of biomaterials is recognized around the world, driven by market need. An effort to achieve higher standards of living, in search of a greater longevity, was made in the area of biomaterials, which has gained increasing importance in the repair and replacement of living tissues victimized by trauma or pathology [32–34]. There are many definitions found in the literature to express biomaterial concept, given the wide range of areas involved in the design and characterization of the materials used in biomedical applications [32]. Consequently, "Biomaterial" can be considered as a synthetic or natural material that comprises whole or part of a living structure or a biomedical device which performs, augments or replaces a function that has been lost through disease or injury with no negative influence on the biological environment [35]. Associated with the definition of biomaterials, the concept of biocompatibility arises, since only biocompatible materials may be used in implants under the risk of failure. However, it is difficult to find a definition of biocompatibility because it covers various aspects related to material, function and biological response. Some authors define "Biocompatibility of a material" as the ability to perform a particular function in the human body, inducing an adequate response in biological organisms [36,37].

The deployment of biomaterials in the human body enables the restoration of biological and mechanical functions, increasing the quality of patients' life, and they are now commonly used as prostheses in cardiovascular, orthopaedic, dental, ophthalmological, and reconstructive surgery, and in other interventions such as surgical sutures, bioadhesives, and controlled drug release devices.

Among the possible applications of biomaterials it must be pointed out, by its importance, hip replacements, since it often presents itself as the only solution to restore quality of life to the patient.

Researches in the area of biomaterials for use in hip prostheses date from the first half of XIX century. Nowadays, it is one of the most explored areas of the branch orthopaedic biomedicine, due to the growing increase of the necessity for replacement of the hip joint. So, it is essential to explain the inherent requirements of biomaterials used in the hip joint, as well as the limitations associated to the joint material combinations.

1.3.1 Inherent Requirements

All materials used in hip replacements must display certain properties that enhance their life span. Considering the aggressive environmental conditions to which they are subjected to, these materials must meet several requirements, as biocompatibility, tribologial resistance, and corrosion strength.

Biocompatibility

Biomaterials must not cause any damage to the cells of the organism in which they are implanted. So, their physical and chemical properties must not interact negatively with the living tissue interface [34].

Tribological Resistance

A small friction coefficient favours the sliding motion between contact surfaces and generally leads to a lower wear rate, also preventing the release of potentially toxic debris. Considering the repeated cyclic loads to which these devices are subjected to, fatigue strength is crucial determining the long-term success of the implant [27].

Corrosion Strength

The chemical environment inside the human body is highly aggressive. Given the nature of certain materials used in orthopaedic prosthesis, this environment can act as an electrolyte and trigger electrochemical reactions. The products released from this corrosion can be toxic, and they can interfere with the normal functioning of the organism [38–40]. High corrosion and wear resistance is indispensable in the development of implants to ensure the longevity of the material in the human body [27].

Mechanical Strength

The prosthesis must have suitable mechanical properties to endure the strengths involved in the motion. Some of these properties are of prime importance as hardness, tensile strength, modulus and elongation [27].

1.3.2 Joint Material Combinations: Tribological Limitations

The type of implant and its constitution are carefully selected by surgeons, pondering several variables such as the patient's age, lifestyle and activity level. The combinations of materials applied in replacement of femoral and acetabular components have different friction coefficients and wear rates. The joint pairs used are: metal-on-polymer (MoP); metal-on-metal (MoM); ceramic-on-polymer (CoP) and ceramic-on-ceramic (CoC).

Simulation results from the, *in vitro,* interaction of some of these materials, where it is possible compare the different wear rates, as well as the average wear particles size of different joint pairs used in hip prosthesis, are summarized in the table 1.2.

Table 1.2 Wear rates and average wear particles size resulting from *in vitro* simulation of several materials pairs [41,42]

Materials pairs	Wear rates ($mm^3/10^6$ cycles)	Average wear debris size (nm)
Metal / UHMWPE	35-45 [41]	300 ± 200 (of UHMWPE)
CoCrMo alloy / CoCrMo alloy	1.23 ± 0.5	30 ± 2.25 (of CoCrMo alloy)
ZrO_2 / UHMWPE	31 ± 4.0	300 ± 200 (of UHMWPE)
Al_2O_3 / Al_2O_3	0.05 ± 0.02	9 ± 0.5 (of Al_2O_3)

Metal-on-polymer

UHMWPE (ultrahigh molecular weight polyethylene) is still the most commonly used material in prostheses as acetabular component with a metal for femoral component [16]. UHMWPE is recognized for its biocompatibility [3], hence it has been used as a biomaterial. It has good

tribological characteristics as low friction and low wear [43]. However, the wear particles released from the UHMWPE component cause serious adverse reactions within the human body, as osteolysis (tissue bone destruction) in the surrounding tissues [44]. In this combination of polymer materials with metal, most of the wear debris comes from the grooves of smoother surface (polymer). As a result, these polymer residues can be transferred to the metal material, forming a film that promotes wear adhesive type. Generally, the harder material (metal) exhibits a higher resistance to abrasive wear, being the softer material which suffers, typically, greater wear. For this reason, the presence of imperfections in metal surface may promote abrasive wear on the polymeric component surface.

Metal-on-metal

Total hip prostheses type MoM have aroused interest because of the problems highlighted by the pair MoP [45], mainly by presenting wear rates that are significantly lower than those of the prostheses type MoP [42]. Some studies have reported that wear rate of MoM hip prosthesis is 1–6 mm^3 per year, comparing to 30–100 mm^3 for MoP hips [46–48]. Materials with similar chemical properties usually exhibit high adhesion forces, it can form chemical bonds more quickly, which is why wear rates are lower. However, there is a serious problem associated with this materials pair, because of its ions released that are toxic to the blood. In the case of cobalt-chromium alloys, metal ions which are released to synovial fluid produce water-soluble metal salts which migrate to blood and posteriorly are excreted in the urine [49]. Nickel, ion released by steel stainless, is usually eliminated through the urine but cobalt and chromium remain longer in the body and may even be retained in organ tissues [23].

Ceramic-on-polymer

When using a ceramic femoral head, the polymeric component wear may be reduced by 50 %, which still involves a large number of particles released [42]. Therefore, due to the problems that this materials pair presents, it has emerged an interest in studying of materials pairs (CoC).

Ceramic-on-ceramic

Prostheses CoC produce a low number of wear particles (1 mm^3 / year) [47,50], this being fairly value lower than the joint articular MOP wear rate (100 mm^3 / 10^6 cycles) [51]. The most widely used ceramic materials in the field of prostheses are alumina (Al_2O_3) and zirconia (ZrO_2), featuring biocompatibility, wear and corrosion resistance. Oxides correspond to the maximum state of oxidation of a metal, being stable in harsh environments, providing this way

a weak degradation [52]. In the 1970s, it was developed the first hip prosthesis of Al_2O_3. Studies revealed that the concentration of wear particles generated in joint pair CoC (Al_2O_3 / Al_2O_3) was around 20 times lower than that observed in the joints of MoP [53–55]. In addition to the number, also its size is fairly inferior when compared to the size of the polymer particles resulting from the action of wear (table1.2). However, this material exhibits a brittle tendency and is sensitive to microstructural flaws [55]. Consequently, the interest in zirconia as a result of the processing mechanisms with a fracture resistance much higher than for alumina arises. ZrO_2 was being recognized for its high strength and surface finish, becoming suitable for the highly loaded environments found in joint replacement [55]. The measure of a ceramic material's ability to resist fracture when a crack is present is specified in terms of fracture toughness (table 1.3).

Long-term results with this type of combination (CoC) can be considered interesting, especially in younger patients. In older patients with pathology of rheumatoid arthritis or osteoporosis, it has been found sometimes the occurrence of osteolysis and, therefore, dislocation of the acetabular component, which may be related to the effect of "stress-shielding" induced by the high elasticity module of alumina (table 1.3) [36,56,57]. This effect is caused by the discrepancy between elasticity modulus of the bone and the materials used in implanted devices to withstand the structural loads, which makes the ceramic component promotes an uneven distribution of the load on the bone [58]. Over time, this phenomenon leads to deterioration in the quality of bone, causing a weakening, loss of bone mass and eventually the dislocation of the prosthesis [58]. Considering only the low wear rates of these materials, these could be considered the most suitable materials for use in orthopaedic implants such as hip case. However, since Young's modulus values are very high, this suggests that are poorly deformable and more susceptible to fracture, causing the unbalanced release of particles, preventing surgical removal of the implant [56].

Table 1.3 shows fracture toughness and elasticity modules values of two natural materials comparatively with some materials used in artificial synovial joints.

Table 1.3 Young's modulus of natural or synthetic materials in joints [56,59]

Joint material	Fracture toughness, K_{Ic} ($MPa \cdot m^{1/2}$)	Young's modulus, E (GPa)
Articular cartilage		0. 001 – 0.17 [56]
Bone	3 – 6 [60]	10 – 30
Ti6Al4V alloy	55	100 – 110
Stainless steel 316L	50 – 200	190
CoCrMo alloy	100	210
UHMWPE		0.8 – 2.7
ZrO_2	7 – 12	150 – 208
Al_2O_3	3 – 5	350 – 400

Summarizing, the main cause of hip implants failure is the degradation of the biomaterial surface, caused by the combination of electrochemical corrosion effects and mechanical effects of cyclic loads, which promote the debris release. As shown in table 1.2, the pairs joint that suffer more degradation are those that have polymer in the composition, since they have a higher wear rate and larger wear debris size. The release of particles in the form of ions can induce accumulation in tissues, causing inflammation, and discomfort in the patient, and in extreme situations implant rejection. Such release occurs in the form of debris, the body treats them as microorganisms, releasing enzymes to attack and destroy. However, while these enzymes attack these particles also kill adjacent bone cells, a process known as osteolysis. This process causes bone re-sorption and aseptic implant dislocation which eventually leads to the necessity for a revision arthroplasty [40].

1.4 Surface modification

The need to prevent the release of wear debris into the body reflects the importance of the optimization of the implant surface. However, the development of a biomaterial is a very complex challenge, especially regarding its surface. So, a biomaterial must be carefully designed and characterized in order to facilitate the understanding of its interaction with the biological environment, which is quite complex and not fully understood. Numerous studies are continuously carried out with a view to solve this kind of problems leading to a competitive and diverse hip prostheses market. Accordingly, and given the difficulty in developing a

material that meets all the requirements for the application in question, the research in this field has been strongly directed to the surface modification of biomaterials, allowing not only the improvement of the mechanical and tribological properties, the minimization of the production of wear debris, but also the increase of the biocompatibility of the material [27]. Within the various techniques that enable the surface modification, those that permit to obtain new materials from the vapour phase should be highlighted. The most important techniques are chemical vapour deposition (CVD), physical vapour deposition (PVD), ion deposition and plasma discharge [27]. Through these techniques, and through the selection of the deposition parameters, it is possible to create materials with virtually all of the desired properties. Changing the parameters of suitable deposition it is possible to obtain crystalline structures with varied grain sizes and different growth preferential orientations, and eventually amorphous structures for a material with the same chemical composition. For example, the coatings of metal nitrides and metal carbides can achieve hardness of 40 GPa when dispersed in the form of nanocrystals (about 15 nm) embedded in the amorphous phase [61].

1.4.1 Mechanical and tribological properties of coatings

The development of ceramic coatings has been perceived as one of the solutions to increase the average life span of orthopaedic prosthesis. The strong characteristics displayed by ceramic materials, such as the resistance to corrosion and a high mechanical strength and resistance to wear, have outweighed their biggest limitation, brittleness [62]. Amongst the different coatings under study, the nitrides, the transition metal carbonitrides (mainly Cr and Ti) and the DLC's (Diamond-like carbon) stand out and have been subject to several scientific investigations concerning biomaterials, as well as in other fields demanding strong mechanical and tribological characteristics, and a high level of resistance to corrosion. TiNbN (titanium niobium nitride) is one of the commercially available coatings used in hip replacements. However, the number of tribological studies focused on this type of surface is very scant. From what is known concerning these coatings, the wear and the release of metal ions have been significantly reduced when compared with a MoM prosthetic implant [63].

Titanium nitride coatings (TiN), on the other hand, have been known and studied for several decades, owing to their inherent properties and, above all, because they display increased levels of hardness. Additionally, the oxidized TiN increases the resistance to corrosion and promotes the nucleation of calcium phosphates, favouring the integration of the implant in the

human bone [64]. However, TiN is known for a high friction coefficient and consequently a weak resistance to wear, an unwanted characteristic in hip replacement prosthetics [65]. The development of TiC coatings with an increased hardness has tried to overcome this limitation. Despite their solid tribologic properties, these coatings pose adhesion problems [66]. Over in the last few years, the TiCN system has been subject to some investigation, with the purpose of bringing together the isolated qualities of both the TiN and the TiC. TiCN forms a solid TiN-TiC solution with an increased hardness (intrinsic to TiC and TiN), a friction coefficient 3 to 4 times lower than TiN and a wear rate 5 to 7 times lower than TiN [27,62,67–70]. Therefore, TiCN coatings are widely applied in medical tools, owing to their great biocompatibility and their excellent tribological behaviour [71]. However, according to the available literature, these coatings have never been applied in hip replacement prosthetics [63]. Notwithstanding, biotribological *in vitro* ball-on-disk short-term tests, using Hanks' balanced salt solution as lubricant, have revealed that the TiCN / TiCN pair has a higher wear resistance than the pair that is currently available, TiNbN / TiNbN. The wear rate observed in the pair TiCN / TiCN, by Serro *et al.* [63], correspond to 6.3×10^{-17} m^3/Nm, in comparison to the 3.1×10^{-16} m^3/Nm of the pair TiNbN / TiNbN. A study of Martínez-Martínez *et al.* [72] reported that in TiCN coatings deposited by magnetron sputtering, a C enrichment led to the formation of an amorphous carbon phase that can help to decrease the friction coefficient and the wear rate, although promoting a hardness reduction. A similar behaviour is reported by Silva *et al.* [73] that used ZrCN coatings deposited by magnetron sputtering with N_2 flows ranging from 2 to 10 sccm in order to investigate the influence of the nitrogen incorporation on structure and properties. These results show that an amorphous phase CN_x formation could act as a lubricant resulting in a low coefficient of friction.

Moreover, DLC coatings have also been proposed as surface alternatives in orthopaedic implants, owing to the excellent properties they have displayed in several *in vitro* studies, namely an increased hardness (ranging between 1 – 60 GPa), a solid resistance to wear and corrosion, a low friction coefficient and a high biocompatibility [74]. However, the main downside of these coatings, generally produced with PVD and CVD techniques, concerns their adhesion problems that are connected to high residual stresses, especially when deposited in steel or titanium substrates, the most commonly used in biomaterials [28,68].

1.4.2 Antimicrobial coatings

Infections, as already referred, are one of the main causes of hip replacement failure, and are triggered by the microbial adhesion and biofilm formation on the surface of biomaterials. In fact, in the U.S.A., studies developed by the *Centers for Disease Control and Prevention,* concluded that 60% of biofilm induced infections are associated with biomedical implants [75]. Biofilms are characterized by communities of microorganisms strongly attached to each other and to a biomaterial surface, embedded in an exopolymeric matrix. Biofilm matrix is composed by a mixture of components, such as extracellular polymeric substances (EPS), nucleic acids, and other substances [76]. The EPS constituted mainly by polysaccharides and proteins [77] are produced by a wide variety of bacteria. These substances are very important for intercellular binding during surface colonization [78] and protection against the host immune system and resistance to antibiotics [79]. For these reasons, biofilms are difficultly eradicated making them important in infections. The process of biofilm formation which included several steps is illustrated in Figure 1.3.

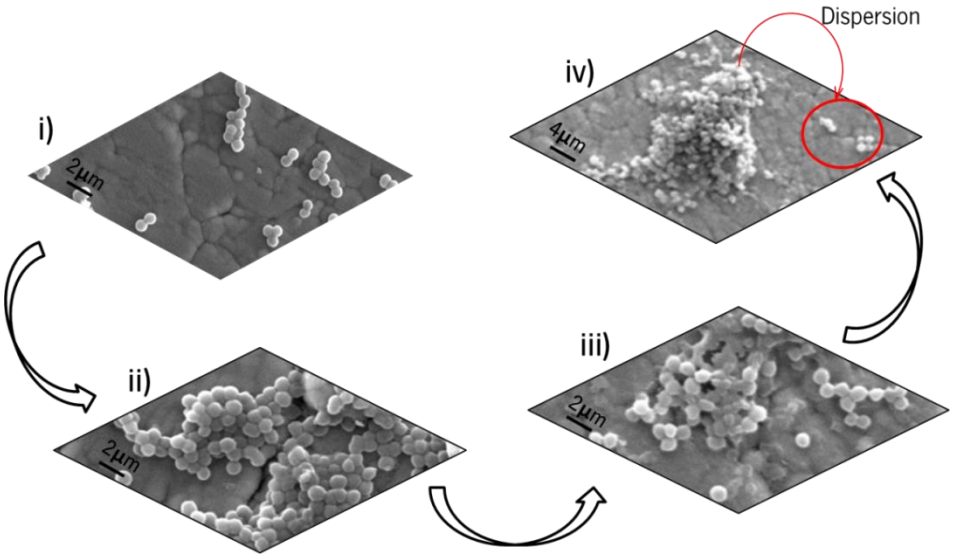

Figure 1.3 Stages of biofilm development i) initial attachment of microbial cells to surface; ii) multiplication of the microbial cells forming microcolonies; iii) maturation of the biofilm of cells and production of an extracellular matrix and iv) detachment of some biofilm cells leading to colonization in other parts of surface.

One of the microorganisms associated to biofilm formation and consequent implant rejection is *Staphylococcus epidermidis* (Figure 1.4)

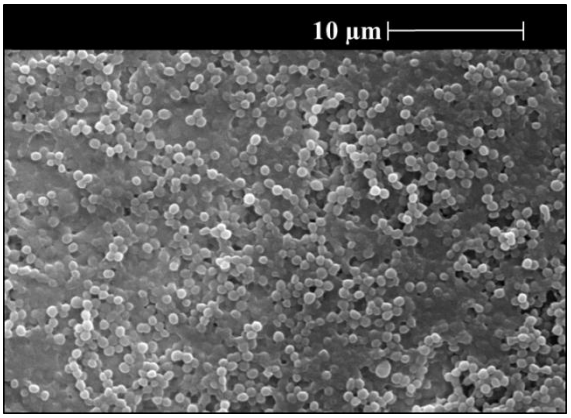

Figure 1.3 Biofilm of *Staphylococcus epidermidis*

Staphylococcus epidermidis belongs to the genus *Staphylococcus* and is characterized to be gram-positive bacteria (presents violet coloration after Gram staining method, due to the thick peptidoglycan layer in the cell wall, while gram-negative have a thin peptidoglycan layer incapable to retain the Gram stain), coagulase-negative (they do not produce the enzyme coagulase responsible by the blood plasma coagulation) and, present a rounded shape with about 1 µm in diameter. This species colonizes the skin and mucous membranes of the human body, and represents an important part of its normal microflora [80,81], and consequently one of the major nosocomial pathogens associated to infections of implanted medical devices [82]. These microorganisms easily come in contact with the implant during surgeries [83] and are responsible for chronic and profound infections, which can occur months or even years after the prosthesis implantation [80,84]. Prosthetic heart valves, central venous catheters, urinary catheters, contact lenses and prosthetic joints (hip prostheses and other orthopaedic devices) are the medical devices mostly affected by *S. epidermidis* [78,80,84,85].

In addition to their role in infections, biofilm also promotes corrosion, namely in metal surfaces, which leads to their degradation once the change of electrochemical conditions at the metal/solution interface induces or accelerates the corrosion process. This change occurs by the attachment of bacteria to the metal, which release metabolites within biofilms, including several acids that influence the anodic and cathodic reactions, creating conditions for corrosion [86]. Therefore, several strategies have been studied in order to avoid biofilm formation in medical prostheses. The main line of research has focused on reducing the

attractive forces between bacteria and the surface of the biomaterial, optimizing the physical and chemical properties of the latter. These studies have shown that the interactions between the biological environment and the biomaterial are influenced by the surface properties of the material [87]. However, the alteration of surface properties alone does not effectively eliminate the production of biofilm [79,88]. It is therefore necessary to adopt different approaches that hinder the adhesion of microorganisms. This can be achieved with biomaterials that are capable of releasing antimicrobial agents. The incorporation of silver, Ag, clusters in TiCN systems may be a solution. The antimicrobial properties of this metal are widely known since ancient times. The antimicrobial activity of silver has been attributed to its oxidized form, Ag^{+}. The antimicrobial action of the silver ions (Ag^{+}) is effective in fighting different types of bacteria and fungus, since Ag^{+} destabilize microbial cell walls, interrupting the metabolism of their cells and inhibiting their reproduction [89–91]. In addition to its antimicrobial properties, the incorporation of controlled percentages of silver has revealed solid tribological properties, acting as a solid lubricant, raising the interest around this metal [92–94]. In this sense, the development of coatings with good tribological properties and an antibacterial character can be crucial to overcome the main limitations of hip replacements.

In the last few years, different systems have been the target of several studies for the development of prostheses replacement coatings, such as Ag doped TiN [65,95,96], CrN [95,97], ZrN [95], TaN [98,99] as well as DLC's [100]. Although the results observed by different authors revealed that the Ag incorporation leads to the development of antimicrobial properties, Kelly *et al.* [95] observed that the incorporation of Ag percentages above 10 at. % in TiN, CrN, ZrN coatings leads to a significant decrease in the hardness, wear and corrosion resistance, unwanted effects in a tribological behaviour. Tseng *et al.* [101], observed an identical behaviour in TaN-Ag systems when Ag was introduced in percentages close to 10 at. %. Accordingly, the incorporation of high silver contents does not favour these applications. In addition to its impact on tribological properties, the incorporation of high silver contents can promote cytotoxicity, leading to the rejection of the biomaterial [99,102]. In fact, few studies have reported that concentrations of silver above 10 mg/L can be toxic to some types of human cells [103,104]. Other authors have shown that the size of silver nanoparticles can influence antimicrobial activity [105]. Studies done by Kelly *et al.* [65,95] with TiN/Ag coatings, showed that in addition to the quantity and size there is also a relationship between shape and distribution density of the silver particles and the nature of the surrounding matrix,

which could also influence the antimicrobial activity. The high chemical stability in the formation of Ag^{+}, responsible for the antimicrobial properties, may not be meaningful. Furthermore, it is still necessary a better understand the silver action mode as an antimicrobial agent.

So, the improvement in the development, design and production of materials and techniques for implants is imperative to maintain a good quality of patient life. Moreover, an accurate characterization of the materials and their interaction with host tissues is required, so that the main property of a biomaterial, which is the absence of any adverse reaction in the body, is satisfied.

References

[1] Cereatti A, Margheritini F, Donati M and Cappozzo A 2010 Is the human acetabulofemoral joint spherical? *J. Bone Joint Surg. Br.* **92** 311–4

[2] Mellon S J, Liddle A D and Pandit H 2013 Hip replacement: landmark surgery in modern medical history *Maturitas* **75** 221–6

[3] Park J and Lakes R 2007 Hard Tissue Replacement—II: Joints and Teeth *Biomaterials* pp 395–458

[4] Schmidt T A and Sah R L 2007 Effect of synovial fluid on boundary lubrication of articular cartilage *Osteoarthritis Cartilage* **15** 35–47

[5] Suh J, Scherping S, Marui T, Steadman J R and Woo S L Y 1995 Basic science of articular cartilage injury and repair *Oper. Tech. Sports Med.* **3** 78–86

[6] Kheir E and Shaw D 2009 Hyaline articular cartilage *Orthop. Trauma* **23** 450–5

[7] Knox P, Levick J R and Mcdonald J N 1988 Synovial fluid-its mass, macromolecular content and pressure in major limb joints of the rabbit *Exp. Physiol.* **73** 33–45

[8] Roba M, Naka M, Gautier E, Spencer N D and Crockett R 2009 The adsorption and lubrication behavior of synovial fluid proteins and glycoproteins on the bearing-surface materials of hip replacements *Biomaterials* **30** 2072–8

[9] Pawaskar S S, Ingham E, Fisher J and Jin Z 2011 Fluid load support and contact mechanics of hemiarthroplasty in the natural hip joint *Med. Eng. Phys.* **33** 96–105

[10] Myant C and Cann P 2014 On the matter of synovial fluid lubrication: Implications for Metal-on-Metal hip tribology *J. Mech. Behav. Biomed. Mater.*

[11] Mattei L, Di Puccio F, Piccigallo B and Ciulli E 2011 Lubrication and wear modelling of artificial hip joints: A review *Tribol. Int.* **44** 532–49

[12] Tandon P and Chaurasia A 1990 Microstructural effects on hip joint articulation *Appl. Math. Model.* **14** 312–9

[13] Ateshian G A 2009 The role of interstitial fluid pressurization in articular cartilage lubrication *J. Biomech.* **42** 1163–76

[14] Suh J K, Li Z and Woo S L 1995 Dynamic behavior of a biphasic cartilage model under cyclic compressive loading *J. Biomech.* **28** 357–64

[15] Wong M and Carter D . 2003 Articular cartilage functional histomorphology and mechanobiology: a research perspective *Bone* **33** 1–13

[16] Gispert M P, Serro A P, Colaço R, Pires E and Saramago B 2008 The effect of roughness on the tribological behavior of the prosthetic pair UHMWPE/TiN-coated stainless steel *J. Biomed. Mater. Res. B. Appl. Biomater.* **84** 98–107

[17] Gispert M P, Serro A P, Colaço R and Saramago B 2006 Friction and wear mechanisms in hip prosthesis: Comparison of joint materials behaviour in several lubricants *Wear* **260** 149–58

[18] Hall R M and Unsworth A 1997 Review Friction in hip prostheses *Biomaterials* **18** 1017–26

[19] Saikko V and Ahlroos T 1997 Phospholipids as boundary lubricants in wear tests of prosthetic joint materials *Wear* **207** 86–91

[20] Yoshida H, Faust A, Wilckens J, Kitagawa M, Fetto J and Chao E Y-S 2006 Three-dimensional dynamic hip contact area and pressure distribution during activities of daily living *J. Biomech.* **39** 1996–2004

[21] Genda E, Iwasaki N, Li G, MacWilliams B A, Barrance P J and Chao E Y 2001 Normal hip joint contact pressure distribution in single-leg standing–effect of gender and anatomic parameters *J. Biomech.* **34** 895–905

[22] Anderson A, Ellis B, Maas S and Weiss J 2010 Effects of idealized joint geometry on finite element predictions of cartilage contact stresses in the hip *J. Biomech.* **43** 1351–7

[23] Pramanik S, Agarwal A and Rai K 2005 Chronology of total hip joint replacement and materials development *Trends Biomater. Artif. Organs* **19** 15–26

[24] Pivec R, Johnson A J, Mears S C and Mont M A 2012 Hip arthroplasty *Lancet* **380** 1768–77

[25] Jassim S S, Vanhegan I S and Haddad F S 2012 The Epidemiology of Total Hip Arthroplasty in England and Wales *Semin. Arthroplasty* **23** 197–9

[26] Bozic K J, Kurtz S M, Lau E, Ong K, Vail T P and Berry D J 2009 The epidemiology of revision total hip arthroplasty in the United States *J. Bone Joint Surg. Am.* **91** 128–33

[27] Geetha M, Singh A K, Asokamani R and Gogia A K 2009 Ti based biomaterials, the ultimate choice for orthopaedic implants – A review *Prog. Mater. Sci.* **54** 397–425

[28] Love C A, Cook R B, Harvey T J, Dearnley P A and Wood R J K 2013 Diamond like carbon coatings for potential application in biological implants—a review *Tribol. Int.* **63** 141–50

[29] Corbett K L, Losina E, Nti A A, Prokopetz J J Z and Katz J N 2010 Population-based rates of revision of primary total hip arthroplasty: a systematic review ed F P Rannou *PLoS One* **5** e13520

[30] Bozic K J, Katz P, Cisternas M, Ono L, Ries M D and Showstack J 2005 Hospital resource utilization for primary and revision total hip arthroplasty *J. Bone Joint Surg. Am.* **87** 570–6

[31] Jafari S M, Coyle C, Mortazavi S M J, Sharkey P F and Parvizi J 2010 Revision hip arthroplasty: infection is the most common cause of failure *Clin. Orthop. Relat. Res.* **468** 2046–51

[32] Ratner B D, Hoffman A S, Schoen F J and Lemons J E 1996 An Introduction to Materials in Medicine *Biomaterials Science* (Academic Press) pp 1–484

[33] Hench L L and Polak J M 2002 Third-generation biomedical materials *Science* **295** 1014–7

[34] Williams D F 2008 On the mechanisms of biocompatibility *Biomaterials* **29** 2941–53

[35] Williams DF 1987 *Definitions in biomaterials* (Amsterdam: Elsevier)

[36] Liu X, Chu P and Ding C 2004 Surface modification of titanium, titanium alloys, and related materials for biomedical applications *Mater. Sci. Eng. R Reports* **47** 49–121

[37] Williams D F 1987 Advanced applications for materials implanted within the human body *Mater. Sci. Technol.* **3** 797–806

[38] Hallab N and Anderson S 2005 Lymphocyte responses in patients with total hip arthroplasty *J. Orthop. Res.* **23** 384–91

[39] Igual Muñoz A and Mischler S 2011 Effect of the environment on wear ranking and corrosion of biomedical CoCrMo alloys *J. Mater. Sci. Mater. Med.* **22** 437–50

[40] Sargeant A and Goswami T 2006 Hip implants: Paper V. Physiological effects *Mater. Des.* **27** 287–307

[41] Barbour P S M, Stone M H and Fisher J 1999 A hip joint simulator study using simplified loading and motion cycles generating physiological wear paths and rates *Proc. Inst. Mech. Eng. Part H J. Eng. Med.* **213** 455–67

[42] Tipper J L, Firkins P J, Besong A A, Barbour P S M, Nevelos J, Stone M H, Ingham E and Fisher J 2001 Characterisation of wear debris from UHMWPE on zirconia ceramic, metal-on-metal and alumina ceramic-on-ceramic hip prostheses generated in a physiological anatomical hip joint simulator *Wear* **250** 120–8

[43] Sawae Y, Yamamoto A and Murakami T 2008 Influence of protein and lipid concentration of the test lubricant on the wear of ultra high molecular weight polyethylene *Tribol. Int.* **41** 648–56

[44] Ollivere B, Wimhurst J A, Clark I M and Donell S T 2012 Current concepts in osteolysis *J. Bone Joint Surg. Br.* **94** 10–5

[45] Wang F C, Brockett C, Williams S, Udofia I, Fisher J and Jin Z M 2008 Lubrication and friction prediction in metal-on-metal hip implants *Phys. Med. Biol.* **53** 1277–93

[46] Amstutz H C and Grigoris P 1996 Metal on metal bearings in hip arthroplasty *Clin. Orthop. Relat. Res.* S11–34

[47] Firkins P J, Tipper J L, Ingham E, Stone M H, Farrar R and Fisher J 2001 A novel low wearing differential hardness, ceramic-on-metal hip joint prosthesis *J. Biomech.* **34** 1291–8

[48] McKellop H, Park S H, Chiesa R, Doorn P, Lu B, Normand P, Grigoris P and Amstutz H 1996 In vivo wear of three types of metal on metal hip prostheses during two decades of use *Clin. Orthop. Relat. Res.* S128–40

[49] Delaunay C, Petit I, Learmonth I D, Oger P and Vendittoli P A 2010 Metal-on-metal bearings total hip arthroplasty: The cobalt and chromium ions release concern *Orthop. Traumatol. Surg. Res.* **96** 894–904

[50] Nevelos J E, Ingham E, Doyle C, Fisher J and Nevelos A B 1999 Analysis of retrieved alumina ceramic components from Mittelmeier total hip prostheses *Biomaterials* **20** 1833–40

[51] Doorn P F, Campbell P A, Worrall J, Benya P D, McKellop H A and Amstutz H C 1998 Metal wear particle characterization from metal on metal total hip replacements: transmission electron microscopy study of periprosthetic tissues and isolated particles *J. Biomed. Mater. Res.* **42** 103–11

[52] Lo K H, Shek C H and Lai J K L 2009 Recent developments in stainless steels *Mater. Sci. Eng. R Reports* **65** 39–104

[53] Davidson J A 1993 Characteristics of metal and ceramic total hip bearing surfaces and their effect on long-term ultra high molecular weight polyethylene wear *Clin. Orthop. Relat. Res.* 361–78

[54] Slonaker M and Goswami T 2004 Review of wear mechanisms in hip implants: Paper II – ceramics IG004712 *Mater. Des.* **25** 395–405

[55] Yen S K, Guo M J and Zan H Z 2001 Characterization of electrolytic ZrO2 coating on Co-Cr-Mo implant alloys of hip prosthesis *Biomaterials* **22** 125–33

[56] Long M and Rack H J 1998 Titanium alloys in total joint replacement–a materials science perspective *Biomaterials* **19** 1621–39

[57] Ribeiro M, Monteiro F J and Ferraz M P 2012 Infection of orthopedic implants with emphasis on bacterial adhesion process and techniques used in studying bacterial-material interactions *Biomatter* **2** 176–94

[58] Katti K S 2004 Biomaterials in total joint replacement *Colloids Surf. B. Biointerfaces* **39** 133–42

[59] Bauer S, Schmuki P, von der Mark K and Park J 2013 Engineering biocompatible implant surfaces *Prog. Mater. Sci.* **58** 261–326

[60] Ritchie R O, Koester K J, Ionova S, Yao W, Lane N E and Ager J W 2008 Measurement of the toughness of bone: a tutorial with special reference to small animal studies. *Bone* **43** 798–812

[61] Veprek S, Zhang R F, Veprek-Heijman M G J, Sheng S H and Argon A S 2010 Superhard nanocomposites: Origin of hardness enhancement, properties and applications *Surf. Coatings Technol.* **204** 1898–906

[62] Serro A P, Completo C, Colaço R, dos Santos F, da Silva C L, Cabral J M S, Araújo H, Pires E and Saramago B 2009 A comparative study of titanium nitrides, TiN, TiNbN and TiCN, as coatings for biomedical applications *Surf. Coatings Technol.* **203** 3701–7

[63] Gispert M P, Serro A P, Colaço R, Pires E and Saramago B 2007 Wear of ceramic coated metal-on-metal bearings used for hip replacement *Wear* **263** 1060–5

[64] Piscanec S 2004 Bioactivity of TiN-coated titanium implants *Acta Mater.* **52** 1237–45

[65] Kelly P J, Li H, Whitehead K A, Verran J, Arnell R D and Iordanova I 2009 A study of the antimicrobial and tribological properties of TiN/Ag nanocomposite coatings *Surf. Coatings Technol.* **204** 1137–40

[66] Bull S 2003 Properties and performance of commercial TiCN coatings. Part 1: coating architecture and hardness modelling *Surf. Coatings Technol.* **163** 499–506

[67] Feng W, Liu C, Chen G, Zhang G, Gu W, Niu E and Yang S-Z 2007 Titanium carbonitride films on cemented carbide cutting tool prepared by pulsed high energy density plasma *Appl. Surf. Sci.* **253** 4923–7

[68] Robertson J 2002 Diamond-like amorphous carbon *Mater. Sci. Eng. R Reports* **37** 129–281

[69] Takadoum J, Bennani H H and Allouard M 1997 Friction and wear characteristics of TiN , TiCN and diamond-like carbon films *Surf. Coatings Technol.* **88** 232–8

[70] Zhang G, Li B, Jiang B, Yan F and Chen D 2009 Microstructure and tribological properties of TiN, TiC and Ti(C, N) thin films prepared by closed-field unbalanced magnetron sputtering ion plating *Appl. Surf. Sci.* **255** 8788–93

[71] Lackner J M, Waldhauser W and Ebner R 2004 Large-area high-rate pulsed laser deposition of smooth TiCxN1−x coatings at room temperature—mechanical and tribological properties *Surf. Coatings Technol.* **188-189** 519–24

[72] Martínez-Martínez D, Sánchez-López J C, Rojas T C, Fernández A, Eaton P and Belin M 2005 Structural and microtribological studies of Ti–C–N based nanocomposite coatings prepared by reactive sputtering *Thin Solid Films* **472** 64–70

[73] Silva E, Rebelo de Figueiredo M, Franz R, Escobar Galindo R, Palacio C, Espinosa A, Calderon V. S, Mitterer C, Carvalho S, Figueiredo M R De, Galindo R E and Calderon S V 2010 Structure – property relations in ZrCN coatings for tribological applications *Surf. Coat. Technol.* **205** 2134–41

[74] Grill A 1993 Review of the tribology of diamond-like carbon *Wear* **168** 143–53

[75] Archibald L K and Gaynes R P 1997 Hospital-acquired infections in the United States. The importance of interhospital comparisons *Infect. Dis. Clin. North Am.* **11** 245–55

[76] Davey M E, George A O and Toole G A O 2000 Microbial Biofilms : from Ecology to Molecular Genetics Microbial Biofilms : from Ecology to Molecular Genetics *Microbiol. Mol. Biol. Rev.* **64** 847–67

[77] Sutherland I W 2001 The biofilm matrix–an immobilized but dynamic microbial environment *Trends Microbiol.* **9** 222–7

[78] Donlan R M 2001 Biofilms and device-associated infections *Emerg. Infect. Dis.* **7** 277–81

[79] An Y H and Friedman R J 1998 Concise review of mechanisms of bacterial adhesion to biomaterial surfaces *J. Biomed. Mater. Res.* **43** 338–48

[80] Vuong C and Otto M 2002 Staphylococcus epidermidis infections *Microbes Infect.* **4** 481–9

[81] O'Gara J P and Humphreys H 2001 Staphylococcus epidermidis biofilms: importance and implications *J. Med. Microbiol.* **50** 582–7

[82] Fitzpatrick F, Humphreys H, Smyth E, Kennedy C A and O'Gara J P 2002 Environmental regulation of biofilm formation in intensive care unit isolates of Staphylococcus epidermidis *J. Hosp. Infect.* **42** 212–8

[83] Pishbin F, Mouriño V, Gilchrist J B, Kreppel S, Salih V, Ryan M P and Boccaccini A R 2013 Single-step electrochemical deposition of antimicrobial orthopaedic coatings based on a bioactive glass/chitosan/nano-silver composite system *Acta Biomater.* **9** 7469–79

[84] An Y H and Friedman R J 1996 Prevention of sepsis in total joint arthroplasty *J. Hosp. Infect.* **33** 93–108

[85] Rohde H, Burdelski C, Bartscht K, Hussain M, Buck F, Horstkotte M a, Knobloch J K-M, Heilmann C, Herrmann M and Mack D 2005 Induction of Staphylococcus epidermidis biofilm formation via proteolytic processing of the accumulation-associated protein by staphylococcal and host proteases *Mol. Microbiol.* **55** 1883–95

[86] Moura M, Pontual E, Paiva P and Coelho L 2013 An Outline to Corrosive Bacteria *methods* **18** 19

[87] Ratner B D 1983 Surface characterization of biomaterials by electron spectroscopy for chemical analysis *Ann. Biomed. Eng.* **11** 313–36

[88] Katsikogianni M and Missirlis Y F 2004 Concise review of mechanisms of bacterial adhesion to biomaterials and of techniques used in estimating bacteria-material interactions *Eur. Cell. Mater.* **8** 37–57

[89] Bellantone M, Williams H D and Hench L L 2002 Broad-Spectrum Bactericidal Activity of Ag 2 O-Doped Bioactive Glass **46** 1940–5

[90] Feng Q, Wu J and Chen G 2000 A mechanistic study of the antibacterial effect of silver ions on Escherichia coli and Staphylococcus aureus *J. Biomed. Mater. Res.* **52** 662–8

[91] Kim T N, Feng Q L, Kim J O, Wu J, Wang H, Chen G C and Cui F Z 1998 Antimicrobial effects of metal ions (Ag+, Cu2+, Zn2+) in hydroxyapatite *J. Mater. Sci. Mater. Med.* **9** 129–34

[92] Babonneau D, Cabioc'h T, Naudon A, Girard J . and Denanot M . 1998 Silver nanoparticles encapsulated in carbon cages obtained by co-sputtering of the metal and graphite *Surf. Sci.* **409** 358–71

[93] Endrino J L, Nainaparampil J J and Krzanowski J E 2002 Microstructure and vacuum tribology of TiC–Ag composite coatings deposited by magnetron sputtering-pulsed laser deposition *Surf. Coatings Technol.* **157** 95–101

[94] Yao S H, Su Y L, Kao W H and Cheng K W 2006 Evaluation on wear behavior of Cr–Ag–N and Cr–W–N PVD nanocomposite coatings using two different types of tribometer *Surf. Coatings Technol.* **201** 2520–6

[95] Kelly P J, Li H, Benson P S, Whitehead K A, Verran J, Arnell R D and Iordanova I 2010 Comparison of the tribological and antimicrobial properties of CrN/Ag, ZrN/Ag, TiN/Ag, and TiN/Cu nanocomposite coatings *Surf. Coatings Technol.* **205** 1606–10

[96] Zhao J, Cai X M, Tang H Q, Liu T, Gu H Q and Cui R Z 2009 Bactericidal and biocompatible properties of TiN/Ag multilayered films by ion beam assisted deposition *J. Mater. Sci. Mater. Med.* **20** 101–5

[97] Mulligan C P and Gall D 2005 CrN–Ag self-lubricating hard coatings *Surf. Coatings Technol.* **200** 1495–500

[98] Huang H-L, Chang Y-Y, Lai M-C, Lin C-R, Lai C-H and Shieh T-M 2010 Antibacterial TaN-Ag coatings on titanium dental implants *Surf. Coatings Technol.* **205** 1636–41

[99] Hsieh J H, Tseng C C, Chang Y K, Chang S Y and Wu W 2008 Antibacterial behavior of TaN–Ag nanocomposite thin films with and without annealing *Surf. Coatings Technol.* **202** 5586–9

[100] Morrison M L, Buchanan R A, Liaw P K, Berry C J, Brigmon R L, Riester L, Abernathy H, Jin C and Narayan R J 2006 Electrochemical and antimicrobial properties of diamondlike carbon-metal composite films *Diam. Relat. Mater.* **15** 138–46

[101] Tseng C C, Hsieh J H, Jang S C, Chang Y Y and Wu W 2009 Microstructural analysis and mechanical properties of TaN–Ag nanocomposite thin films *Thin Solid Films* **517** 4970–4

[102] Jamuna-Thevi K, Bakar S A, Ibrahim S, Shahab N and Toff M R M 2011 Quantification of silver ion release, in vitro cytotoxicity and antibacterial properties of nanostuctured Ag doped TiO2 coatings on stainless steel deposited by RF magnetron sputtering *Vacuum* **86** 235–41

[103] Betts A, Dowling D, Mcconnell M and Pope C 2005 The influence of platinum on the performance of silver–platinum anti-bacterial coatings *Mater. Des.* **26** 217–22

[104] Chen W, Liu Y, Courtney H S, Bettenga M, Agrawal C M, Bumgardner J D and Ong J L 2006 In vitro anti-bacterial and biological properties of magnetron co-sputtered silver-containing hydroxyapatite coating *Biomaterials* **27** 5512–7

[105] Kim J S, Kuk E, Yu K N, Kim J-H, Park S J, Lee H J, Kim S H, Park Y K, Park Y H, Hwang C-Y, Kim Y-K, Lee Y-S, Jeong D H and Cho M-H 2007 Antimicrobial effects of silver nanoparticles *Nanomedicine* **3** 95–101

Chapter II – Coatings characterization

The work presented in this chapter was based on the two published papers:

- **Carvalho, Isabel**; Henriques, M.; Oliveira, J.C.; Alves, C.F.A.; Piedade, A.P.; Carvalho, S. Science and Technology of Advanced Materials, 14(3), 1-10, 2013

- Sánchez-López, J.C.; Abad, M.D.; **Carvalho, Isabel**; Escobar Galindo, R.; Benito, N.; Ribeiro, S.; Henriques, M.; Cavaleiro, A.; Carvalho, S. Surface and Coatings Technology, 206(8-9), 2192-2198, 2012

Chapter II – Coatings characterization

2.1 Introduction

Application of thin films in the biomedical engineering field represents an attractive challenge due to the multiple situations where they may improve or even functionalize a certain part of the human body. Although the use of hip implants is continuously increasing, implant failure is a huge problem for both the patient and governmental agencies, once it involves repeated surgeries and consequently considerable economical resources, as well as patients' health risks. This failure can be attributed to excessive wear and wear debris and also to microbial infection, which promotes the short durability [1]. For these reasons the investigation of new biomaterials is required to obtain good mechanical, tribological and biological properties that allow the development of better prostheses. To overcome the problem of particle generation, the uses of a very low wear coating material as diamond-like carbon (DLC), transition-metal carbides (MeC_x), nitrides (MeN_x), or other protective thin films, has been proposed [2–5]. In recent years, the research has been directed towards the use of antibacterial materials that could reduce the failure of medical devices provoked by the infections. Many of these studies focus on the use of silver, which is known to be an antimicrobial element [3,6–8].

Early works have studied the combination of hard phases (TiN or TiC), that provide hardness, with silver as soft metal to play the role of lubricant, to investigate their tribological performance [9,10]. In previous studies, the deposition of TiC(O)N-based coatings by direct current (dc) magnetron sputtering gained knowledge about the synthesis conditions that yielded a good compromise between tribological and hardness properties [11,12]. The aim of this study is the production and structural characterization of Ag-TiCN for hip implant applications and the focus is to study the influence of silver addition to the structure of TiCN coatings produced by dc reactive magnetron sputtering. In the present study the addition of variable concentrations of Ag into TiCN films is explored with the goal of maintaining a good tribological performance. To achieve this purpose, the coatings were evaluated in terms of structure and composition and the tribological properties were studied in lubricated conditions using fetal bovine serum (FBS) to simulate the biological conditions. The final mechanical and tribological performances were correlated with the evolution of the ratio of Ag/Ti inside the coatings.

2.2 Materials and methods

2.2.1 Samples preparation

Ag-TiCN samples were deposited by reactive DC magnetron sputtering using a home-made chamber onto polished and ultrasonically cleaned 316L stainless steels (SS 316L) (20 × 20 mm^2) and single crystal silicon (100) (10 × 10 mm^2) substrates. Two types of targets (pure Ti and mixed Ti + Ag) of dimensions 200 × 100 mm^2 were used in Ar + C_2H_2 + N_2 mixtures with the substrates rotating at 70 mm over the target at a constant speed of 7 rpm. Argon flow was kept constant at 60 sccm while the reactive gas fluxes, C_2H_2 and N_2, were changed in the ranges of 1.2 to 8 sccm and 3 to 8.6 sccm, respectively, in order not to change significantly the C and N contents. This represented a variation of the working pressure of the deposition chamber between 0.2 and 0.5 Pa. The films were grown at a constant temperature (373 K) and bias voltage was maintained at −50 V. A set of samples was prepared with Ag content varying from 0 to 15 at. %, by varying the current density applied to each magnetron and the chemical composition of the mixed Ti + Ag target (silver pellets were placed in the preferential erosion area of one Ti target resulting in relative Ag sputtering areas of 15 % for atomic ratio Ag/Ti ≤ 0.20 and 37 % for atomic ratio Ag/Ti ≥ 0.37).

2.2.2 Chemical composition

The chemical composition of the deposited films was measured using a Cameca, Camebax SX 50, electron probe microanalysis (EPMA) equipment. Five measurements were performed for each sample, randomly selecting different areas of the surface. The accelerating voltage of the electron beam was 10 kV and the current 40 nA.

2.2.3 Physical characterization

Ball crater tests were performed with a 15 mm diameter sphere rotating at 700 rpm during 80 s. The film thickness was calculated from the diameters of the rings.

2.2.4 Structural characterization

The structure and phase distribution of the coatings were determined by X-ray diffraction (XRD) using a Siemens diffractometer in a Bragg–Brentano geometry and Co K_α radiation (1.78897 Å).

The crystallite grain sizes was calculated by applying the Scherrer equation after a nonlinear Voigt curve fit on the (111) peaks of the diffractograms using OriginPro 8 software.

The chemical bonds were evaluated by micro-Raman spectroscopy. Raman spectra were acquired with a Renishaw InVia microscope using the 514.5 nm Ar laser line.

2.2.5 Morphology and topography

The morphology of the coatings was assessed by scanning electron microscopy (EDAX-Nova nanoSEM 200) in both backscattering (BSE) and secondary electron (SE) modes, while surface roughness and topography were characterized by atomic force microscopy (AFM NanoScope III Digital Instruments). Ag-TiCN coatings roughness measurements were performed on silicon and SS 316L substrates under a scan range of 5 × 5 μm^2 and 10 x 10 μm^2 respectively, in tapping mode. Measurements were made in three areas randomly chosen in all samples.

2.2.6 Chemical bonds characterization by XPS

XPS spectra were acquired using a hemispherical analyser (SPECS EA-10 Plus).The pass energy was 15 eV giving a constant resolution of 0.9 eV. The Ag 3d5/2 line at 367.9 eV was used in order to calibrate the binding energies. A twin anode (Mg and Al) X-ray source was operated at a constant power of 300W using Al Kα radiation. The samples were sputter-cleaned in situ using a broad 3 keV Ar^+ beam for 10 min.

2.2.7 Mechanical characterization: hardness and residual stress

Hardness measurements were conducted using a Micro Materials Nanotest system equipped with a Berkovich indenter applying a maximum load of 10 mN. Correction of the geometrical defects in the tip of the indenter, thermal drift of the equipment and uncertainty of the initial contact was done [13]. Fifteen tests were performed.

The residual stresses, σ, were obtained by the deflection method from Stoney's equation, using substrate curvature radii, both before and after coating deposition [14].

2.2.8 Tribological characterization: friction coefficient and wear rate

The tribological properties were evaluated by linear reciprocating friction tests using alumina-6-mm balls in diluted fetal bovine serum (FBS, 10% solution in water) in a CSM tribometer.

The assays were performed in triplicate and at least three times. The test parameters were set to 0.5 N of applied load; 3 mm/s of linear speed over a track length of 3 mm and 3000 cycles. The specific film wear rate was estimated after dividing the worn volume by the applied load and the sliding distance.

Scanning electron microscopy (SEM) and energy dispersive X-ray analysis (EDX) of the friction contact region were recorded in a FEG Hitachi S5200 microscopes operating at 5 keV. Raman spectra measurements (200–2000 cm^{-1}) were carried out in a LabRAM Horiba Jobin Yvon spectrometer equipped with a CCD (charge-coupled device) detector and a He–Ne laser (532 nm) at 5 mW.

Table 2.1 Chemical composition, deposition parameters, thickness and deposition rate of deposited coatings

Samples Ag/Ti	Chemical Composition (at. %)					[a] ΦN_2 (sccm)	[a] Φ C_2H_2 (sccm)	Current Density (mA cm^{-2})		Thickness (μm)	Deposition Rate (μm h^{-1})	Hardness, H (GPa)	Stress, σ (GPa)	Friction coefficient, μ	Wear rate, K (x 10^{-6} mm^3/Nm)
	Ti	C	N	O	Ag			Ti	Ti + Ag						
0	39	22	34	5	0	5	2	10	0	2.8	1.6	17.0	-0.5	0.29	7.1
0.05	33	27	31	7	2	6.4	6	10	1.3	2.0	1.6	17.8	-1.0	0.31	19
0.20	30	29	30	5	6	8.5	8	10	6	1.4	1.4	18.0	-1.7	0.26	5.2
0.37	27	20	38	5	10	4	1.7	5.2	3.7	1.8	1.1	15.0	-2.5	0.27	38
0.62	24	22	36	3	15	3	1.2	3.5	3	2.5	1.5	10.0	-1.6	0.28	48

[a] Gas flow

2.3 Results and discussion

2.3.1 Chemical analysis

The chemical composition, thickness and some experimental details of the coatings are summarized in table 2.1. Increasing the J_{Ti+Ag}/J_{Ti} current density ratio promoted an increase in Ag content from 0 to 15 at. %, while the Ti content decreased from 39 to 24 at. %. The C and N content decreases slightly, respectively, from 29 to 20 and 38 to 30 at. %. Oxygen contamination was in the range of 3–7 at. %. The film thicknesses ranged from 1.4 to 2.8 µm. With the increment of $J_{Ti+Ag} + J_{Ti}$, it would be expected an increase in the deposition rate (DR). However, it can be observed a poisoning effect in the samples with 6 (Ag/Ti = 0.20) and 10 (Ag/Ti = 0.37) at. % Ag content, this can be confirmed by the increment in the voltage in both targets during the depositions as shown in figure 2.1.

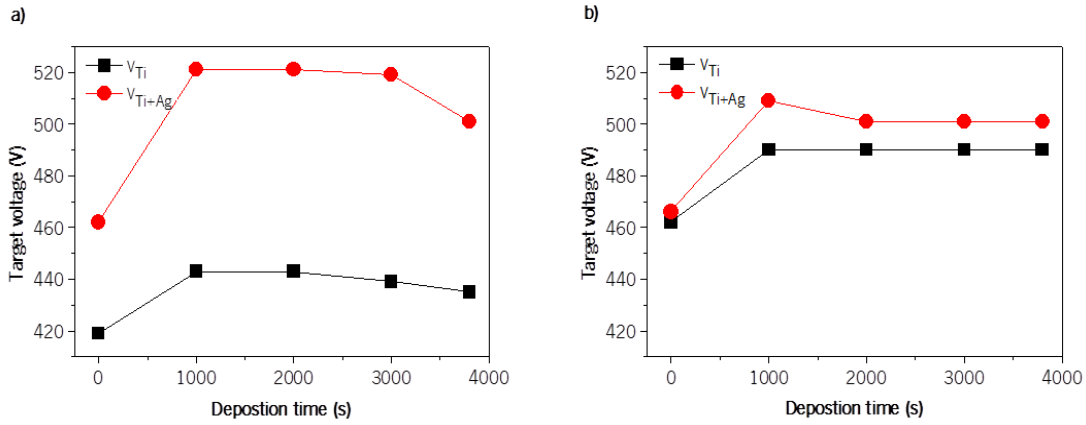

Figure 2.1 Evolution of the potential on the targets V_{Ti+Ag} and V_{Ti} as a function of the deposition time of the sample a) Ag/Ti = 0.20 and b) Ag/Ti = 0.37.

The targets voltage increase is due to the change of the target surface condition. In fact, due to the presence of reactive gases (N_2 +C_2H_2), both TiN and TiC layers should be formed at the Ti and Ti + Ag surfaces targets (a phenomenon called the poisoning effect). As the sputtering yield of both compounds is lower than that of Ti, a decrease in the deposition rate is consequently observed [15,16]. Also, it is possible to observe that the increment on the target voltage is higher for the Ti + Ag target than for the Ti target. Silver nitride is unstable, thus this effect cannot be explained from the formation of a silver nitride phase on the target surface. Depla *et al.* [17] justify the increment on the target voltage during sputtering of silver target in a nitrogen/argon plasma, by the presence on non-reacted N atoms in the target top

surface layers. Concerning the other depositions, no significant changes on the targets voltage values were observed during the deposition time.

2.3.2 Structural analysis

Figure 2.2 shows the XRD diffraction patterns for the deposited coatings with different Ag/Ti atomic ratios (0 to 0.62). The reference peaks, obtained from International Centre for Diffraction Data (ICDD) database, for $TiC_{0.3}N_{0.7}$ (ICDD card nr. 00-042-1488) and Ag (ICDD card n° 00-004-0783), are also included at the top of figure 2.2. The differences in the composition are well correlated with those observed in the structure evolution. In fact, the film without silver crystallizes in a B1-NaCl crystal structure typical for $TiC_{0.3}N_{0.7}$. The diffraction peaks at 2θ = 42.39° and 49.32° were assigned to the (111) and (200) planes of $TiC_{0.3}N_{0.7}$, respectively. Both peaks are shifted to lower angles as compared to the reference values, as a result of a lattice parameter slightly higher than the standard value (a = 4.26 Å). This result may be related to higher C/N atomic ratio in the film than in standard $TiC_{0.3}N_{0.7}$. Moreover, the shift of the XRD peaks towards lower angles may be due to the development of compressive residual stresses which are often associated with the deposition process. A similar behaviour is observed for the samples with low Ag/Ti atomic ratio (0.05, 0.20 and 0.37), although for these two last samples a new diffraction peak attributed to fcc-Ag (111) begins to appear close to 2θ = 44.35°.

The $TiC_{0.3}N_{0.7}$ diffraction peaks become broader with silver incorporation in the films, concurrently with the development of the characteristic pattern of metallic silver. The XRD pattern of the sample deposited with a 0.62 Ag/Ti atomic ratio displays two broad diffraction peaks. Deconvolution of the higher intensity band resulted in two peaks, at 42.44° and 44.19°, which were attributed to $TiC_{0.3}N_{0.7}$ (111) and Ag (111), respectively. Deconvolution of the diffraction band at higher 2θ angles (between 48° and 53°) also resulted in two peaks which were indexed to $TiC_{0.3}N_{0.7}$ (200) and Ag (200).

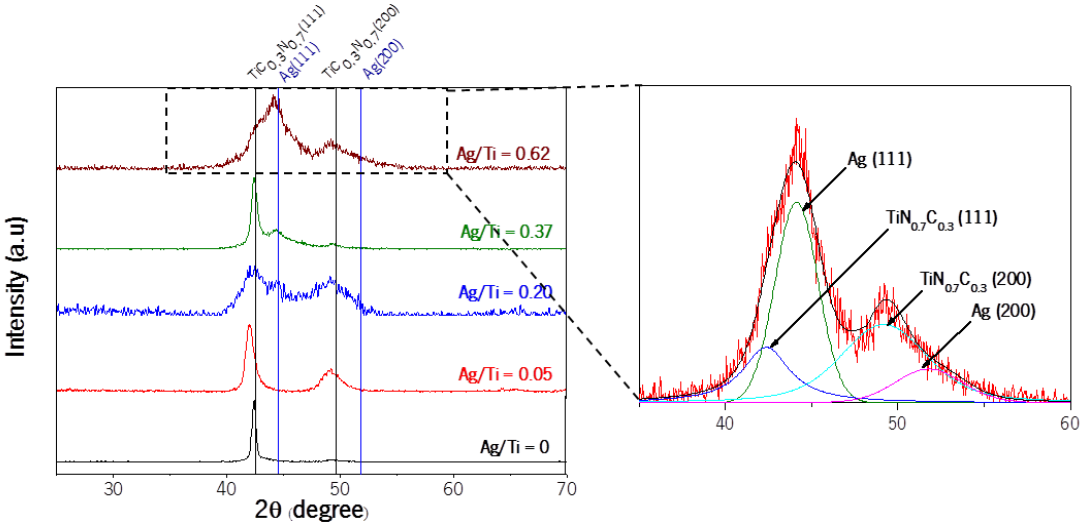

Figure 2.2 XRD patterns of the Ag-TiCN coatings deposited by DC reactive magnetron sputtering on silicon and in the right the deconvolution of peak Ag/Ti = 0.62.

The grain size of TiC_yN_{1-y} and Ag phases was determined by Scherrer formula using the (111) peak. The calculated values varied from 32 down to 5 nm and from 8.5 up to 29 nm with the increase of Ag content, for TiC_yN_{1-y} and Ag phases, respectively. This variation is concomitant with the increase of Ag content in the films which results in the predominance of the fcc-Ag phase while the degree of structural order of the TiC_yN_{1-y} phase decreases. The loss of crystallinity of the TiC_yN_{1-y} phase can be explained by two different mechanisms: (1) the growth interruption of the TiC_yN_{1-y} phase can be affected by the nucleation of Ag nanocrystals or (2) the increase of (C + N)/Ti atomic ratio as consequence of the silver incorporation which leads to the formation of an amorphous layer, a-(C, CN_x) as reported by several authors for TiCN films also deposited by sputtering [18–21]. The relation between the phase composition (CN_x, Ag and TiC_yN_{1-y}), determined from the elemental chemical composition and the Ag/Ti ratio, are shown in figure 2.3. The amorphous CN_x is increasing with the increment the of Ag crystalline phase while the TiC_yN_{1-y} phase decreases. This multiphase structure will certainly have an influence on the functional properties of the coatings (tribological, mechanical and biological) as it will be revised in the next sections.

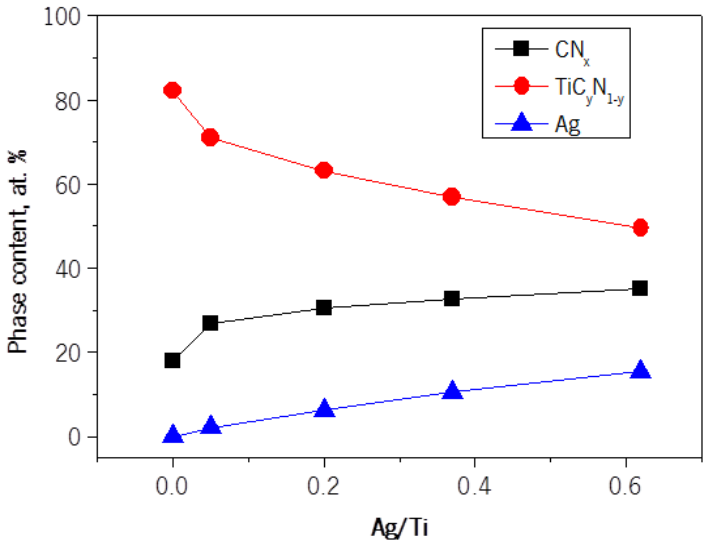

Figure 2.3 Phase composition of the samples prepared with Ag/Ti ratios of 0, 0.05, 0.20, 0.37 and 0.62, using silicon substrate.

Figure 2.4 shows the Raman spectra of deposited Ag-TiCN samples with different Ag/Ti ratio.

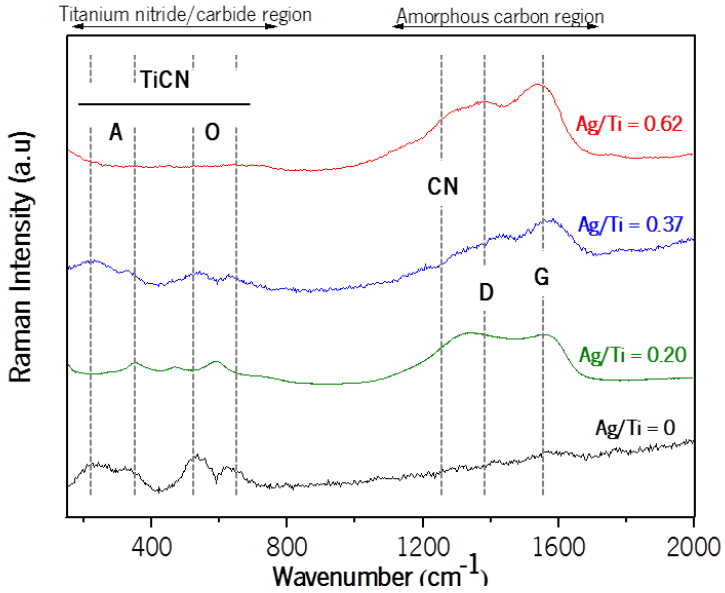

Figure 2.4 Raman spectra of the Ag-TiCN coatings deposited on silicon.

For the samples with 0, 0.20 and 0.37 Ag/Ti atomic ratio two weak and broad bands are detected in the ranges of 200 – 350 cm^{-1} and 500 – 700 cm^{-1}. These bands correspond to acoustic and optical vibrational modes of titanium nitride/carbide, respectively [12,22–24]. According to another study [19], the TiCN bonds should be located between TiN and TiC bands. These results agree well with the XRD patterns as crystalline TiCN was detected for

both samples. For the samples deposited with 0.20, 0.37 and 0.62 Ag/Ti atomic ratio two intense broad bands were detected between 1200 and 1700 cm^{-1}. These bands are assigned by several authors [25–27] to carbon based phases such as D and G bands of carbon materials at 1332 and 1580 cm^{-1}, respectively [26]. Also, C-N vibrational modes have been reported in this region [25]. These results agree well with the formation of an amorphous phase, a-(C, CN_x), already suggested by the analysis of the XRD patterns. The (C + N)/Ti atomic ratio is the highest in the sample deposited with the highest Ag contents, which also shows more intense Raman peaks in the 1200 to 1700 cm^{-1} range. The higher amount of amorphous phase in this coating is responsible for the significant loss of crystallinity of the TiC_yN_{1-y} phase detected by XRD.

2.3.3 Morphology and topography analysis

The morphology and topography of the coatings were studied by cross-sectional SEM micrographs of fractured samples (figure 2.5).

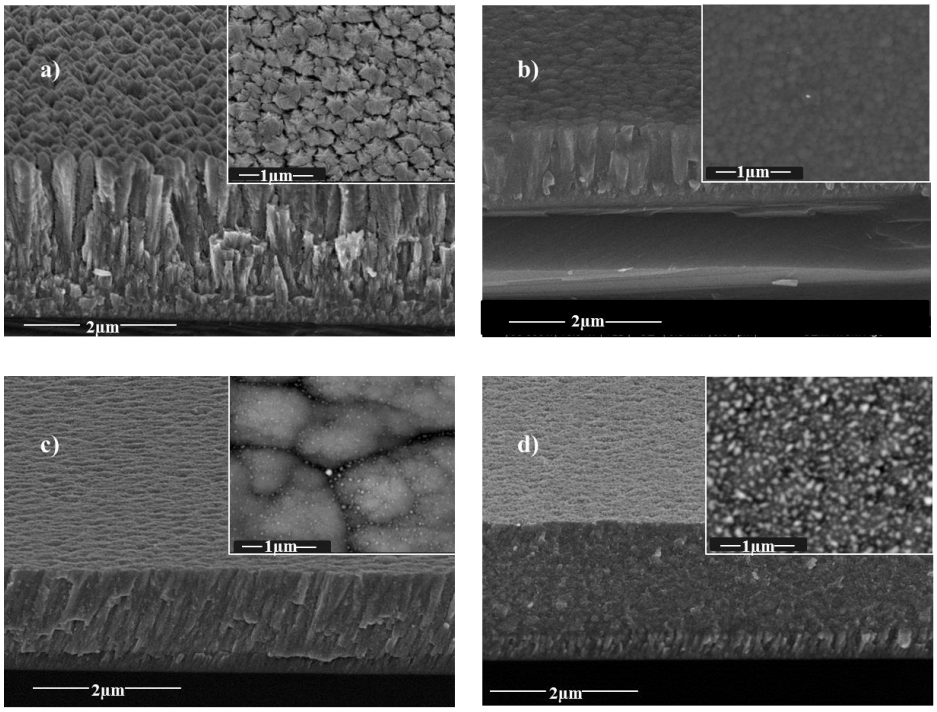

Figure 2.5 Cross-sectional SEM micrographs of coatings on silicon: a) Ag/Ti = 0, b) Ag/Ti = 0.20, c) Ag/Ti = 0.37 and d) Ag/Ti = 0.62. The insets show the SEM image from the sample surface on SS 316L where in a) the top of column TiCN is evident and in b), c) and d) BSE image where Ag clusters are visible only in Ag/Ti = 0.37 and Ag/Ti = 0.62.

The cross-section of the sample without silver (figure 2.5a) shows an open columnar-type structure that terminates in domes at the surface. This structure presents high porosity, as shown in the inset of figure 2.5a, in agreement with zone 1 of the Thornton model [28]. The low deposition temperature (373 K) as compared to the melting temperature of the deposited material, which must be between the melting temperature of TiN and TiC (3203 K and 3413 K, respectively [29,30]), and the low bombardment conditions used in this work resulted in reduced adatom mobility and subsequent formation of a porous structure [19]. The incorporation of Ag (Ag/Ti atomic ratio of 0.20 and 0.37) resulted in a denser film (figure 2.5b and (c) respectively) although the columnar structure is retained. The inset in the figure 2.5c, obtained in BSE mode, clearly shows the formation of Ag nanoclusters dispersed all over the film surface. Increasing the Ag content (Ag/Ti atomic ratio of 0.62) resulted in a further densification of the film and an increase of the number of Ag nanoclusters (figure 2.5d). Although the Ag nanoclusters are dispersed all over the film surface (inset in BSE mode), those formed in the porous zones of the film attained bigger sizes. The columnar growth observed in the other thin films is no longer detected, which agrees well with the loss of crystallinity of the TiC_yN_{1-y} phase and simultaneous formation of an amorphous phase as suggested by XRD and Raman results.

The surface topography of samples was analysed by atomic force microscopy (AFM) (figure 2.6) on silicon (figure 2.6a) and SS 316L substrates (figure 2.6b) in tapping mode.

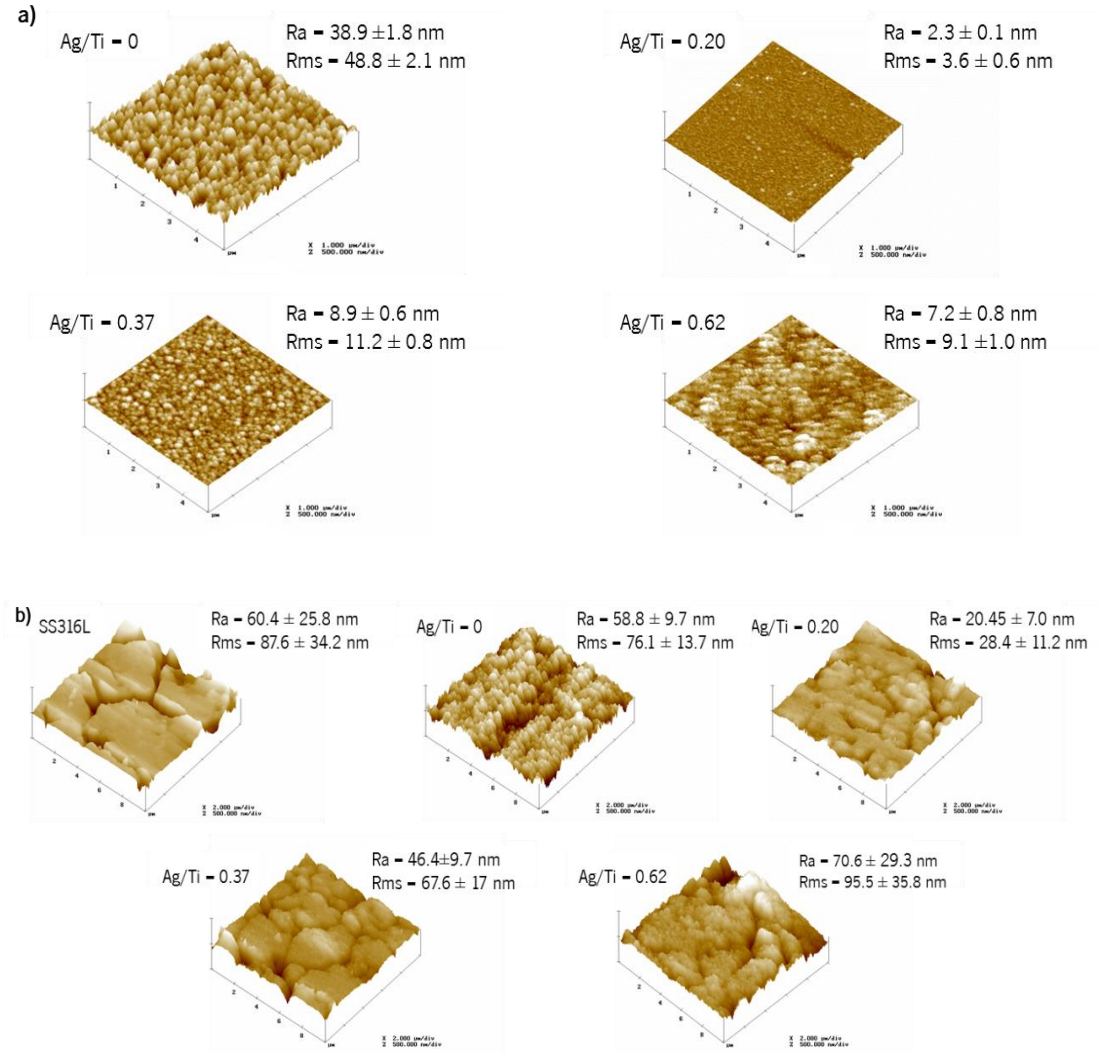

Figure 2.6 AFM images of coatings, a) on silicon with a scan range of 5 × 5 μm^2 and b) on SS 316L with a scan range of 10 × 10 μm^2. Ra is the arithmetic mean of surface roughness of every measurement within the total distance ½ roughness average and Rms is the root mean square roughness.

In order to assess the roughness of TiCN coatings with and without Ag, it is necessary to make the analysis on silicon to avoid the substrate effect, since the SS 316L morphological structure has a great porosity for presenting pronounced grain boundaries, and as TiCN films with and without Ag follows these grain boundaries, one cannot observe any trend in roughness terms. Additionally, the figure 2.6b shows that the standard deviations are very high. Thus, analyses are made to roughness of the surface substrate and not to thin film. Figure 2.6a shows that coatings deposited without Ag have a roughness considerably higher than coatings deposited with Ag. Furthermore through the AFM images in figure 2.6, it can be

seen that TiCN coatings without Ag seem rather less dense than with Ag, highlighting their columnar structure. All these results are in agreement with SEM observations.

2.3.4 Chemical bonding analysis

XPS analysis was carried out with the aim of obtaining further information on the chemical bonding. Figure 2.7 shows the (a) Ti2p, (b) C1s, (c) N1s and (d) Ag3d core level XPS spectra of the deposited Ag-TiCN films with Ag/Ti atomic ratio of 0, 0.20, 0.37 and 0.62.

Figure 2.7a shows the contribution of three doublets clearly identified in the Ti2p spectra in all samples. The first two doublets with Ti2p3/2 components centred at 458.5 eV and 456.6 eV, respectively, can be ascribed to TiO_2 and TiO_x bonds as derived from the analysis of reference samples [19]. The oxygen impurities are due to residual oxygen in the vacuum chamber, in the targets and also due to contamination after deposition by environmental components. For the sample without silver the third contribution is found to be at 455.1 eV (for the Ti2p3/2 component), that is in between the TiC (454.6 eV) and TiN (455.4 eV) bonds. This suggests the formation of a TiC_yN_{1-y} phase in good agreement with the XRD results previously shown. Similar behaviour is found for the sample with Ag/Ti = 0.20.

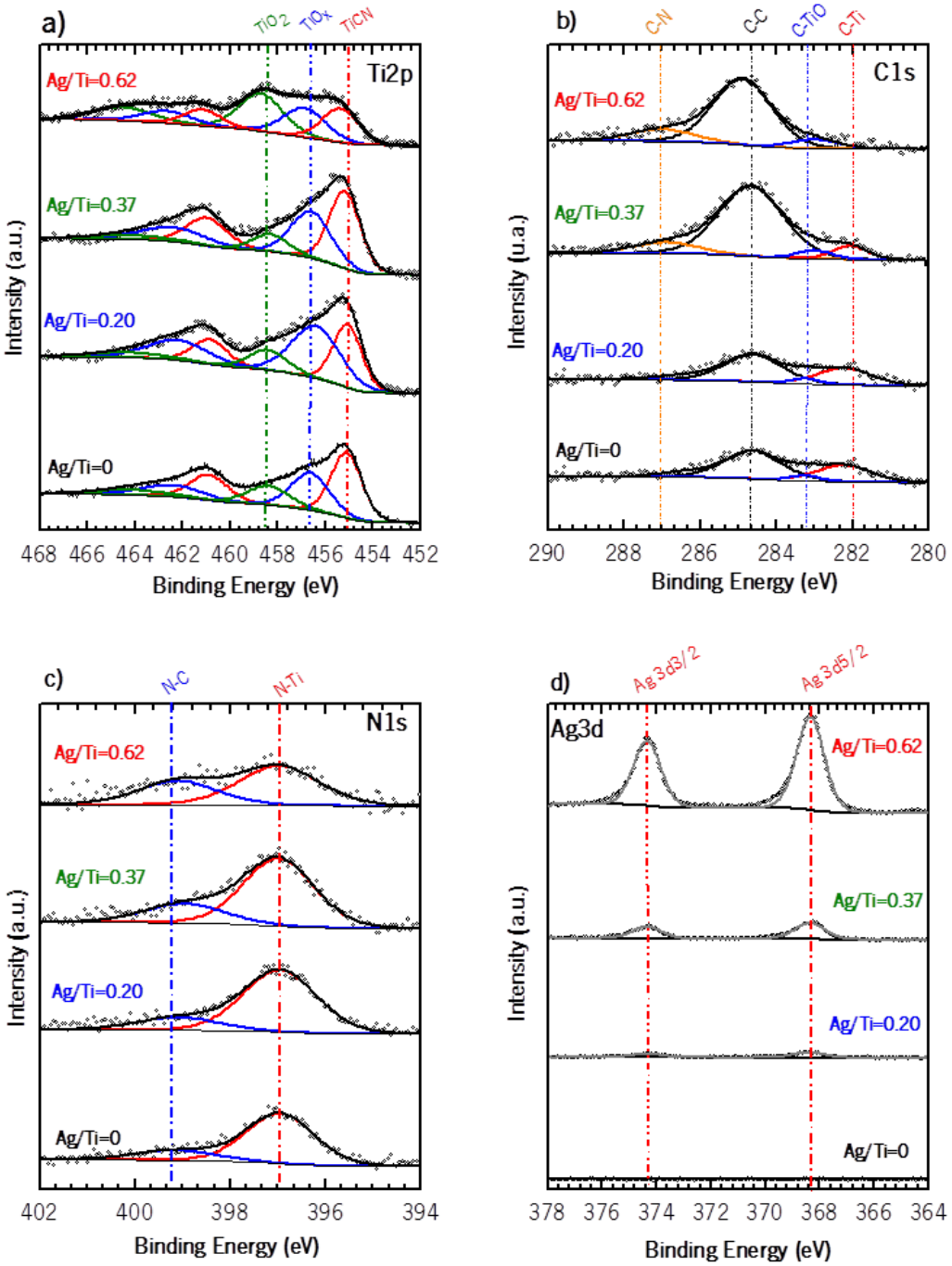

Figure 2.7 XPS spectra of (a) Ti2p, (b) C1s, (c) N1s and (d) Ag3d core levels of the Ag-TiCN coatings deposited by dc reactive magnetron sputtering with different Ag/Ti atomic ratios on silicon.

However, as the silver ratio increases there is a slight, but progressive, shift of this third doublet towards higher binding energies. In the sample with Ag/Ti = 0.37 the third doublet is centred at 455.2 eV while for Ag/Ti = 0.62 it is at 455.4 eV, namely the binding energy of

TiN. This shift is therefore ascribed to a continuous decrease of the titanium bonded to carbon. The Gibbs free energy for the formation of TiN phases is −290 kJ mol^{-1} and for TiC is −180 kJ mol^{-1} [31]. Therefore, with the decreasing of Ti content, there is a clear trend to the formation of the thermodynamically more stable nitride phases. In fact when analysing the C1s spectra in figure 2.7b, the intensity of component ascribed to the C–Ti bonds at 282 eV decreases with the increase in the Ag/Ti ratio. In particular, for the sample with Ag/Ti = 0.62 this contribution simply disappears. For samples with high Ag/Ti ratio there is an increase in the intensity of the component ascribed to C–N bonds (286.9 eV), which is supported by the presence of the contribution assigned to N–C bonds in the N1s spectra (figure 2.7c), reinforcing the idea of the formation of an amorphous C-phase incorporating N. In the N1s spectra of figure 2.7c, two contributions were found at 397.0 eV and 399.2 eV ascribed to N–Ti and N–C bonds, respectively [19]. The intensity of the N–C component becomes significant when the Ag/Ti increases (in agreement with the results for C1s spectra). Therefore, it can be pointed out that the presence of CN bonds is observed in samples with Ag/Ti atomic ratios of 0.37 and 0.62, and the appearance of these bonds is attributed to the decrease in Ti content in the coatings. The excess of C and N (high (C + N)/Ti) ratio, as it is possible to confirm by the composition results, promotes the formation of CN amorphous phases detected in both XPS and Raman spectroscopy analysis. Finally, from the analysis of Ag 3d photoelectron spectra (figure 2.7d) it was possible to confirm that the only contribution is the Ag–Ag metal bonds, which was somehow predictable due to the low solubility of C and N in silver.

2.3.5 Mechanical analysis

The hardness and internal stress values are presented in figure 2.8 as a function of the Ag/Ti ratio. The hardness varied in a range from 10 to 18 GPa, much lower than the typical values reported for pure TiCN coatings, ranging from 30 to 36 GPa [32–34]. These overall lower values should be certainly related with microstructural and chemical composition aspects. Thus, low energetic conditions of the deposition (low negative substrate bias and low deposition temperature) can lead to more opened columnar morphologies, as previously referred. The phase composition of these nanocomposites is also affecting the dependence of the mechanical properties as it influences the balance between hard and soft phases and their distribution. Thus, according to the achieved accuracy, increasing Ag content up to 6 at.

% (Ag/Ti = 0.20) does not affect the hardness; however, further increase is accompanied with a significant hardness decrease.

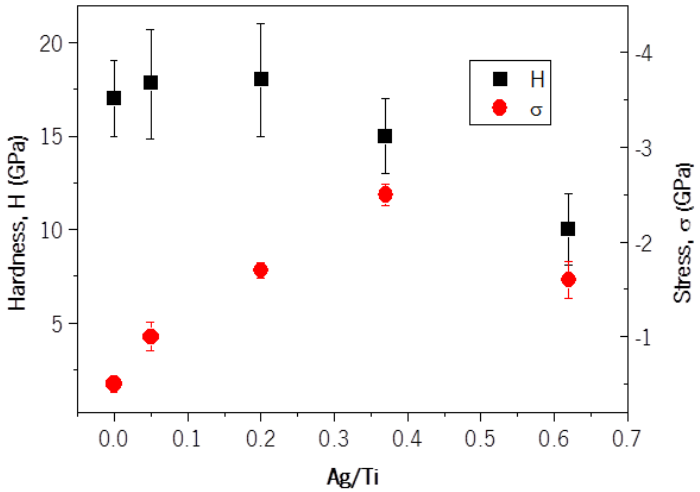

Figure 2.8 Hardness and residual stress values of Ag-TiCN coatings *vs.* the Ag/Ti atomic ratio.

A similar behaviour of soft metals has been reported in the past in other systems, such as ZrN/Cu [35], ZrN/Ni [36], or others including silver, Ag/TiN [3] and Ag/TiC [10]. However, it is also likely that ion-induced defects in the films during the deposition or more compact film microstructure would also contribute to a hardness enhancement. This would imply an increment of the compressive residual stress on the as-deposited coatings, as indeed was observed for Ag/Ti ratios lower than 0.20 (figure 2.8). Moreover, the decrease in the grain size, as a result of the interference of Ag deposition in the grain growth, promoting an increasing nucleation, can also contribute for the higher values of hardness. Further increasing of the Ag/Ti ratio leads to a noticeable hardness reduction, in spite of the maximum in the compressive residual stress, mainly attributed to the increasing presence of either a boundary of amorphous carbon-based phase (a-C and CN_x), or silver nanoparticles that soften the film structure as it was stated in previous studies [37,38]. In figure 2.9, the ratio of the soft phases (Ag + CN_x) with hard carbonitrides (TiC_yN_{1-y}) is calculated for establishing correlations with the tribomechanical properties. Thus, it is clearly illustrated the dependence of the hardness *vs.* this parameter. The wear rate is inversely proportional to the film hardness. Similar dependences have been reported in previous nanocomposites based on CrN/Ag; ZrN/Ag; TiN/Ag and TiN/Cu phases [39]. The excess of C and N segregates to the surface and interface during film growth, forming (C,N)-rich disordered region situated in

the vicinity of TiC_yN_{1-y} grains, causing an effective softening of the film. Moreover, the continuous increase on the Ag/Ti atomic ratio induces the nucleation of silver, a soft metal, which also contributes to further diminution of the hardness.

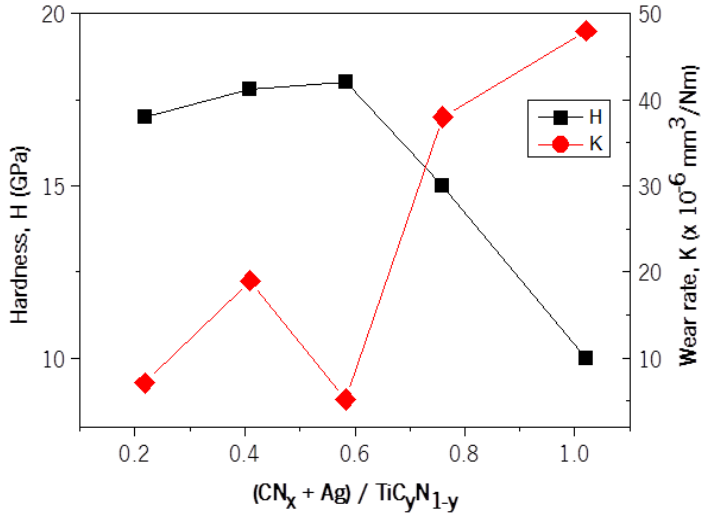

Figure 2.9 Variation of the hardness and wear rate properties as a function of the ratio of soft (Ag + CN_x)/hard (TiC_yN_{1-y}) phases.

2.3.7 Tribological analysis

The tribological properties (friction coefficient and wear rate) were studied in lubricated conditions using 10% FBS solution in order to simulate the tribochemical conditions appearing in an artificial implant. Both properties are shown in figure 2.10 as a function of the Ag/Ti atomic ratio.

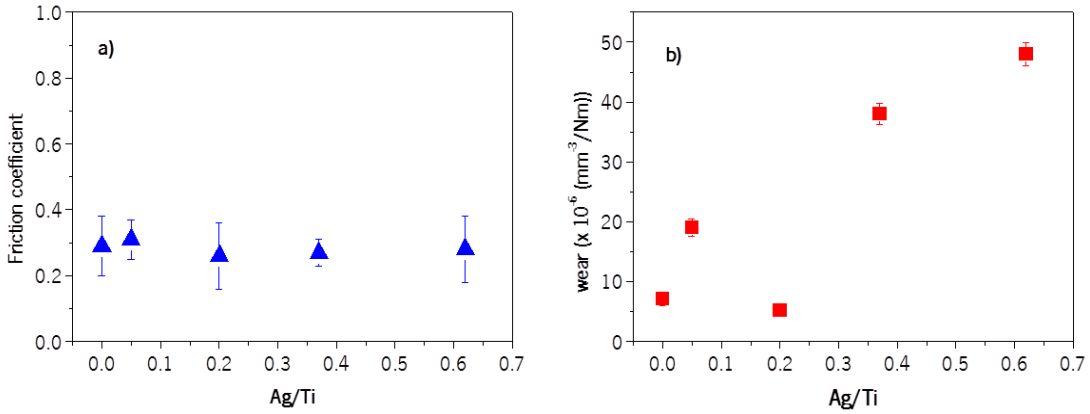

Figure 2.10 Friction coefficients (a) and wear rate (b) values of Ag-TiCN as a function of the Ag/Ti atomic ratio.

The measured friction coefficients were found to be very similar for all the samples (figure 2.10a). Conversely, more differences are noticed in the variation of the film wear rates as displayed in figure 2.10b. The best wear resistance is found for samples with the lowest Ag/Ti ratios (≤ 6 at. % Ag). These coatings show typical values in the range of 5–8 × 10^{-6} mm^3/N m, except for the sample with 0.05 Ag/Ti ratio which presents a value much higher (19 x 10^{-6}) and this is reflected in the friction coefficient also the highest. Further Ag/Ti ratios led to a continuous degradation of the wear resistance. In order to obtain more information about the processes in the sliding contact, the surface of a ball scar from a sample with 10 at. % Ag content was examined by SEM/EDX and Raman spectroscopy.

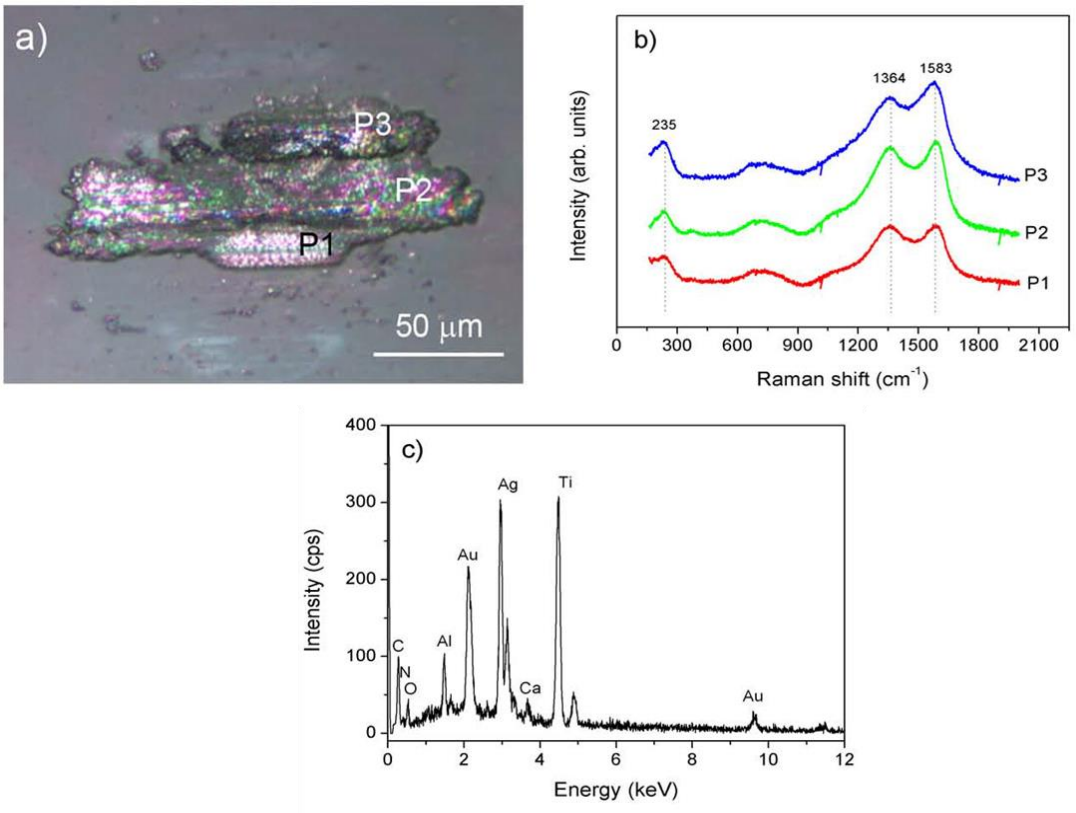

Figure 2.11 Optical micrograph of the alumina ball after the friction test onto the Ag-TiCN coating with 10 at. % of Ag (a) and corresponding Raman spectra (b) and EDX (c) analysis.

Figure 2.11a shows the appearance of the alumina ball after having been tested against the Ag/Ti = 0.37 film. Material from the film and the solution can be detected adhered to the ball. The Raman spectrum obtained from three different points of the transferred material, displayed as P1, P2 and P3 in figure 2.11b, is dominated by the presence of the D and G bands at 1364 and 1583 cm^{-1}, respectively, corresponding to the presence of aromatic six-

membered sp2 clusters and the sp2 C-C bonds. A small peak at 235 cm^{-1} is attributed to TiC_yN_{1-y}, as observed in previous papers of TiCN and TiAlCN coatings [22,40]. A chemical analysis was carried out by SEM/EDX after covering the ball by a thin Au layer in order to avoid the charge effects. The EDX spectrum (shown in figure 2.11c) revealed the presence of the elements forming the film (Ag, Ti, C, N) and Ca, probably from the FBS solution, besides Au and Al, from the cover layer and the alumina ball respectively.

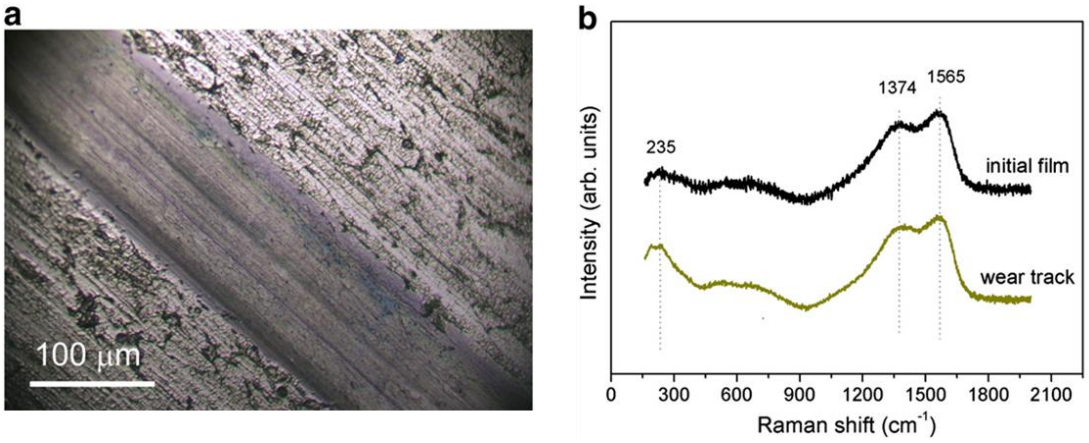

Figure 2.12 Optical micrograph of the wear track after the friction test of the Ag-TiCN coating with 10 at. % of Ag (a) and corresponding Raman spectra (b)

In figure 2.12 the Raman spectra taken from the wear track are depicted and compared with that obtained on the initial film. The spectra look very similar, showing both the D and G bands at 1364 and 1583 cm^{-1}, respectively, characteristic of a disordered carbon-based structure. The main differences are noticed if compared to the transfer film onto the ball (figure 2.11b), where the observed peaks are narrower and more separated, in agreement with the behaviour observed in DLC and other amorphous carbon-based materials after friction modification [41]. Therefore, it can be concluded that the friction process takes place between this adhered layer, mainly formed by graphitic-like carbon, and the modified surface layer in the FBS solution media. The almost constant value of the friction coefficient of ≈ 0.3 measured for the different Ag-TiCN coatings pointed to a similar nature of the counterfaces independently of the lubricant phase contents (Ag and CN_x). Lower friction coefficient values and higher-dependence with phase composition have been usually reported in silver-containing [42,43] and amorphous carbon-based phases [44,45] when tested in dry lubricant conditions. However, in the presence of a liquid media (FBS in this case), the self-lubricant

properties of these soft phases are less influencing [46]. Nevertheless, a beneficial effect in the topmost layers by the supply of self-lubricant silver and a-C phases should not be discarded. On the other hand, there are significant differences in terms of the wear resistance as a function of the Ag content that can be explained by the differences in the phase composition and the mechanical properties of the coating. As denoted in figure 2.9, the samples with higher contribution of hard TiC_yN_{1-y} phases, i.e. those with lower Ag content, are harder and thereby more resistant to the mechanical contact exhibiting lower wear rates.

2.4 Conclusions

Ag-TiCN thin films were deposited by reactive magnetron sputtering with variable silver content (0 to 15 at. %). The coatings were found to be a mixture of TiC_yN_{1-y}, Ag and a-C(N)$_x$ phases whose relative proportion varied depending on the Ag/Ti ratio. By means of XRD and XPS analyses it could be concluded that the proportion of soft phases becomes dominant and there was a substantial reduction in the grain size of TiC_yN_{1-y} for Ag/Ti ≥ 0.37, decreasing the hardness and the wear resistance. The friction coefficient was relatively constant (0.25–0.29) as it proceeds from sliding of a transferred material layer and the modified film surface in the FBS solution media. The best hardness and wear resistant coatings were obtained for low Ag contents (up to 6 at. % of Ag or Ag/Ti ≤ 0.20) with hardness of 18 GPa and specific wear rate values in the range of 10^{-6} mm^3/Nm. It can be concluded that incorporation of silver into protective carbon-based coatings for use in implant and medical devices must be limited up to 6 at. % in order to ensure a good balance between mechanical and tribological properties. However, it is necessary to certify the biological properties as cytotoxicity and antimicrobial effect of silver. In this sense, the next chapter will be worked on these properties.

References

[1] Daniels A U, Barnes F H, Charlebois S J and Smith R A 2000 Macrophage cytokine response to particles and lipopolysaccharide in vitro *J. Biomed. Mater. Res.* **49** 469–78

[2] Hauert R 2003 A review of modified DLC coatings for biological applications *Diam. Relat. Mater.* **12** 583–9

[3] Kelly P J, Li H, Whitehead K A, Verran J, Arnell R D and Iordanova I 2009 A study of the antimicrobial and tribological properties of TiN/Ag nanocomposite coatings *Surf. Coatings Technol.* **204** 1137–40

[4] Rauschenbach B, Mandl S and Mändl S 2002 Improving the biocompatibility of medical implants with plasma immersion ion implantation *Surf. Coatings Technol.* **156** 276–83

[5] Shtansky D V, Gloushankova N A, Sheveiko A N, Kharitonova M A, Moizhess T G, Levashov E A and Rossi F 2005 Design, characterization and testing of Ti-based multicomponent coatings for load-bearing medical applications *Biomaterials* **26** 2909–24

[6] Endrino J L, Anders A, Albella J M, Horton J A, Horton T H, Ayyalasomayajula P R and Allen M 2010 Antibacterial efficacy of advanced silver-amorphous carbon coatings deposited using the pulsed dual cathodic arc technique *J. Phys. Conf. Ser.* **252** 012012

[7] Kwok S C H, Zhang W, Wan G J, McKenzie D R, Bilek M M M and Chu P K 2007 Hemocompatibility and anti-bacterial properties of silver doped diamond-like carbon prepared by pulsed filtered cathodic vacuum arc deposition *Diam. Relat. Mater.* **16** 1353–60

[8] Morrison M L, Buchanan R A, Liaw P K, Berry C J, Brigmon R L, Riester L, Abernathy H, Jin C and Narayan R J 2006 Electrochemical and antimicrobial properties of diamondlike carbon-metal composite films *Diam. Relat. Mater.* **15** 138–46

[9] De los Arcos T, Oelhafen P, Aebi U, Hefti A, Düggelin M, Mathys D and Guggenheim R 2002 Preparation and characterization of TiN–Ag nanocomposite films *Vacuum* **67** 463–70

[10] Endrino J L, Nainaparampil J J and Krzanowski J E 2002 Microstructure and vacuum tribology of TiC–Ag composite coatings deposited by magnetron sputtering-pulsed laser deposition *Surf. Coatings Technol.* **157** 95–101

[11] Oliveira C, Gonçalves L, Almeida B G, Tavares C J, Carvalho S, Vaz F, Escobar Galindo R, Henriques M, Susano M and Oliveira R 2008 XRD and FTIR analysis of Ti–Si–C–ON coatings for biomedical applications *Surf. Coatings Technol.* **203** 490–4

[12] Oliveira C, Galindo R E, Palacio C, Vázquez L, Espinosa A, Almeida B G, Henriques M, V S C and Carvalho S 2010 Influence of the surface morphology and microstructure on the biological properties of Ti–Si–C–N–O coatings *Thin Solid Films* **518** 5694–9

[13] Antunes J and Cavaleiro A 2002 Ultra-microhardness testing procedure with Vickers indenter *Surf. Coatings Technol.* **149** 27–35

[14] Stoney G G 1909 The Tension of Metallic Films Deposited by Electrolysis *Proc. R. Soc. A Math. Phys. Eng. Sci.* **82** 172–5

[15] Berg S and Nyberg T 2005 Fundamental understanding and modeling of reactive sputtering processes *Thin Solid Films* **476** 215–30

[16] Depla D, Buyle G, Haemers J and De Gryse R 2006 Discharge voltage measurements during magnetron sputtering *Surf. Coatings Technol.* **200** 4329–38

[17] Depla D and De Gryse R 2003 Target voltage measurements during DC sputtering of silver in a nitrogen/argon plasma *Vacuum* **69** 529–36

[18] Silva E, Rebelo de Figueiredo M, Franz R, Escobar Galindo R, Palacio C, Espinosa A, Calderon V. S, Mitterer C, Carvalho S, Figueiredo M R De, Galindo R E and Calderon S V 2010 Structure – property relations in ZrCN coatings for tribological applications *Surf. Coat. Technol.* **205** 2134–41

[19] Manninen N K, Galindo R E, Benito N, Figueiredo N M, Cavaleiro A, Palacio C and Carvalho S 2011 Ag–Ti(C, N)-based coatings for biomedical applications: influence of silver content on the structural properties *J. Phys. D. Appl. Phys.* **44** 375501

[20] Lu Y H and Shen Y G 2011 Nanostructure evolution and properties of two-phase nc-Ti(C, N)/a-(C, CN x) nanocomposites by high-resolution transmission electron microscopy, x-ray photoelectron spectroscopy, and Raman spectroscopy *J. Mater. Res.* **22** 2460–9

[21] Martínez-Martínez D, Sánchez-López J C, Rojas T C, Fernández A, Eaton P and Belin M 2005 Structural and microtribological studies of Ti–C–N based nanocomposite coatings prepared by reactive sputtering *Thin Solid Films* **472** 64–70

[22] Constable C, Yarwood J and Münz W 1999 Raman microscopic studies of PVD hard coatings *Surf. Coatings Technol.* **119** 155–9

[23] Dreiling I, Haug A, Holzschuh H and Chassé T 2009 Raman spectroscopy as a tool to study cubic Ti–C–N CVD coatings *Surf. Coatings Technol.* **204** 1008–12

[24] Spengler W, Kaiser R, Christensen A and Müller-Vogt G 1978 Raman scattering, superconductivity, and phonon density of states of stoichiometric and nonstoichiometric TiN *Phys. Rev. B* **17** 1095–101

[25] Ferrari A C, Rodil S E and Robertson J 2003 Resonant Raman spectra of amorphous carbon nitrides: the G peak dispersion *Diam. Relat. Mater.* **12** 905–10

[26] Robertson J 2002 Diamond-like amorphous carbon *Mater. Sci. Eng. R Reports* **37** 129–281

[27] Escobar-Alarcon L, Medina V, Camps E, Romero S, Fernandez M and Solis-Casados D 2011 Microstructural characterization of Ti–C–N thin films prepared by reactive crossed beam pulsed laser deposition *Appl. Surf. Sci.* **257** 9033–7

[28] Thornton J A 1977 High rate thick film growth *Annu. Rev. Mater. Sci.* **7** 239–60

[29] Zhang S 1993 Titanium carbonitride-based cermets: processes and properties *Mater. Sci. Eng. A* **163** 141–8

[30] Simon J G and Langer E L 1994 *ASM Handbook Volume 5: Surface Engineering* (ASM International)

[31] Jung I and Kang S 2000 A study of the characteristics of Ti (CN) solid solutions *J. Mater. Sci.* **35** 87–90

[32] Bull S 2003 Properties and performance of commercial TiCN coatings. Part 1: coating architecture and hardness modelling *Surf. Coatings Technol.* **163** 499–506

[33] Serro A P, Completo C, Colaço R, dos Santos F, da Silva C L, Cabral J M S, Araújo H, Pires E and Saramago B 2009 A comparative study of titanium nitrides, TiN, TiNbN and TiCN, as coatings for biomedical applications *Surf. Coatings Technol.* **203** 3701–7

[34] Bienk E, Reitz H and Mikkelsen N 1995 Wear and friction properties of hard PVD coatings *Surf. Coatings Technol.* **77** 475–80

[35] Musil J 2000 Hard and superhard nanocomposite coatings *Surf. Coatings Technol.* **125** 322–30

[36] Šůna J, Musil J, Ondok V and Han J G 2006 Enhanced hardness in sputtered Zr–Ni–N films *Surf. Coatings Technol.* **200** 6293–7

[37] Martínez-Martínez D, López-Cartes C, Justo A, Fernández A and Sánchez-López J C 2009 Self-lubricating Ti–C–N nanocomposite coatings prepared by double magnetron sputtering *Solid State Sci.* **11** 660–70

[38] Silva E, Rebelo de Figueiredo M, Franz R, Escobar Galindo R, Palacio C, Espinosa A, Calderon V. S, Mitterer C and Carvalho S 2010 Structure–property relations in ZrCN coatings for tribological applications *Surf. Coatings Technol.* **205** 2134–41

[39] Kelly P J, Li H, Benson P S, Whitehead K A, Verran J, Arnell R D and Iordanova I 2010 Comparison of the tribological and antimicrobial properties of CrN/Ag, ZrN/Ag, TiN/Ag, and TiN/Cu nanocomposite coatings *Surf. Coatings Technol.* **205** 1606–10

[40] Lackner J M, Waldhauser W and Ebner R 2004 Large-area high-rate pulsed laser deposition of smooth TiCxN1−x coatings at room temperature—mechanical and tribological properties *Surf. Coatings Technol.* **188-189** 519–24

[41] Donnet C and Erdemir A 2008 *Tribology of diamond-like carbon films: fundamentals and applications* ed C Donnet and A Erdemir (Springer)

[42] Holmberg K, Ronkainen H and Matthews A 2000 Tribology of thin coatings *Ceram. Int.* **26** 787–95

[43] Kelly P J, Li H, Whitehead K A, Verran J, Arnell R D and Iordanova I 2009 A study of the antimicrobial and tribological properties of TiN/Ag nanocomposite coatings *Surf. Coatings Technol.* **204** 1137–40

[44] Martínez-Martínez D, López-Cartes C, Fernández A and Sánchez-López J C 2008 Comparative performance of nanocomposite coatings of TiC or TiN dispersed in a-C matrixes *Surf. Coatings Technol.* **203** 756–60

[45] Sánchez-López J C, Martínez-Martínez D, Abad M D and Fernández A 2009 Metal carbide/amorphous C-based nanocomposite coatings for tribological applications *Surf. Coatings Technol.* **204** 947–54

[46] Endrino J L, Sánchez-López J C, Galindo R E, Horwat D and Anders A 2010 Beneficial silver: antibacterial nanocomposite Ag-DLC coating to reduce osteolysis of orthopaedic implants *J. Phys. Conf. Ser.* **252** 012005

Chapter III – Biological characterization

The work presented in this chapter was based on the published paper:

Carvalho, Isabel; Henriques, M.; Oliveira, J.C.; Alves, C.F.A.; Piedade, A.P.; Carvalho, S.

Science and Technology of Advanced Materials, 14(3), 1-10, 2013

Chapter III – Biological characterization

3.1 Introduction

Nowadays, the use of biomaterials is becoming increasingly common, for total or partial replacement of human's organs and tissues. A mandatory requirement is that these materials must be biocompatible, having no toxic effect when interacting with the living organisms.

Nevertheless, these materials are susceptible to microbial colonization. Adhesion of bacteria to human tissue and implanted biomaterial surfaces is an important step in the infection process [1]. Bacteria have the ability to adhere to biomaterials surface and develop biofilms, responsible for infection in these devices. Stainless steel 316L (SS 316L), cobalt–chromium alloys and titanium and its alloys are the most commonly biomaterials used in the development of medical devices [2,3]. They are used in orthopaedics in implant surgery since they present good mechanical properties and, in the case of stainless steel, also low cost [2–4]. However, SS 316L is a material susceptible to corrosion when in prolonged contact with body fluids [4,5]. To overcome this problem, the surface modification of SS 316L with TiCN coatings, to improve and control the corrosion resistance and biocompatible properties, is a promising process. Titanium carbonitride (TiCN) presents good mechanical and tribological properties [6], in which wear and fatigue behaviours were extensively studied [6–8]. In the literature, it is also reported the good corrosion resistance of TiCN [4] and its non-cytotoxic character [9], resulting in an interesting material for biomedical applications. Nevertheless, this material does not present any antimicrobial effect and the infection caused by microorganisms is one of the causes of failure of these devices. Hence, surface modification by coatings doped with silver is one the most used approaches to control the bacterial adhesion and colonization. As silver demonstrates high antimicrobial activity and a relatively low cytotoxicity has been the most used metal [10–18].

The mechanism of action of silver on microbes is still not clear, but it is suggested that silver ions act by strongly binding to critical biological molecules (proteins, DNA, RNA) and disrupting their functions [19–23].

So, the aim of the present work is to assess the Ag-TiCN coatings biocompatibility, their antibacterial activity and the surface properties ruling adhesion of *S. epidermidis* to these coatings.

3.2 Materials and methods

3.2.1 Coatings preparation

Ag-TiCN coatings produced under the conditions indicated in chapter II, were sterilized at 121 °C for 15 min in autoclave for further biological tests.

3.2.2 Cytotoxicity assays

Cytotoxicity tests were performed using fibroblasts 3T3 (CCL-163) obtained from American Type Cell Collection. Coated coupons were inserted in six well plates and 3 mL of Dulbecco modified eagle medium DMEM (Gibco) were added to each well. The plates with the materials were then incubated with 5 % CO_2 at 37 °C for 7 days. Meanwhile, the cells were grown in DMEM containing 10 % of fetal bovine serum (FBS-Gibco) and 1 % penicillin streptomycin (PS, Gibco). The cells were allowed to grow until attaining 80 % confluence and, after detachment, 500 μL of cell suspension with 1×10^5 cells/mL were added to each well of a 24 wells' plate. In parallel, materials were placed in contact with cell medium for 7 days and 500 μL were removed from each well and added to the plates with cells. The plates were incubated with 5 % CO_2 at 37 °C for 48 h. After that time, all the medium was removed and a solution containing 100 μL of MTS (3-(4,5-dimethylthiazol-2-yl)-5-(3-carboxymethoxyphenyl)-2-(4-sulfophenyl)-2H-tetrazolium) inner salt (Promega CellTiter 96® AQueous Non-Radioactive Cell Proliferation Assay) and 1 mL of DMEM without phenol red was added to each well, in the dark. After 1 h, the absorbance of the resulting solution was read at 490 nm. The percentage of fibroblasts death was determined by the ratio of the difference between cell growth in the absence of Ag-TiCN sample (control – 100 %) and the growth in the presence of a sample over the control growth (equation 3.1). The assays were performed in triplicate and at least in three independent tests.

$$\%\ \text{inhibition} = \frac{(\text{control - sample})}{\text{control}} \times 100 \qquad (3.1)$$

3.2.3 Antibacterial assays

Bacterial colonization assays were performed using two clinical strains of *S. epidermidis*, IE186 and 1457, belonging to the CEB Biofilm group collection. The strains were stored at -80 °C in glycerol stocks. Cells were firstly grown for approximately 36 hours in plates of Tryptic Soy Agar (TSA, Merck), and then incubated for 18 hours in Tryptic Soy Broth (TSB,

Merck), at 37 °C under a constant agitation of 120 rpm. After this period, cells were centrifuged for 5 minutes, at 8900× g and 4 °C, and washed twice with a phosphate buffer saline (PBS 1×). The cellular suspension was adjusted to a final concentration of approximately 1 × 10^8 cells/mL, determined by optical density at 640 nm, prior to usage in the adhesion and biofilm formation assays. Coated coupons (Ag/Ti atomic ratios of 0, 0.37 and 0.62) were inserted in six well plates and 3 mL of cellular suspension were added to each well. The plates with the materials were then incubated at 37 °C under a constant agitation of 120 rpm for 2 and 24 h.

After incubation the cellular suspension was removed from each well and the coatings were gently washed with PBS to remove non-attached bacteria. Thereafter the adherent bacteria were detached from the coatings using an ultrasonic bath for 10 min. The bacteria were plated in serial dilutions on TSB agar plates at 37 °C for 24 h, and then the number of CFUs (colonies forming units) was counted. All experiments were done in triplicate and repeated at least in two independent assays.

Scanning electron microscopy was used to observe the bacteria adhesion and biofilm formation on the surface of the coatings. After adhesion and biofilm formation the coatings were carefully washed three times with distilled water. Samples were dehydrated by an immersion in increasing ethanol concentration solutions: 70, 95 and 100 % (v/v) for 10, 10 and 20 minutes, respectively, and placed in a sealed desiccator. Afterwards, the samples were mounted on aluminium bases with carbon tape, sputter-coated with gold and observed with a Leica S360 scanning electron microscope. In order to assess the extent of bacterial adhesion and biofilm formation in each sample, three fields were used for image analysis. All photographs were taken using a magnification of 1000×.

3.2.4 Surface hydrophobicity characterization

Hydrophobicity parameters of surfaces were determined through the sessile drop contact angle technique, using an automated contact angle measurement apparatus (OCA 15 Plus; Dataphysics, Germany). Cleaned and dried surfaces were used for determining the hydrophobicity parameters of Ag-TiCN coatings. All measurements were performed at room temperature and water, formamide and α-bromonaphtalene, with known surface energy

components [24,25], were used as reference liquids. Contact angle measurements allowed the calculation of substrata hydrophobicity parameters, using the van Oss approach [26].

3.2.5 Topography characterization

Ag-TiCN coatings topography was achieved by AFM under the conditions displayed in chapter II.

3.2.6 Statistical analysis

Results from biological assays were compared using one-way analysis of variance (ANOVA) by applying the Bonferroni multiple comparisons test, using the software Statistical Package for the Social Sciences Inc., (SPSS). All tests were performed with a confidence level of 95 %.

3.3 Results and discussion

3.3.1 Cytotoxicity

In order to verify the applicability of the coated samples as biomaterials, their cytotoxicity was assessed in fibroblast cells. The cytotoxicity of the coatings was analysed using the MTS assay which gives the indication of materials' toxicity on cells in a precise, fast and reliable way [27]. The cellular inhibition as a function of the Ag/Ti atomic ratio is shown in Fig. 3.1.

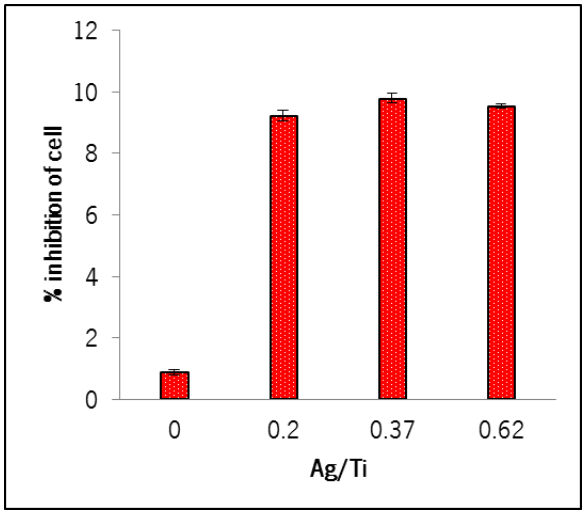

Figure 3.1 Rate of inhibition of fibroblast cell growth as a function of the Ag/Ti atomic ratio.

All samples present an inhibition below 10 % independently of the silver concentration. Several recent studies have already highlighted the toxicity of silver nanoparticles to various

cultured cells [28,29]. However, in the present study, all samples show a mortality rate inferior to 10 %, which is in accordance with ISO standard 10993-5:2009 [30] that only considers cytotoxic effect when the reduction in cell viability is higher than 30% and so, samples with different Ag content were used for the evaluation of their antibacterial properties.

3.3.2 Antibacterial activity

In order to assess the number of viable cells, the cellular concentration was determined by CFU (figure 3.2) in terms of logarithm of bacterial concentration (CFU/mL) for each *S. epidermidis* strain (IE186, figure 3.2a and 1457, figure 3.2b).

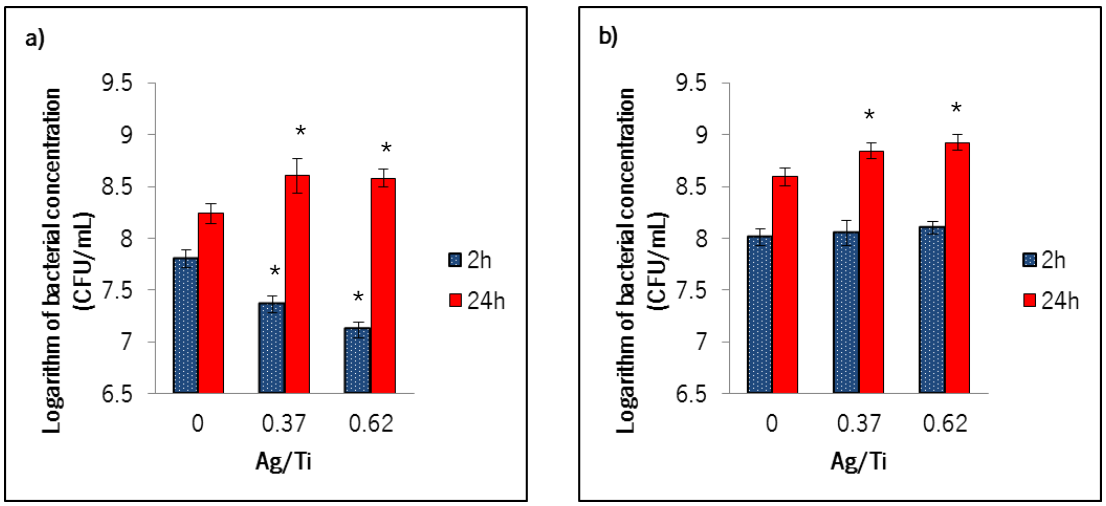

Figure 3.2 Logarithm of bacterial concentration after 2 h and 24 h contact between Ag-TiCN coatings (with different ratios) and *S. epidermidis* strains: IE186 (a) and 1457 (b). (*) indicates that the samples are statistically different from the control (Ag/Ti =0).

The selection of these two strains was based on their propensity to form biofilms in previous studies [31,32]. According to the study of Sousa *et al.* [31], *S. epidermidis* 1457 produces a larger amount of extracellular polymeric substances (EPS) than *S. epidermidis* IE 186. These substances are components of the biofilm matrix and consist mainly of polysaccharides and proteins [33]. The extracellular matrix is very important for intercellular binding during surface colonization [34] and protection against the host immune system and resistance to antibiotics [1], as referred previously in chapter I. Figure 3.2a shows that the addition of silver to TiCN coatings promotes a statistically significant decrease ($P < 0.05$) in the bacterial adhesion.

Nevertheless, this decrease does not represent antibacterial activity since the difference in the logarithmic value of viable cell counts between TiCN coatings with and without silver incorporation is not higher than 2.0. According to Japanese Industrial Standard Z 2801: 2000 [35], if the difference in the logarithmic value of viable cells counts between antimicrobial products and untreated products is less than 2.0, the antimicrobial activity should not be considered. Regarding *S. epidermidis* 1457, it is possible to observe (figure 3.2b) that with increasing silver concentration the increase in the bacteria adhesion (2 h) is not statistically significant ($P > 0.05$). The results of the biofilm formation (24 h) for both strains show that the addition of silver in the coatings promotes a statistically significant increase ($P < 0.05$) in bacterial concentration. This fact was not expected since silver is known for its antibacterial effect [19–21,36,37].

SEM images, presented in figures 3.3 and 3.4, confirm that silver does not prevent adhesion and that biofilm formed by *S. epidermidis* 1457 is greater than *S. epidermidis* IE 186 strains.

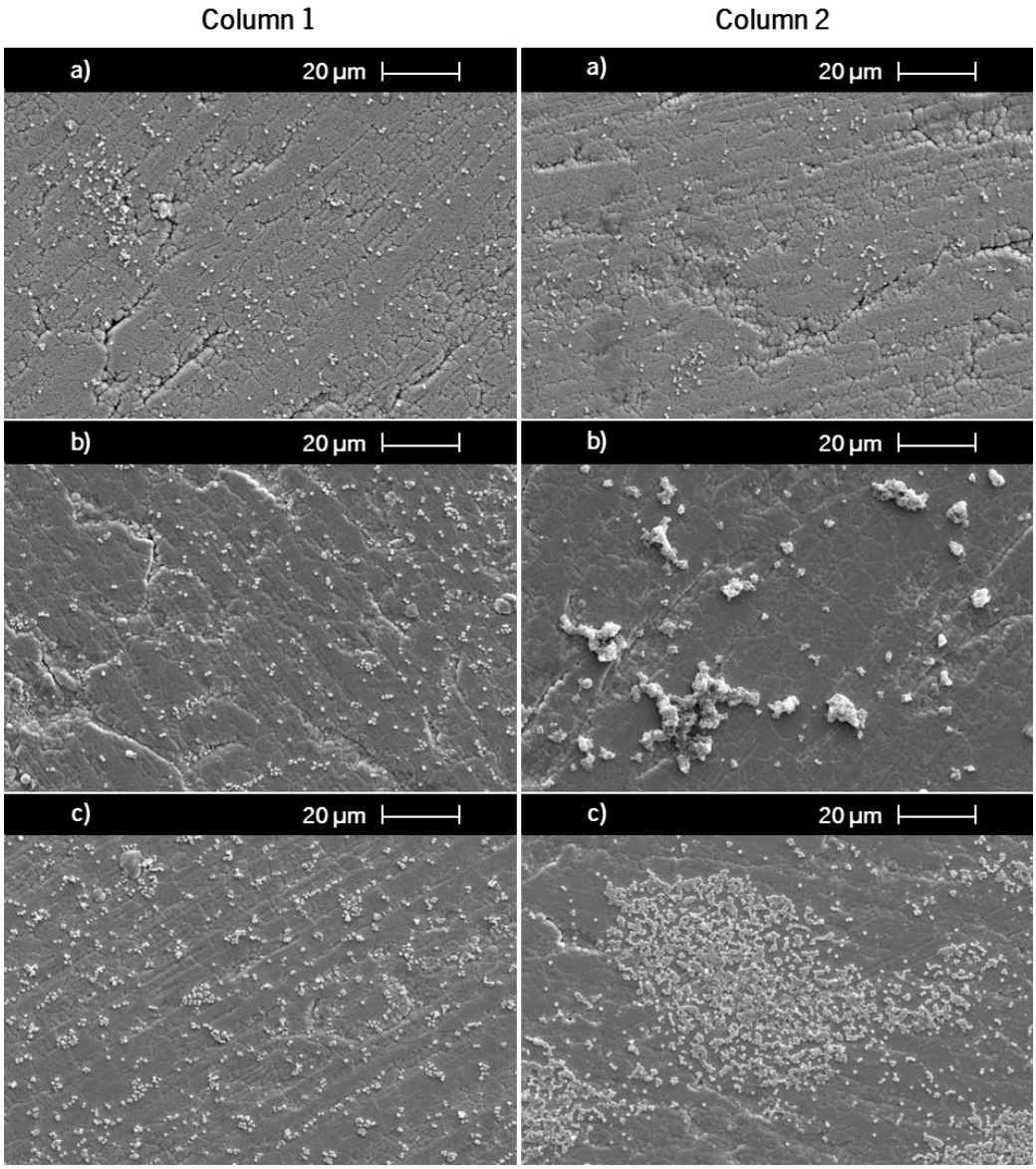

Figure 3.3 SEM micrographs of *S. epidermidis* IE186 adhered to Ag-TiCN coatings after 2 h (column 1) and 24 h (column 2) period of contact: adhesion and biofilm formation to Ag/Ti = 0 (a); to Ag/Ti = 0.37 (b); to Ag/Ti = 0.62 (c).

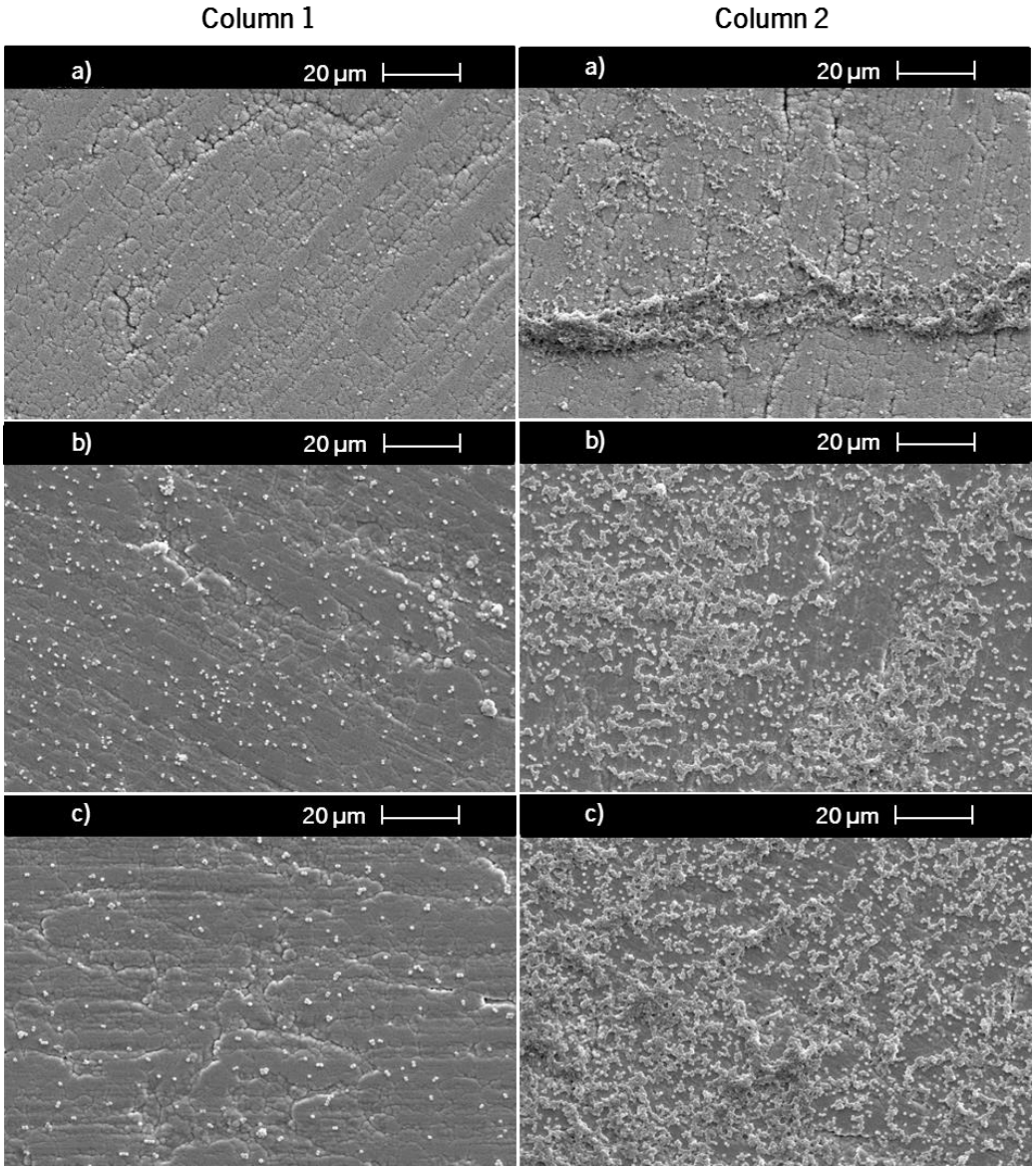

Figure 3.4 SEM micrographs of *S. epidermidis* 1457 adhered to Ag-TiCN coatings after 2 h (column 1) and 24 h (column 2) period of contact: adhesion and biofilm formation to Ag/Ti = 0 (a); to Ag/Ti = 0.37 (b); to Ag/Ti = 0.62 (c).

The results presented may be due to the amount of ionic silver released from the surfaces which may be insufficient or even non-existent. In fact, SEM images reveal that silver coatings seem to favour adhesion and biofilm formation. So, this absence of antibacterial activity can be explained by coatings' morphology and/or by their hydrophobicity characteristics. Therefore these parameters were also evaluated.

The introduction of silver causes the formation of a second crystalline phase (fcc-Ag), which usually tends to develop in the grain boundaries as shown in chapter II, increasing the contact opportunities between bacteria and surface coatings (figure 3.5a), as the non-silver coatings have a columnar structure with a width of approximately 300 nm (L = 283.20 nm) (figure 3.5b) and as these bacteria have a diameter of around 1 μm, the contact opportunities between bacteria and these surfaces are lower than to the surfaces with silver.

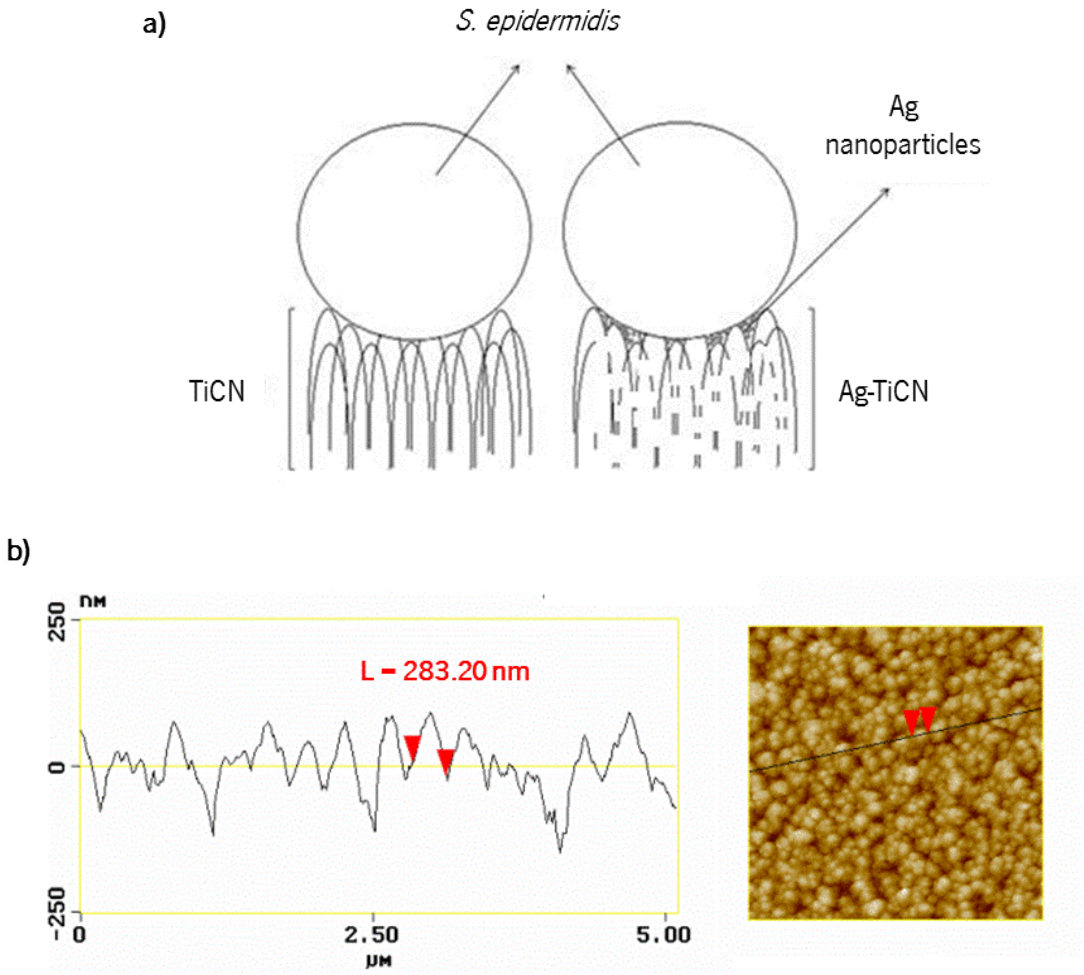

Figure 3.5 Schematic representation of bacterial adhesion (not to scale) (a). AFM section profile of Ag-TiCN coating with zero Ag/Ti atomic ratio (b).

Indeed, in chapter II, the analysis of Ag 3d photoelectron spectra showed that the only contribution was of Ag–Ag metal bonds. As silver produces no antibacterial effect, leads one to believe that its ionization does not happen or occurs at very low concentrations which do not cause the death of the bacteria.

3.3.3 Surface hydrophobicity analysis

Hydrophobicity of Ag-TiCN coatings surface was evaluated through contact angle measurements, using the van Oss approach [26]. According to that author, the hydrophobicity of a given material is defined in terms of the variation of the free energy (ΔG) of interaction between material's surface (s) immersed in water (w), ΔG_{sws}. When ΔG_{sws} is negative, the free energy of interaction between molecules is attractive revealing a greater interaction with each other than with water, making the material surface hydrophobic. In opposition, a surface is hydrophilic when ΔG_{sws} is positive. Contact angles, surface energy parameters and the degree of hydrophobicity of coatings are presented in table 3.1.

Table 3.1 Water (θ_w), formamide (θ_F), and α-bromonaphtalene ($\theta_{\alpha B}$) contact angles, surface energy components (apolar Lifshitz-van der Waals surface free energy component, γ^{LW}, electron acceptor surface free energy component, γ^+, and electron donor surface free energy component, γ^-), and degree of hydrophobicity (ΔG_{sws}) of the Ag-TiCN coatings surface

Samples Ag/Ti	Contact angle ± [a]SD (°)			Surface energy components (mJ/m²)			ΔG_{sws} (mJ/m²)
	θ_W	θ_F	$\theta_{\alpha B}$	γ^{LW}	γ^+	γ^-	
0	112.6±2.9	60.7±2.6	74.1±2.7	18.0	9.0	0.0	-41.7
0.37	99.3±2.4	78.5±2.0	65.1±1.4	22.4	0.2	1.3	-70.6
0.62	114.6±2.0	102.0±1.7	91.5±4.5	10.5	0.0	1.1	-82.3

[a] standard deviation

The water contact angles obtained for the coatings surfaces are higher than 90°, suggesting a hydrophobic character [38,39], also, confirmed by the negative values of ΔG_{sws}. The coatings without Ag present a monopolar surface (γ^+ = 9 mJ/m² and γ^-= 0 mJ/m²) and the coatings with Ag present a surface slightly polar, both surface energy component values (γ^+ and γ^-) are quite close to zero, and this fact may highlight the surfaces' high densities of apolar areas which may promote the adhesion of microorganisms to those coatings with Ag [40]. The hydrophobic character of these coatings may be due to the incorporation of silver preferably in

grain boundaries lessening the roughness of coatings which makes them more homogeneous topographically.

3.4 Conclusions

All Ag/Ti atomic ratios have shown to be biocompatible. However, these coatings do not present any antibacterial effect. These results may be due to the absence of silver ionization or in very low concentrations, and consequently being insufficient to cause the bacteria death. Additionally, silver phases and a-(C, CN_x) tends to segregate in the grain boundaries of $TiC_{0.3}N_{0.7}$ causing a reduction in the grain size and a densification of the coatings as concluded in chapter II, resulting in a higher number of contact zones between the bacteria and the film surface. The increase of silver in coatings leads to less rough and more hydrophobic surfaces. The hydrophobic behaviour of the coatings promotes a favourable bacterial adhesion. Ag-TiCN coatings with Ag/Ti atomic ratios of 0.37 and 0.62 possess sites with high densities of apolar areas that can justify the bacterial adhesion to the surface via hydrophobic effect. So, as the results point to an increase of bacterial adhesion to coatings with silver, it is important to better understand how the surfaces properties rule bacterial adhesion.

References

[1] An Y H and Friedman R J 1998 Concise review of mechanisms of bacterial adhesion to biomaterial surfaces *J. Biomed. Mater. Res.* **43** 338–48

[2] Batory D, Reczulska M C –, Kolodziejczyk L and Szymanski W 2013 Gradient titanium and silver based carbon coatings deposited on AISI316L *Appl. Surf. Sci.* **275** 303–10

[3] Kannan S, Balamurugan A and Rajeswari S 2003 Hydroxyapatite coatings on sulfuric acid treated type 316L SS and its electrochemical behaviour in Ringer's solution *Mater. Lett.* **57** 2382–9

[4] Antunes R A, Rodas A C D, Lima N B, Higa O Z and Costa I 2010 Study of the corrosion resistance and in vitro biocompatibility of PVD TiCN-coated AISI 316L austenitic stainless steel for orthopedic applications *Surf. Coatings Technol.* **205** 2074–81

[5] Valero Vidal C and Igual Muñoz A 2008 Electrochemical characterisation of biomedical alloys for surgical implants in simulated body fluids *Corros. Sci.* **50** 1954–61

[6] Sánchez-López J C, Abad M D, Carvalho I, Escobar Galindo R, Benito N, Ribeiro S, Henriques M, Cavaleiro A and Carvalho S 2012 Influence of silver content on the tribomechanical behavior on Ag-TiCN bioactive coatings *Surf. Coatings Technol.* **206** 2192–8

[7] Martínez-Martínez D, Sánchez-López J C, Rojas T C, Fernández A, Eaton P and Belin M 2005 Structural and microtribological studies of Ti–C–N based nanocomposite coatings prepared by reactive sputtering *Thin Solid Films* **472** 64–70

[8] Serro A P, Completo C, Colaço R, dos Santos F, da Silva C L, Cabral J M S, Araújo H, Pires E and Saramago B 2009 A comparative study of titanium nitrides, TiN, TiNbN and TiCN, as coatings for biomedical applications *Surf. Coatings Technol.* **203** 3701–7

[9] Feng H-P, Hsu C-H, Lu J-K and Shy Y-H 2003 Effects of PVD sputtered coatings on the corrosion resistance of AISI 304 stainless steel *Mater. Sci. Eng. A* **347** 123–9

[10] Chekan N M, Beliauski N M, Akulich V V, Pozdniak L V, Sergeeva E K, Chernov A N, Kazbanov V V and Kulchitsky V A 2009 Biological activity of silver-doped DLC films *Diam. Relat. Mater.* **18** 1006–9

[11] Chen W, Liu Y, Courtney H S, Bettenga M, Agrawal C M, Bumgardner J D and Ong J L 2006 In vitro anti-bacterial and biological properties of magnetron co-sputtered silver-containing hydroxyapatite coating *Biomaterials* **27** 5512–7

[12] Ewald A, Hösel D, Patel S, Grover L M, Barralet J E and Gbureck U 2011 Silver-doped calcium phosphate cements with antimicrobial activity *Acta Biomater.* **7** 4064–70

[13] Fielding G A, Roy M, Bandyopadhyay A and Bose S 2012 Antibacterial and biological characteristics of silver containing and strontium doped plasma sprayed hydroxyapatite coatings *Acta Biomater.* **8** 3144–52

[14] Huang H-L, Chang Y-Y, Lai M-C, Lin C-R, Lai C-H and Shieh T-M 2010 Antibacterial TaN-Ag coatings on titanium dental implants *Surf. Coatings Technol.* **205** 1636–41

[15] Endrino J L, Sánchez-López J C, Galindo R E, Horwat D and Anders A 2010 Beneficial silver: antibacterial nanocomposite Ag-DLC coating to reduce osteolysis of orthopaedic implants *J. Phys. Conf. Ser.* **252** 012005

[16] Böswald M, Mende K and Bernschneider W 1999 Biocompatibility testing of a new silver-impregnated catheterin vivo *Infection* **27** 38–42

[17] Kelly P J, Li H, Whitehead K A, Verran J, Arnell R D and Iordanova I 2009 A study of the antimicrobial and tribological properties of TiN/Ag nanocomposite coatings *Surf. Coatings Technol.* **204** 1137–40

[18] Chiang W-C, Tseng I-S, Møller P, Hilbert L R, Tolker-Nielsen T and Wu J-K 2010 Influence of silver additions to type 316 stainless steels on bacterial inhibition, mechanical properties, and corrosion resistance *Mater. Chem. Phys.* **119** 123–30

[19] Morones J R, Elechiguerra J L, Camacho A, Holt K, Kouri J B, Ramírez J T and Yacaman M J 2005 The bactericidal effect of silver nanoparticles *Nanotechnology* **16** 2346–53

[20] Rai M, Yadav A and Gade A 2009 Silver nanoparticles as a new generation of antimicrobials *Biotechnol. Adv.* **27** 76–83

[21] Feng Q, Wu J and Chen G 2000 A mechanistic study of the antibacterial effect of silver ions on Escherichia coli and Staphylococcus aureus *J. Biomed. Mater. Res.* **52** 662–8

[22] Brutel de la Riviere A, Dossche K M, Birnbaum D E and Hacker R 2000 First clinical experience with a mechanical valve with silver coating *J. Heart Valve Dis.* **9** 123–9; discussion 129–30

[23] Hollinger M A 1996 Toxicological aspects of topical silver pharmaceuticals *Crit. Rev. Toxicol.* **26** 255–60

[24] Janczuk B, Chibowski E, Bruque J, Kerkeb M and Caballero F 1993 On the consistency of surface free energy components as calculated from contact angles of different liquids: an application to the cholesterol surface *J. Colloid Interface Sci.* **159** 421–8

[25] Oliveira R, Azeredo J, Teixeira P and Fonseca A P 2001 *The role of hydrophobicity in bacterial adhesion* ed P Gilbert, D Allison, M Brading, J Verran and J Walker (Cardiff: BioLine)

[26] Van Oss C J and Giese R F 1995 The hydrophilicity and hydrophobicity of clay minerals *Clays Clay Miner.* **43** 474–7

[27] Malich G, Markovic B and Winder C 1997 The sensitivity and specificity of the MTS tetrazolium assay for detecting the in vitro cytotoxicity of 20 chemicals using human cell lines *Toxicology* **124** 179–92

[28] AshaRani P V, Low Kah Mun G, Hande M P and Valiyaveettil S 2009 Cytotoxicity and genotoxicity of silver nanoparticles in human cells *ACS Nano* **3** 279–90

[29] Kawata K, Osawa M and Okabe S 2009 In vitro toxicity of silver nanoparticles at noncytotoxic doses to HepG2 human hepatoma cells *Environ. Sci. Technol.* **43** 6046–51

[30] I.S. EN ISO 10993-5:2009 2009 Biological evaluation of medical devices - Part 5: Tests for in vitro cytotoxicity (ISO 1 0993-5:2009)

[31] Sousa C, Teixeira P and Oliveira R 2009 The role of extracellular polymers on Staphylococcus epidermidis biofilm biomass and metabolic activity *J. Basic Microbiol.* **49** 363–70

[32] Cerca N, Pier G B, Vilanova M, Oliveira R and Azeredo J 2005 Quantitative analysis of adhesion and biofilm formation on hydrophilic and hydrophobic surfaces of clinical isolates of Staphylococcus epidermidis *Res. Microbiol.* **156** 506–14

[33] Sutherland I W 2001 The biofilm matrix–an immobilized but dynamic microbial environment *Trends Microbiol.* **9** 222–7

[34] Donlan R M 2001 Biofilms and device-associated infections *Emerg. Infect. Dis.* **7** 277–81

[35] Standard J I 2000 Jis z 2801 :2000 **2000**

[36] Hsieh J H, Tseng C C, Chang Y K, Chang S Y and Wu W 2008 Antibacterial behavior of TaN–Ag nanocomposite thin films with and without annealing *Surf. Coatings Technol.* **202** 5586–9

[37] Kelly P J, Li H, Benson P S, Whitehead K A, Verran J, Arnell R D and Iordanova I 2010 Comparison of the tribological and antimicrobial properties of CrN/Ag, ZrN/Ag, TiN/Ag, and TiN/Cu nanocomposite coatings *Surf. Coatings Technol.* **205** 1606–10

[38] Kapoor R and Eagar T 1989 Tin-based reactive solders for ceramic/metal joints *Metall. Mater. Trans. B* **20** 919–24

[39] Nascimento R M Do, Martinelli A E and Buschinelli A J A 2003 Review Article: recent advances in metal-ceramic brazing *Cerâmica* **49** 178–98

[40] Doyle R J 2000 Contribution of the hydrophobic effect to microbial infection *Microbes Infect.* **2** 391–400

Chapter IV – Theoretical approach to silver antibacterial inactivity in Ag-TiCN coatings

The work presented in this chapter was based on the published book chapter:

Carvalho, Isabel; Henriques, M.; Carvalho, S.

Microbial Pathogens and Strategies for Combating Them: Science, Technology and Education, Formatex, Badajoz, 1, 170-178, 2013

Chapter IV – Theoretical approach to silver antibacterial inactivity in Ag-TiCN coatings

4.1 Introduction

Microorganisms play an important role in nature and in various technological processes [1]. Microbial adhesion to solid surfaces is a fundamental step in biofilm formation. Biofilms are a community of microorganisms strongly attached to each other and to a surface, embedded in an extracellular matrix. Moreover, due to their complex structure these communities are hardly eradicated by antibiotics. The medical devices are easily susceptible to microbial colonization, and to be able to reduce or even eliminate this effect, it is necessary to deeply understand the adhesion step. This is a complex process, involving microbiological factors of microorganisms, as the production of extracellular polymeric substances (EPS) [2], physicochemical properties of bacteria and materials' surface like hydrophobicity and roughness [3,4], and also environmental factors [5]. The interactions involved in bacterial adhesion to materials' surface can be classified as nonspecific or specific [6]. The nonspecific interactions comprehend physicochemical interactions between bacterial cell wall and materials' surface. These interactions involve van der Waals forces, electrostatic interactions and hydrophobic effects. This is the first stage where the adhesion is still reversible. The specific interactions are those in which the adhesion becomes irreversible. At this point, microorganisms have the ability to synthesize a variety of structural components, such as EPS that can fix to the surface of the materials. Moreover, bacteria can also bond to surface through appendages such as pili, fimbria, fibrils and flagella, when these are part of their structure [7]. In this sense, the aim of this chapter consists on the study on the mechanisms of bacterial adhesion, highlighting the surface characterization of TiCN coatings doped with silver.

4.2 Surface parameters ruling bacterial adhesion

Hydrophobicity, roughness and chemical composition appear to play an important role in the microbial adhesion process.

4.2.1 Free energy of interaction

The initial phase of the adhesion process of bacteria to non-living surfaces is usually mediated by non-specific interactions. The approach of microorganisms to the surface substrate is ruled by diffusion due to Brownian motions in fluids, arbitrary movements of particles in a fluid as a result of collisions between all the molecules or atoms present in this fluid [8]. The initial adhesion of the microorganism to the surface occurs in the distances of approximately 50 nm, in which the microorganisms and the surface can interact by short-and long-range forces leading to adhesion. The long-range forces involve van der Waals and electrostatic forces. The former are the only operating at distances greater than 50 nm. When the distance is approximately 10 and 20 nm, the interactions occur as a result of electrostatic forces, which are originated by the interaction of charges between microbial and material surfaces [7]. At the distance of approximately 0.5 and 2 nm, the interactions become stronger and are due to hydrophobic effects. These hydrophobic interactions between bacteria and material surfaces play an important role in initial adhesion of bacteria [9] by removing water films from the interacting surfaces. In this way, bacteria can attach to surfaces of material and simultaneously have the ability to segregate the EPS to colonize irreversibly on the surface of the material.

In the adhesion process, the interactions between microorganisms and the surfaces are carried out by a set of thermodynamic, physicochemical and microbiological phenomena. There are three physicochemical approaches that allow quantifying the energies involved in the interactions between surfaces, the thermodynamic, the DLVO and xDLVO approaches.

4.2.1.1 Thermodynamic approach

The adhesion of a microorganism to a solid surface in aqueous solution can only be established if the film of water between both surfaces is removed. This approach describes the energy of interaction between material and bacteria surfaces and considers Van der Waals attractive forces and acid–base interactions. The acid–base interactions are based on electron-donor and electron-acceptor interactions or polar interactions. The influence of the acid–base interactions is enormous when compared with electrostatic and van der Waals interactions, once that surrounding medium of the particles (bacteria, materials surface), is especially polar. However, the acid–base interactions are also relatively short ranged, and a

close approach between the interacting surfaces (less than 5 nm) is required before these forces can become operative [10].

According to van Oss [11], the hydrogen-bonding energy of cohesion of water molecules originate hydrophobic interactions. As known hydrogen-bonding can be seen as a form of more general electron-donor, electron-acceptor, and thus the interactions sensed are due to acid-base interactions defined by Lewis interactions. The surface tension (γ) can be divided into a Lifshitz–van der Waals (LW) component (γ^{LW}) and an acid–base (AB) component (γ^{AB}) where γ^{LW} comprises dispersion, orientation and induction contributions to the van der Waals interactions. LW interactions when compared with the AB are tiniest, since these latest come to exceed 10 to 100 times [12,13]. Consequently, the sole origin of the hydrophobic interaction would be the strong hydrogen bonding of water causing the high internal cohesiveness of water. So, the hydrophobicity of a given material is defined in terms of the variation of the free energy of interaction (ΔG) between material's surface (s) immersed in water (w), ΔG_{sws}, and is given using the following equation:

$$\Delta G_{sws}=\Delta G_{sws}^{LW}+\Delta G_{sws}^{AB} \quad (4.1)$$

Where ΔG_{sws}^{LW} and ΔG_{sws}^{AB} are free apolar energy of Lifshitz–van der Waals and free polar energy of Lewis components, respectively. When ΔG_{sws} is negative, the free energy of interaction between molecules is attractive revealing a greater interaction with each other than with water, making the material surface hydrophobic. In opposition, a surface is hydrophilic when ΔG_{sws} is positive.

It is possible to determined ΔG_{sws}^{LW} and ΔG_{sws}^{AB} by the following equations:

$$\Delta G_{sws}^{LW}=-2(\sqrt{\gamma_s^{LW}}-\sqrt{\gamma_w^{LW}})^2 \quad (4.2)$$

$$\Delta G_{sws}^{AB}=-4\left[\left(\sqrt{\gamma_s^{+}\gamma_s^{-}}\right)+\left(\sqrt{\gamma_w^{+}\gamma_w^{-}}\right)-\left(\sqrt{\gamma_s^{+}\gamma_w^{-}}\right)-\left(\sqrt{\gamma_w^{+}\gamma_s^{-}}\right)\right] \quad (4.3)$$

Where γ_s^{+} and γ_s^{-} are, respectively, the electron-acceptor and electron-donor surface tension parameters. The surface tension components (γ_s^{LW}, γ_s^{+} and γ_s^{-}) can be determined by measuring the contact angles formed by three different liquids on material or bacterial

surface, one of them apolar and two polar liquids, which one should be water. Each component of surface tension is known and presented in table 4.1.

Table 4.1 Surface tension parameters (mJ/m²) of the liquids commonly used in contact angle measurements

Liquids	γ^{TOT}	γ^{LW}	γ^{+}	γ^{-}
Water	72.8	21.8	25.5	25.5
Glycerol	64.0	34.0	3.9	57.4
Formamide	58.0	39.0	2.3	39.6
Diiodomethane	50.8	50.8	0	0
n-Decane	23.8	23.8	0	0
α-Bromonaphthalene	44.4	44.4	0	0

Afterward, using the following equation, resulting from Young's equation, for all the three liquids and solving the three unknowns system, it is possible to obtain each surface tension component (γ_s^{LW}, γ_s^{+} and γ_s^{-}).

$$\gamma_l^{TOT}(1+\cos\theta)=2\sqrt{(\gamma_S^{LW}\gamma_l^{LW})}+2\sqrt{(\gamma_S^{-}\gamma_l^{+})}+2\sqrt{(\gamma_S^{+}\gamma_l^{-})} \qquad (4.4)$$

Where, θ is the contact angle formed between the surface (of material or bacteria) and the liquid.

Surface hydrophobicity is one of the most important properties involved in the adhesion process [6]. As it has been previously mentioned, the hydrophobicity can be modified to increase the capacity of removing the film of water that interacts between two surfaces [14,15], but this definition is not sufficient since electrostatic interactions are not taken into account. van Oss and Giese [11], defined hydrophobic interactions as the attraction among apolar, or slightly polar, cells or other molecules themselves, when immersed in an aqueous solution. As mentioned above, LW forces do not contribute much to the total interaction energy between apolar entities. The value of apolar surface tension component of water (γ_w^{LW}) is 21.8 mJ/m² at 20°C and as the majority of compounds have a γ_s^{LW} values proximally of

γ_w^{LW} [11], by applying of the Eq. (4.2), ΔG_{sws}^{LW} have a very low value comparatively with ΔG_{sws}^{AB}. Thus, often the sole contribution driving force of hydrophobic attraction is the AB, or more precisely the hydrogen bonding component of the free energy of cohesion of water [16]. For completely apolar compounds the value of ΔG_{sws}^{AB} = -102 mJ/m^2, once the electron-acceptor surface tension parameter (γ_s^+) as well as the electron donor surface tension parameter (γ_s^-) are zero, substituting in the Eq. (4.3), one has: $\Delta G_{sws}^{AB} = -4\left[\left(\sqrt{\gamma_w^+ \gamma_w^-}\right)\right]$ which represents the hydrogen-bonding energy of cohesion of water. As $\gamma_w^+ = \gamma_w^-$ = 25.5 mJ/m^2 at 20 °C, the ΔG_{sws}^{AB} = -102 mJ/m^2 for apolar compounds, immersed in water. The ΔG_{sws}^{LW} have a low contribution for the total free energy of hydrophobic attraction (ΔG_{sws}^{TOT}), according to van Oss [11], the contribution of ΔG_{sws}^{LW} is about 2% of the total ΔG_{sws}^{TOT}. When ΔG_{sws}^{TOT} is negative, the free energy of interaction between molecules of material surface is attractive revealing a poor or even no interaction with water, making the material surface hydrophobic. When ΔG_{sws}^{TOT} is positive, the material surface makes hydrophilic. In this sense the bacteria are more prone to attach the hydrophobic surfaces than hydrophilic. Bacteria and other microorganisms have developed several means to use hydrophobic effects, in order to adhere to material's surfaces. According to Doyle [17], a microorganism may adhere to a material surface via the hydrophobic effect since that surface has seats where the density of apolar areas is high. Several studies have shown that bacterial adhesion is promoted by the hydrophobic effect [18,19].The hydrophobicity of the cell surface is important in adhesion since hydrophobic interactions tend to increase with an increasing apolar zones of one or both surfaces involved [19]. According to Drenkard and Ausubel [20], the ability of bacteria to attach to each other and to surfaces depends in part on the interaction of hydrophobic domains.

However, in this theory the electrostatic interactions are not accounted and these interactions are very important in aqueous systems, so this theory can only be applied if the energy barrier between the two surfaces is exceeded.

4.2.1.2 DLVO approach

The adhesion of microorganisms to surfaces can be interpreted according to the DLVO theory, developed by Derjaguin e Landau (1941) e Verwey e Overbeek (1948). This approach describes the energy of interaction between material and bacteria surfaces and considers only the interactions of long-range as van der Waals attractive forces and electrostatic repulsive forces. The van der Waals forces can be the London dispersion force, the Keesom dipole–dipole force, and the Debye dipole-induced dipole force, these forces are attractive and their intensity depends on the particles size involved. The electrostatic interactions are due to the formation, in aqueous solutions, of a charged layer, diffusely distributed around the bulk which is usually negative as a result of ionization of surface functional groups. The positive ions present in the solution neutralize the negative charge of the bacteria and material surfaces creating an electrical double layer. These interactions are due to overlapping of electrical double layer of bacteria surface with the double layer of the material surface, and as both surfaces have the same charge, the interaction between them is repulsive. This repulsive energy increases when the ionic strength of an aqueous solution decreases since the shield of the surface charges due to the ions present in the electrical double layers decreases. At low ionic strengths, when a bacterial cell approaches a surface, there is an energy barrier which is difficult overcome [21]. The total free energy (ΔG_{adh}^{TOT}) of these interactions is the result of the sum of the free energies of each interaction forces, according to equation 4.5.

$$\Delta G_{adh}^{TOT} = \Delta G^{LW} + \Delta G^{DL} \quad (4.5)$$

Where ΔG^{DL} is the electric double layer free energy of electrostatic interaction. As mentioned above this theory contemplates only the interactions of long-range, thus allowing only the prediction that microorganisms approach up to a certain distance from the material surface.
Both approaches have proven merit for microbial adhesion. However, so far, they presented only partially interpretation of the phenomena. Consequently, van Oss et al. [22] introduced an extended DLVO theory which integrated the thermodynamic aspects of adhesion to the DLVO theory.

4.2.1.3 Extended DLVO approach

This theory considers three fundamental interactions: Lifshitz–van der Waals (LW), electrostatic (DL) and Lewis acid–base (AB) forces. The total free energy of these interactions is the result of the sum of the free energies of each interaction forces, according to equation 4.6.

$$\Delta G_{adh}^{TOT} = \Delta G^{LW} + \Delta G^{AB} + \Delta G^{DL} \quad (4.6)$$

4.2.2 Roughness

Biomaterial surface roughness is another relevant property for bacterial adhesion process. The roughness of these materials' surface usually promotes bacterial adhesion and consequently biofilm formation. According to some authors surface irregularities caused by the increased surface roughness provide shelter bacterial cells by inducing their attachment [23,24]. This is because shear forces are diminished, and surface area is higher on rougher surfaces [19,25]. Nevertheless, the growth of these microorganisms depends also on their sizes, cell morphology and their reproduction [26,27]. There are many different roughness parameters for measurement of surface roughness, such as Ra (arithmetical mean of surface roughness of every measurement within the total distance ½ roughness average), Rmax (maximum roughness within the distance measured), Rms (root mean square roughness) and among others [28]. Ra is the most universally used roughness parameter since it is easy to define and to measure, providing a good general description of height variations [29]. However, this parameter alone is not enough to describe to whole topography of a surface, so, the other roughness parameters should always be used together. These parameters can be measured by atomic force microscope. Several studies shows that bacterial adhesion forces increase with increasing roughness of the substratum surfaces [30,31]. However, according to other authors, the influence of surface roughness on bacterial adhesion and biofilm formation is not that significant [30,32,33]. Some *in vivo* studies suggested a threshold surface roughness for bacterial retention (Ra = 0.2 μm) below which no further reduction in bacterial accumulation could be expected. An increase in surface roughness above this threshold roughness, however, resulted in a simultaneous increase in plaque accumulation [34]. In accordance to these studies, it was also reported that, when the surface

roughness is lower than 0.2 μm, surface roughness has no significant effect on plaque accumulation and microbial composition on titanium abutments in vivo [35,36] nor on adhesion and colonization by *Staphylococcus epidermidis* of silicone surfaces in vitro [30,37]. Another study demonstrated that the attachment to and removal of microorganisms from stainless steel surfaces did not depend on surface roughness when varied between Ra values of 0.01 and 0.9 μm [33]. Some studies suggested that adhesion of different bacteria to surface substrate is not influenced by roughness. The adhesion of *S. epidermidis* and *Pseudomonas aeruginosa* are dependent on pyrolytic carbon surface roughness, although *Staphylococcus aureus* adhesion appears to be independent of these factors [38].

In the literature, the opinions vary in relation to the effect of bacterial attachment to surface features. Some researchers report that there is a positive correlation between adhesion and increase roughness [4,39], while other researchers do not report any correlation between the ability of bacteria to adhere and irregularities or roughness of surfaces [40]. This apparent conflict is related with the different roughness parameters determined, with the bacterial species studied, the physicochemical parameters of the surface and the method used to detect the bacteria on the surface.

4.2.3 Chemical composition

Another factor that influences bacteria adherence to a biomaterial surface is the chemical composition of the latter. Material surfaces are composed by different functional groups. Hydrophobicity and charges which involved the biomaterial surface depend of those groups, influencing the bacterial adhesion. Tegoulia and Cooper [41] showed that *S. aureus* adhesion on self-assembled monolayers (SAMs), was lower on ethylene oxide-bearing surfaces followed by the hydroxyl surfaces and higher on carboxylic acid and methyl terminated SAMs. They measured the contact angle for all surfaces, and found that the ethylene oxide terminated SAM was more hydrophobic than the hydroxyl and carboxylic acid surface, which suggests that some methylene groups was exposed to water. In this study, it was demonstrated that surface hydrophobicity and the presence of specific functional groups such as ethylene oxide moieties can significantly affect the amount of cells that attach to the surface. Kiremitci-Gumustederelioglou and Pesmen [42] studied the microbial adhesion to polymeric biomaterials used in implants and showed that microbial adhesion was reduced on the

negatively charged polymeric implants, while it was increased on the positively charged. Amanatides *et al.* [43] investigated the effect of plasma surface treatment of polyethylene terephthalate (PET) films, based in He/O_2 rf discharges, on the *S. epidermidis* adhesion and showed that the treatment increased the surface hydrophilicity leading to promote the bacterial adhesion, and this might be due to the incorporation of oxygenated functional groups. Oliveira et al [44,45] studied the structural properties of Ti-Si-C-O-N coatings, including the biofilm formation of *S. epidermidis* to their surfaces and concluded that the biofilm formation could be related to the surface chemical composition. According to these authors coating's surfaces were less prone to be colonized with a decrease on the N/O atomic ratio since a decrease on the TiN structure promotes an increase on the Ti-O compounds. The change or modification in surface chemistry can hinder the bacterial adhesion to these surfaces.

4.3 Control of bacterial adhesion

4.3.1 Surface modification

The risk of microbial infection associated with the biomaterials used in implants happens more often at the time of implantation and revision surgeries [46]. Due to this fact, these materials are susceptible to colonization caused mainly by nosocomial pathogens. The most popular materials used in orthopaedic devices have already been mentioned earlier, being stainless steel the most appealing in terms of cost. However, this biomaterial has a serious problem with corrosion. In this sense, different types of physical vapour deposition, PVD, hard ceramic coatings are frequently considered to overcome this drawback. Titanium carbonitride (TiCN) for instance presents good mechanical and tribological properties [47]. The wear and fatigue behaviours of TiCN coatings are extensively studied [47–49]. In the literature the good corrosion resistance of TiCN, is also reported [50]. Feng *et al.* [51] reported a significant decrease of the corrosion current density of TiCN-coated stainless steel 304. Besides, its non-cytotoxic character allied with mechanical and corrosion properties make it a very interesting material for biomedical applications. Concomitant to all these factors and has already referred, the risk of bacterial infection is also one of the causes of failure of these devices. Thus, surface modification by coatings doped with silver is one the most used approaches to control the bacterial adhesion and their colonization. Silver has been the most used metal by

demonstrating high antimicrobial activity and a relatively low cytotoxicity [52–56]. It is important that addition of silver do not change the good mechanical and tribological properties of coatings.

4.4 Conclusions

In chapter II, it was concluded that the incorporation of silver in TiCN coatings alters chemically the surface, in fact XRD and XPS analyses, showed that, as the silver content increases, the appearance of two new soft phases (Ag and amorphous phases) are evidenced and their preferable growth location is in the grain boundary in the TiCN coatings, making them smoother. Moreover, these phases are responsible for making the surface more hydrophobic, increasing apolar area density promoting thereby the bacterial adhesion, as seen in chapter III. The surface roughness of these samples was also measured and it was concluded that, according to the studies mentioned above, its influence could be not significant since all coatings had a roughness lower than 200 nm. So, the modification of the material surfaces by the addition of an element like the case of silver alters the chemical composition and the structure/morphology and consequently the roughness and hydrophobicity, and as it has been described all these features can influence bacterial adhesion.

As it is well known, an ideal coating would present silver ions release which will be translated in their antibacterial activity. In this work, this fact is not verified verify. Thus, it is essential to know what can be conditioning the release of silver ions. A hypothesis that arises is the possible influence of the culture media used in the biological assays in the Ag^{+} ions release. In this sense, this hypothesis will be explored in the next chapter.

References

[1] Ubbink J and Schär-Zammaretti P 2007 Colloidal properties and specific interactions of bacterial surfaces *Curr. Opin. Colloid Interface Sci.* **12** 263–70

[2] Truong V K, Rundell S, Lapovok R, Estrin Y, Wang J Y, Berndt C C, Barnes D G, Fluke C J, Crawford R J and Ivanova E P 2009 Effect of ultrafine-grained titanium surfaces on adhesion of bacteria. *Appl. Microbiol. Biotechnol.* **83** 925–37

[3] Bruinsma G M, van der Mei H C and Busscher H J 2001 Bacterial adhesion to surface hydrophilic and hydrophobic contact lenses. *Biomaterials* **22** 3217–24

[4] Kawai K, Urano M and Ebisu S 2000 Effect of surface roughness of porcelain on adhesion of bacteria and their synthesizing glucans. *J. Prosthet. Dent.* **83** 664–7

[5] An Y H and Friedman R J 1998 Concise review of mechanisms of bacterial adhesion to biomaterial surfaces *J. Biomed. Mater. Res.* **43** 338–48

[6] Busscher H 1987 Specific and non-specific interactions in bacterial adhesion to solid substrata *FEMS Microbiol. Lett.* **46** 165–73

[7] Daeschel M and McGuire J 1998 Interrelationships between protein surface adsorption and bacterial adhesion *Biotechnol. Genet. Eng. Rev.* **15** 413–38

[8] Teughels W, Van Assche N, Sliepen I and Quirynen M 2006 Effect of material characteristics and/or surface topography on biofilm development. *Clin. Oral Implants Res.* **17 Suppl 2** 68–81

[9] Oliveira R, Azeredo J, Teixeira P and Fonseca A P 2001 *The role of hydrophobicity in bacterial adhesion* ed P Gilbert, D Allison, M Brading, J Verran and J Walker (Cardiff: BioLine)

[10] Van Oss C J, Chaudhury M K and Good R J 1988 Interfacial Lifshitz-van der Waals and polar interactions in macroscopic systems *Chem. Rev.* **88** 927–41

[11] Van Oss C J 1995 Hydrophobic, Hydrophilic and Other Interaction in Epitope-Paratope Binding *Mol. Immunol.* **32** 199–211

[12] Hermansson M 1999 The DLVO theory in microbial adhesion *Colloids Surfaces B Biointerfaces* **14** 105–19

[13] Van Oss C J and Good R J 1989 Surface Tension and the Solubility of Polymers and Biopolymers: The Role of Polar and Apolar Interfacial Free Energies *J. Macromol. Sci. Part A - Chem.* **26** 1183–203

[14] Busscher H J, Cowan M M and van der Mei H C 1992 On the relative importance of specific and non-specific approaches to oral microbial adhesion. *FEMS Microbiol. Rev.* **8** 199–209

[15] Loosdrecht M van, Norde W, Lyklema J and Zehnder A J B 1990 Hydrophobic and electrostatic parameters in bacterial adhesion *Aquat. Sci.* **52** 103–14

[16] Van Oss C J 1997 Hydrophobicity and hydrophilicity of biosurfaces *Curr. Opin. Colloid Interface Sci.* **2** 503–12

[17] Doyle R J 2000 Contribution of the hydrophobic effect to microbial infection *Microbes Infect.* **2** 391–400

[18] Li B and Logan B E 2004 Bacterial adhesion to glass and metal-oxide surfaces. *Colloids Surf. B. Biointerfaces* **36** 81–90

[19] Donlan R M 2002 Biofilms: microbial life on surfaces *Emerg. Infect. Dis.* **8** 881–90

[20] Drenkard E and Ausubel F M 2002 Pseudomonas biofilm formation and antibiotic resistance are linked to phenotypic variation. *Nature* **416** 740–3

[21] Hori K and Matsumoto S 2010 Bacterial adhesion: From mechanism to control *Biochem. Eng. J.* **48** 424–34

[22] Van Oss C ., Good R . and Chaudhury M . 1986 The role of van der Waals forces and hydrogen bonds in "hydrophobic interactions" between biopolymers and low energy surfaces *J. Colloid Interface Sci.* **111** 378–90

[23] Al-Radha A S D, Dymock D, Younes C and O'Sullivan D 2012 Surface properties of titanium and zirconia dental implant materials and their effect on bacterial adhesion. *J. Dent.* **40** 146–53

[24] Amoroso P F, Pier-Francesco A, Adams R J, Waters M G J and Williams D W 2006 Titanium surface modification and its effect on the adherence of Porphyromonas gingivalis: an in vitro study. *Clin. Oral Implants Res.* **17** 633–7

[25] Katsikogianni M and Missirlis Y F 2004 Concise review of mechanisms of bacterial adhesion to biomaterials and of techniques used in estimating bacteria-material interactions *Eur. Cell. Mater.* **8** 37–57

[26] Katainen J, Paajanen M, Ahtola E, Pore V and Lahtinen J 2006 Adhesion as an interplay between particle size and surface roughness. *J. Colloid Interface Sci.* **304** 524–9

[27] Messing R A and Oppermann R A 1979 Pore dimensions for accumulating biomass. I. Microbes that reproduce by fission or by budding *Biotechnol. Bioeng.* **21** 49–58

[28] Truong V K, Lapovok R, Estrin Y S, Rundell S, Wang J Y, Fluke C J, Crawford R J and Ivanova E P 2010 The influence of nano-scale surface roughness on bacterial adhesion to ultrafine-grained titanium. *Biomaterials* **31** 3674–83

[29] Gadelmawla E S, Koura M M, Maksoud T M A, Elewa I M and Soliman H H 2002 Roughness parameters *J. Mater. Process. Technol.* **123** 133–45

[30] Mei L, Busscher H J, van der Mei H C and Ren Y 2011 Influence of surface roughness on streptococcal adhesion forces to composite resins. *Dent. Mater.* **27** 770–8

[31] Zhao Q, Liu Y, Wang C, Wang S, Peng N and Jeynes C 2008 Reduction of bacterial adhesion on ion-implanted stainless steel surfaces *Med. Eng. Phys.* **30** 341–9

[32] Größner-Schreiber B, Griepentrog M, Ingrun Haustein, Wolf-Dieter Muller, Gobel K-P L, Briedigkeit H and Ulf Berthold Gobel 2001 Plaque formation on surface modified dental implants *Clin. Oral Implants Res.* **12** 543–51

[33] Hilbert L R, Bagge-Ravn D, Kold J and Gram L 2003 Influence of surface roughness of stainless steel on microbial adhesion and corrosion resistance *Int. Biodeterior. Biodegradation* **52** 175–85

[34] Bollen C M, Lambrechts P and Quirynen M 1997 Comparison of surface roughness of oral hard materials to the threshold surface roughness for bacterial plaque retention: a review of the literature. *Dent. Mater.* **13** 258–69

[35] Bollen C M, Papaioanno W, Van Eldere J, Schepers E, Quirynen M and van Steenberghe D 1996 The influence of abutment surface roughness on plaque accumulation and peri-implant mucositis. *Clin. Oral Implants Res.* **7** 201–11

[36] Quirynen M, Bollen C M, Papaioannou W, Van Eldere J and van Steenberghe D The influence of titanium abutment surface roughness on plaque accumulation and gingivitis: short-term observations. *Int. J. Oral Maxillofac. Implants* **11** 169–78

[37] Tang H, Cao T, Liang X, Wang A, Salley S O, McAllister J and Ng K Y S 2009 Influence of silicone surface roughness and hydrophobicity on adhesion and colonization of Staphylococcus epidermidis. *J. Biomed. Mater. Res. A* **88** 454–63

[38] Litzler P-Y, Benard L, Barbier-Frebourg N, Vilain S, Jouenne T, Beucher E, Bunel C, Lemeland J-F and Bessou J-P 2007 Biofilm formation on pyrolytic carbon heart valves:

influence of surface free energy, roughness, and bacterial species *J. Thorac. Cardiovasc. Surg.* **134** 1025–32

[39] Carlén a, Nikdel K, Wennerberg a, Holmberg K and Olsson J 2001 Surface characteristics and in vitro biofilm formation on glass ionomer and composite resin. *Biomaterials* **22** 481–7

[40] Buergers R, Rosentritt M and Handel G 2007 Bacterial adhesion of Streptococcus mutans to provisional fixed prosthodontic material. *J. Prosthet. Dent.* **98** 461–9

[41] Tegoulia V A and Cooper S L 2002 Staphylococcus aureus adhesion to self-assembled monolayers: effect of surface chemistry and fibrinogen presence *Colloids Surfaces B Biointerfaces* **24** 217–28

[42] Kiremitci-Gumusderelioglu M and Pesmen a 1996 Microbial adhesion to ionogenic PHEMA, PU and PP implants. *Biomaterials* **17** 443–9

[43] Amanatides E, Mataras D, Katsikogianni M and Missirlis Y F 2006 Plasma surface treatment of polyethylene terephthalate films for bacterial repellence *Surf. Coatings Technol.* **200** 6331–5

[44] Oliveira C, Gonçalves L, Almeida B G, Tavares C J, Carvalho S, Vaz F, Escobar Galindo R, Henriques M, Susano M and Oliveira R 2008 XRD and FTIR analysis of Ti–Si–C–ON coatings for biomedical applications *Surf. Coatings Technol.* **203** 490–4

[45] Oliveira C, Galindo R E, Palacio C, Vázquez L, Espinosa A, Almeida B G, Henriques M, V S C and Carvalho S 2010 Influence of the surface morphology and microstructure on the biological properties of Ti–Si–C–N–O coatings *Thin Solid Films* **518** 5694–9

[46] Pishbin F, Mouriño V, Gilchrist J B, Kreppel S, Salih V, Ryan M P and Boccaccini A R 2013 Single-step electrochemical deposition of antimicrobial orthopaedic coatings based on a bioactive glass/chitosan/nano-silver composite system *Acta Biomater.* **9** 7469–79

[47] Sánchez-López J C, Abad M D, Carvalho I, Escobar Galindo R, Benito N, Ribeiro S, Henriques M, Cavaleiro A and Carvalho S 2012 Influence of silver content on the tribomechanical behavior on Ag-TiCN bioactive coatings *Surf. Coatings Technol.* **206** 2192–8

[48] Serro A P, Completo C, Colaço R, dos Santos F, da Silva C L, Cabral J M S, Araújo H, Pires E and Saramago B 2009 A comparative study of titanium nitrides, TiN, TiNbN

and TiCN, as coatings for biomedical applications *Surf. Coatings Technol.* **203** 3701–7

[49] Martínez-Martínez D, Sánchez-López J C, Rojas T C, Fernández A, Eaton P and Belin M 2005 Structural and microtribological studies of Ti–C–N based nanocomposite coatings prepared by reactive sputtering *Thin Solid Films* **472** 64–70

[50] Antunes R A, Rodas A C D, Lima N B, Higa O Z and Costa I 2010 Study of the corrosion resistance and in vitro biocompatibility of PVD TiCN-coated AISI 316L austenitic stainless steel for orthopedic applications *Surf. Coatings Technol.* **205** 2074–81

[51] Feng H-P, Hsu C-H, Lu J-K and Shy Y-H 2003 Effects of PVD sputtered coatings on the corrosion resistance of AISI 304 stainless steel *Mater. Sci. Eng. A* **347** 123–9

[52] Chekan N M, Beliauski N M, Akulich V V, Pozdniak L V, Sergeeva E K, Chernov A N, Kazbanov V V and Kulchitsky V A 2009 Biological activity of silver-doped DLC films *Diam. Relat. Mater.* **18** 1006–9

[53] Chen W, Liu Y, Courtney H S, Bettenga M, Agrawal C M, Bumgardner J D and Ong J L 2006 In vitro anti-bacterial and biological properties of magnetron co-sputtered silver-containing hydroxyapatite coating *Biomaterials* **27** 5512–7

[54] Ewald A, Hösel D, Patel S, Grover L M, Barralet J E and Gbureck U 2011 Silver-doped calcium phosphate cements with antimicrobial activity *Acta Biomater.* **7** 4064–70

[55] Fielding G A, Roy M, Bandyopadhyay A and Bose S 2012 Antibacterial and biological characteristics of silver containing and strontium doped plasma sprayed hydroxyapatite coatings *Acta Biomater.* **8** 3144–52

[56] Huang H-L, Chang Y-Y, Lai M-C, Lin C-R, Lai C-H and Shieh T-M 2010 Antibacterial TaN-Ag coatings on titanium dental implants *Surf. Coatings Technol.* **205** 1636–41

Chapter V – Seeking for an explanation for the antibacterial inactivity of the Ag -TiCN coatings

The work presented in this chapter was based on the published paper:

- **Carvalho, Isabel**; Escobar Galindo, R.; Henriques, M.;Palacio, C.; Carvalho, S.

Journal of Physics D: Applied Physics

Chapter V – Seeking for an explanation for the antibacterial inactivity of the Ag-TiCN coatings

5.1 Introduction

As seen in the previous chapter, bacterial adhesion is a complex process dependent on several factors. In the chapter III, it was reported the antibacterial inactivity of Ag-TiCN coatings, even for relatively large quantities of silver (15 at. %), conflicting with other published results [1–8]. In this part of study, the silver nanoparticles embedded in the TiCN matrix did not produce any antibacterial effect, since there was no ionization, or it occurred at very low concentrations. In this sense, one explanation for the inactivity of antibacterial activity may be related with the culture medium used in microbiological assays, Tryptic soy broth (TSB), which can somehow influence the release of silver ions. Additionally, as cytotoxicity of coatings was also tested, Dulbecco's Modified Eagle's medium (DMEM), a culture medium of animal cells was also used. Accordingly, the aim of this part of work is to evaluate the possible physical and chemical changes that may occur in the coatings surfaces after being exposed to TSB and DMEM. In order to achieve such goal, advanced surface characterization techniques were used, glow discharge optical emission spectroscopy (GDOES), Rutherford backscattering spectroscopy (RBS) and X-ray photoelectron spectroscopy (XPS). Two different samples were selected with Ag/Ti ratios of 0 and 0.20, corresponding to 0 and 6 at.% of Ag content, respectively, subsequently to what has been reported in Chapter II, where the tribological tests revealed that the wear resistance was enhanced for Ag/Ti ratios lower than 0.20 (Ag content < 6 at.%).

5.2 Materials and methods

5.2.1 Coatings preparation

Ag-TiCN coatings produced under the conditions indicated in chapter II, (previously sterilized at 121 °C for 15 min) were immersed into 3 ml of TSB or DMEM for 24 h, at 37 °C under a constant agitation of 120 rpm. Afterwards the supernatants were removed and the coatings were placed in a sealed desiccator.

This treatment was done with the purpose to evaluate the possible changes on the coatings surface after their exposure to the culture media referred above and the potential influence in

the antimicrobial inactivity. The choice of 24 h was taken to be the minimum time to obtain a considerable development of microbial biofilms [9,10] responsible for infections [11–13].

5.2.2 Chemical and physical analysis

Glow discharge optical emission spectroscopy (GDOES) and Rutherford backscattering spectrometry (RBS) were used in order to detect small variations in the composition of coatings surface and in the elementary distribution in depth, with particular focus on the distribution of silver after 0 and 24 h of immersion. GDOES experiments were performed using a Jobin Yvon RF GD Profiler equipped with a 4 mm diameter anode and operating at a typical radio frequency discharge pressure of 650 Pa and a power of 40 W. RBS experiments were performed using 3.7 MeV He^+ at an ion dose of 10 μC. The data were acquired simultaneously with two silicon surface barrier detectors located at scattering angles of 170° and 135°, respectively, with an energy resolution of 16 keV. RBS spectra were fitted with the software program RBX [14].

X-ray photoelectron spectroscopy (XPS) was carried out to analyse the chemical bonds of the compounds on the coatings surface, also after coatings treatment. The tests were performed using a hemispherical analyser (SPECS EA-10 Plus) and Al Kα radiation as exciting source at a constant power of 300 W. The pass energy was 15 eV giving a constant resolution of 0.9 eV. The Ag 3d5/2 line at 367.9 eV was used to calibrate the binding energies (BE). All samples (those that were in contact or not with the culture media) were not sputter-cleaned in order to obtain the effect of the electrolytes on the surface. The curve-fitting analysis of all core levels was performed by using Gaussian curve fitting function, in CasaXPS software.

5.3 Results and discussion

5.3.1 Depth profile characterization

GDOES profiles of coatings with 0 and 0.20 Ag/Ti atomic ratios before and after immersion in the culture media are presented in figures 5.1 and 5.2, respectively.

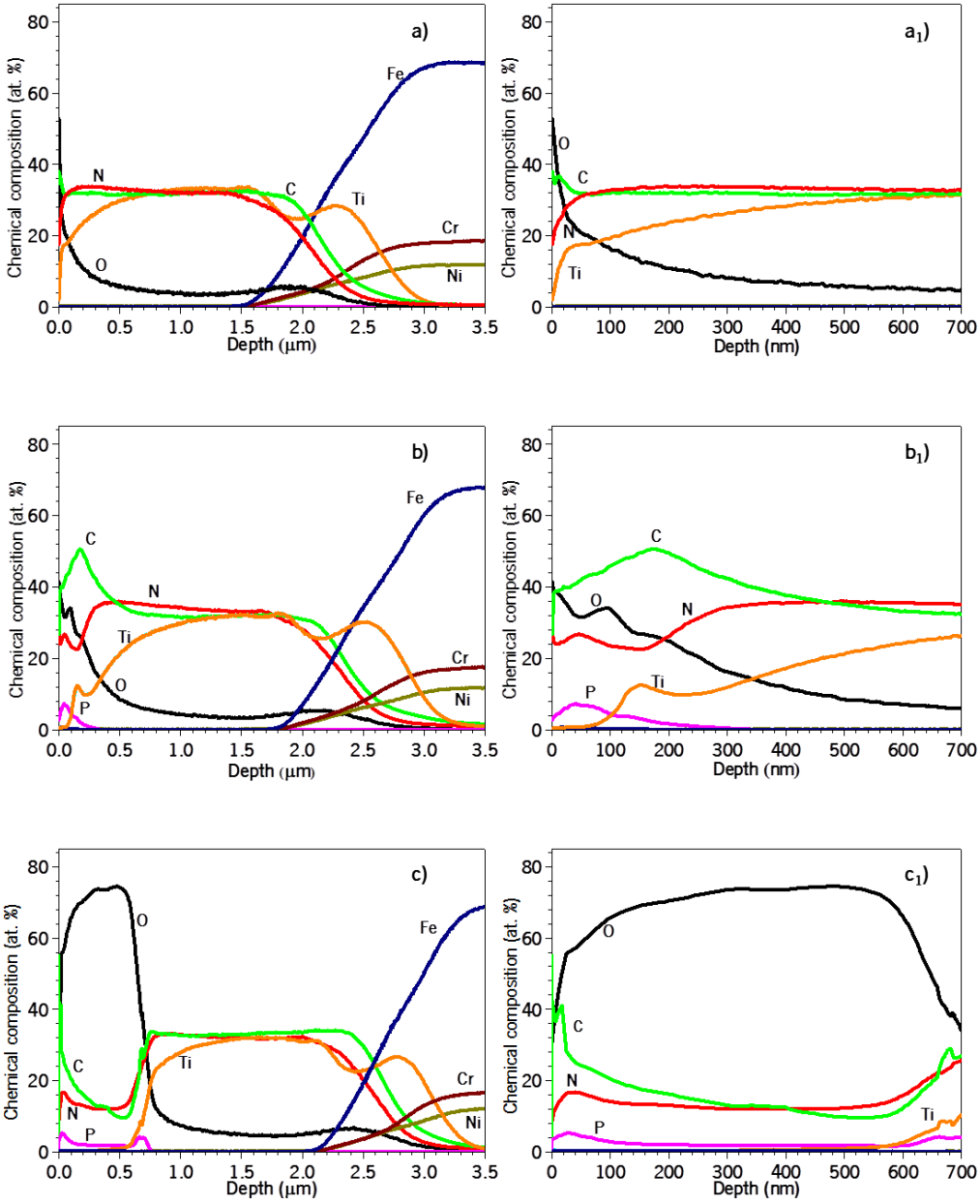

Figure 5.1 GDOES depth profile of Ag/Ti = 0. a) control samples, b) samples immersed 24 h in TSB and, c) samples immersed 24 h in DMEM. a), b) and c) extended depth profiles up to 3.5 μm and a_1), b_1) and c_1) the depth profiles near surface (< 700 nm).

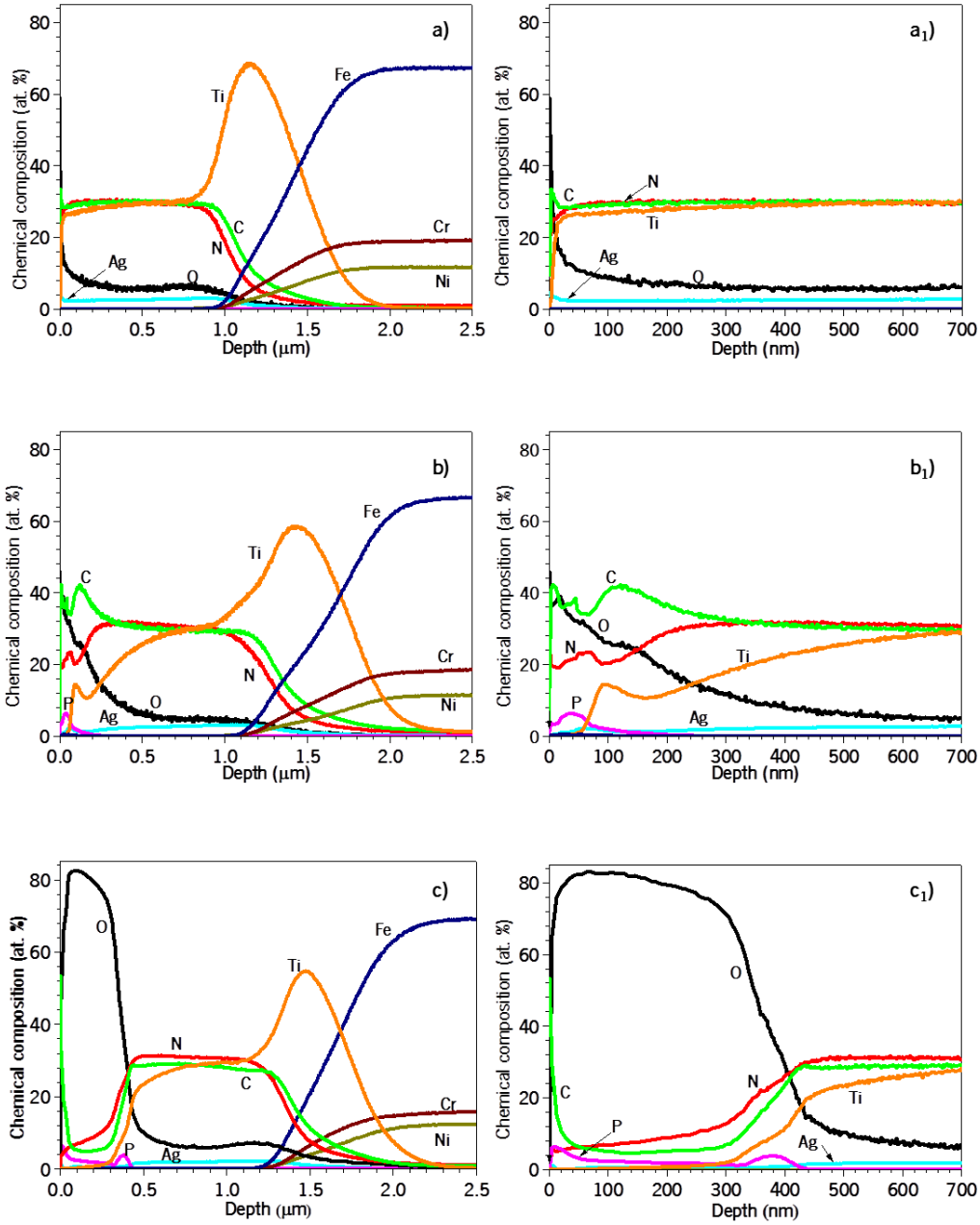

Figure 5.2 GDOES depth profile of Ag/Ti = 0.20. a) control samples, b) samples immersed 24 h in TSB and, c) samples immersed 24 h in DMEM. a), b) and c) extended depth profiles up to 2.5 μm and a1), b1) and c1) the depth profiles near surface (< 700 nm).

The spectra of control samples (without media immersion) without and with silver (figure 5.1a and 5.2a, respectively) present an oxidation in the top surface (< 200 nm), with the oxygen content decreasing progressively within the bulk coating. This effect is more noticeable in figures 5.1a$_1$ and 5.2a$_1$, where the first 700 nm of the samples are zoomed. The oxidation in

the surface is probably due to some contamination by exposure to environment. The oxygen inside the coating probably stems from the residual oxygen in the deposition chamber during the production, as well as a small amount due to natural oxidation from the target surface, constituted by metals, which occurs unavoidably when the samples are in contact with moisture in the environment [15], as referred previously in chapter II. In these figures, it can be observed the homogeneous elemental composition within the bulk deposited coating (thickness above 500 nm and 20 nm for Ag/Ti = 0 and Ag/Ti = 0.20, respectively) until reaching the Ti interlayer. The chemical composition of these control samples corroborates with that obtained by EPMA (analysed in chapter II).

GDOES profiles for samples with 0 and 0.20 Ag/Ti atomic ratios, which were 24 h in contact with TSB (figure 5.1b and 5.2b) show the presence of phosphorus on the surface. However, this presence was not confirmed either by RBS or by XPS as it will be discussed later. Figures 5.1b$_1$ and 5.2b$_1$ show a high heterogeneity in the chemical composition on the first 700 nm nanometres of both samples. It can be seen an increase in the carbon content, reaching the maximum concentration approximately at 170 nm and 120 nm in depth for the samples without and with silver, respectively. Moreover, it should be noted that for both samples there is a very thin surface layer (with a thickness of 70 and 50 nm for samples Ag/Ti = 0 and Ag/Ti = 0.20, respectively) where neither titanium nor silver is detected. This layer may indicate the presence of organic compounds on top of the deposited coatings, since there is only the contribution of carbons, nitrogen and oxygen (and, to a smaller extent, phosphorus), and these elements are principal constituents of proteins, an important component of TSB.

Finally, GDOES profiles of samples subjected to immersion in DMEM (figures 5.1c and 5.2c) exhibit a wide oxidized surface of about 600 and 400 nm of thickness for the coatings without and with silver, respectively. In this same coating thickness, it can be seen the emergence of phosphorus, and in this case, its presence was confirmed by RBS and XPS as will be discussed later. Underneath the oxidized layer it can be observed that the film remains quite homogeneous, showing the same behaviour found in the control samples.

Figure 5.3 shows RBS spectra for coatings with Ag/Ti atomic ratio of a) 0 and b) 0.20 before and after 24 h of immersion in both culture media (TSB and DMEM).

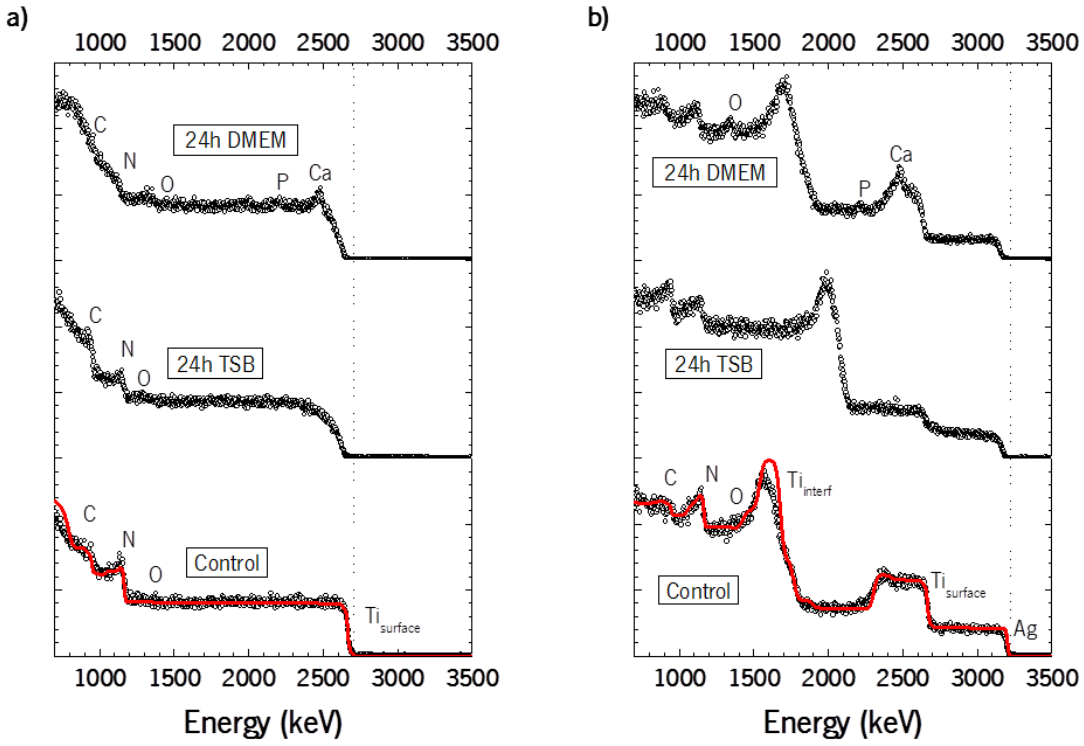

Figure 5.3 RBS spectra of: a) Ag/Ti = 0 and b) Ag/Ti = 0.20 of samples immersed in DMEM (top), in TSB (middle) and control (bottom).

RBS results (figure 5.3) confirm the presence of a surface layer on top of the Ag-TiCN coatings for both samples, in agreement with GDOES observations (see figure 5.1 and 5.2). The surface Ti signal for the control samples with Ag/Ti = 0 sharply appears at an energy of 2660 keV in the RBS spectrum of figure 5.3a (bottom). However, after 24 h of immersion in TSB or DMEM, the titanium signals appear slightly shifted towards lower energy, while the signals of C, N and O remain at their original energies. This is an indication of the deposition of a C-N-O based coating on the control TiCN film. The decrease in the energy of the titanium signal is due to the loss of energy of He^+ ions within this top layer until reaching the buried titanium. In a similar way the surface Ag signal for Ag/Ti = 0.20 samples immersed in TSB and DMEM appears shifted towards energies lower than 3190 keV (energy of the surface Ag for the control sample) in the RBS spectra of figure 5.3b. In addition, for samples immersed in DMEM, there are evidences in the RBS spectra of the presence of two new surface elements (phosphorus and calcium) that are main constituents of the DMEM media. The phosphorus was already detected by GDOES (see figures 5.1 and 5.2), but since GDOES setup was not

equipped with a photodetector for the calcium wavelength, it was only by using RBS that the calcium content in these films could be revealed.

5.3.2 Chemical bonding analysis by XPS

Further information on the chemical bonding of samples in contact with the culture media was obtained using XPS. The analysis was performed on both samples, with and without silver. Since both results are very similar, only the results of the sample with silver are presented and discussed.

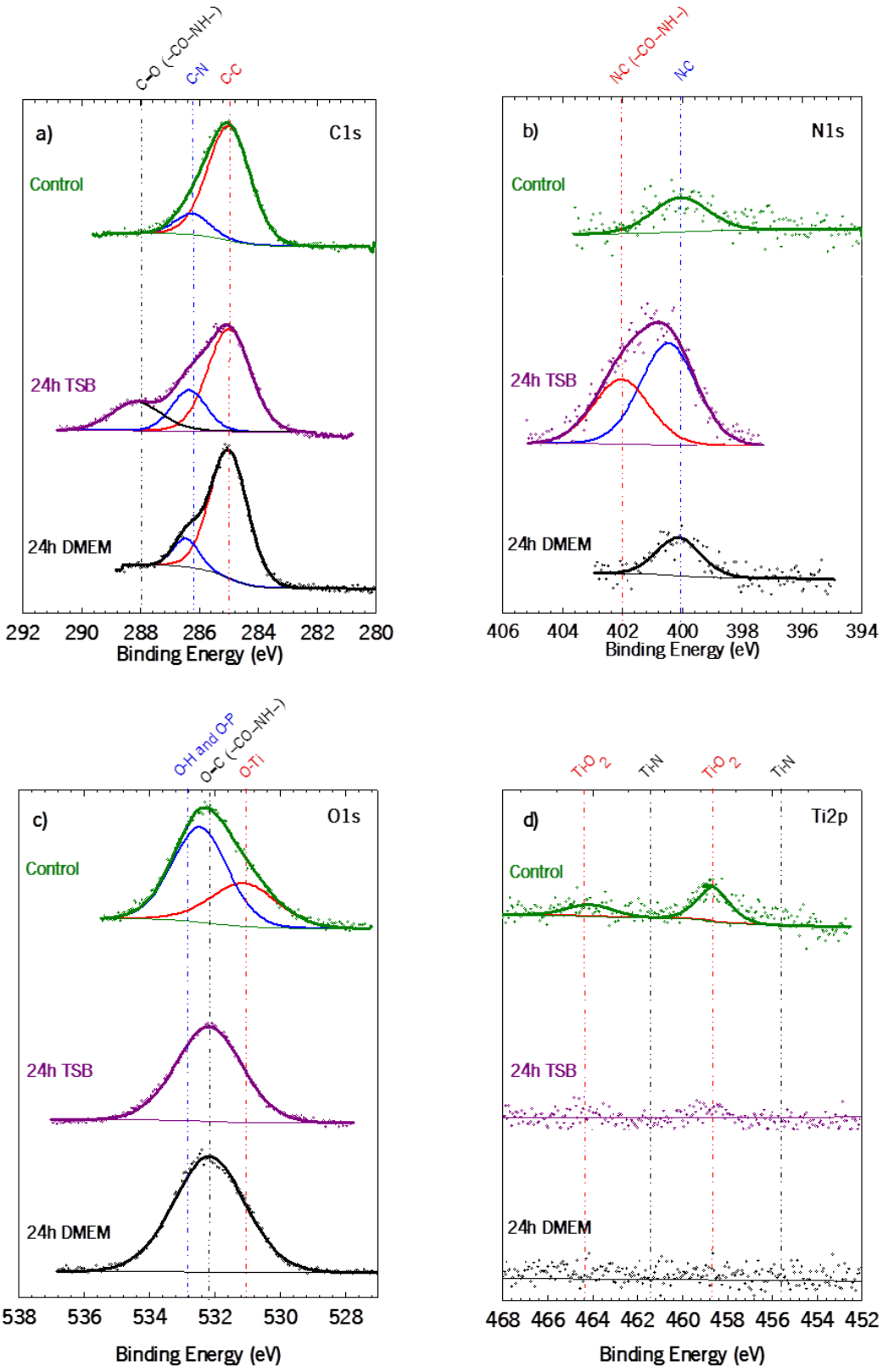

Figure 5.4 XPS spectra of: a) C 1s, b) N 1s, c) O 1s and d) Ti 2p core levels of Ag/Ti = 0.20 in control samples (top), and samples exposed to 24 h in TSB (middle) and in DMEM (bottom).

The effect of BE's shift due to charging effects of the samples upon x-ray irradiation were corrected referring all XPS energies to that of C 1s band at 285.0 eV. In order to relate the chemical changes in the sample surface to the antibacterial effect in the coating, the C1s, N1s, O1s and Ti 2p XPS bands after BE's correction of the control sample as well as of the samples immersed in TSB and DMEM were represented in figure 5.4. As can be seen in figure 5.4a the C1s band, related to the sample immersed in TSB, shows three contributions at 285.0 eV, 286.4 eV and 288.1 eV, respectively. The C 1s band at 285.0 eV is assigned to C-C bonds related to amorphous carbon phase in good agreement with Raman spectroscopy results previously published [16].

The band at 286.4 eV is attributed to C-N bonds in a CN amorphous phase. This interpretation is supported by the presence of a contribution at around 400 eV within the N 1s band (see figure 5.4b) [17–20]. The peak at 288.1 is only observed in samples treated with TSB and should be assigned to C=O. The counterpart is also observed in the O 1s band at around 531.7 eV. The carboxylic group points to the presence of organic species which were also identified in other studies [19–22] and has been corroborated from GDOES analysis. In addition to that, the N1s band for the sample treated with TSB show another contribution at ~401.5 eV which should be attributed to C-N bonds in organic matrix [21,23]. This organic material being adsorbed on the coating surface prevents the silver diffusion to the surface and consequently its ion release. For the samples either sterilized or immersed in DMEM, the O1s band shows a peak at ~532.3 eV that could be attributed either to O-H or O-P bonds, respectively. The presence of O-H bonds in the control sample has been also observed with GDOES and is attributed to surface contamination by environmental components. However, as it will be discussed later, the presence of O-P bonds in the samples treated with DMEM is attributed to the formation on the surface of a phosphate thin layer. The peaks at 531.1 eV for the O1s band and that at 458.4 eV for the Ti 2p3/2 band (see figure 5.4c and 5.4d) in the control sample are attributed to the formation to oxygen bonded to titanium in good agreement with previously published results [16]. It is worth to note that Ti contribution disappear upon immersion of the samples in the culture media. This is consistent with GDOES and RBS results which show also the absence of Ti on the coating surface. For the sample immersed in TSB, the explanation of this behaviour should be found in the formation

of a film of proteins on the surface, from TSB constituent, while for the sample immersed in DMEM it is attributed to the formation of a thin calcium phosphate layer.

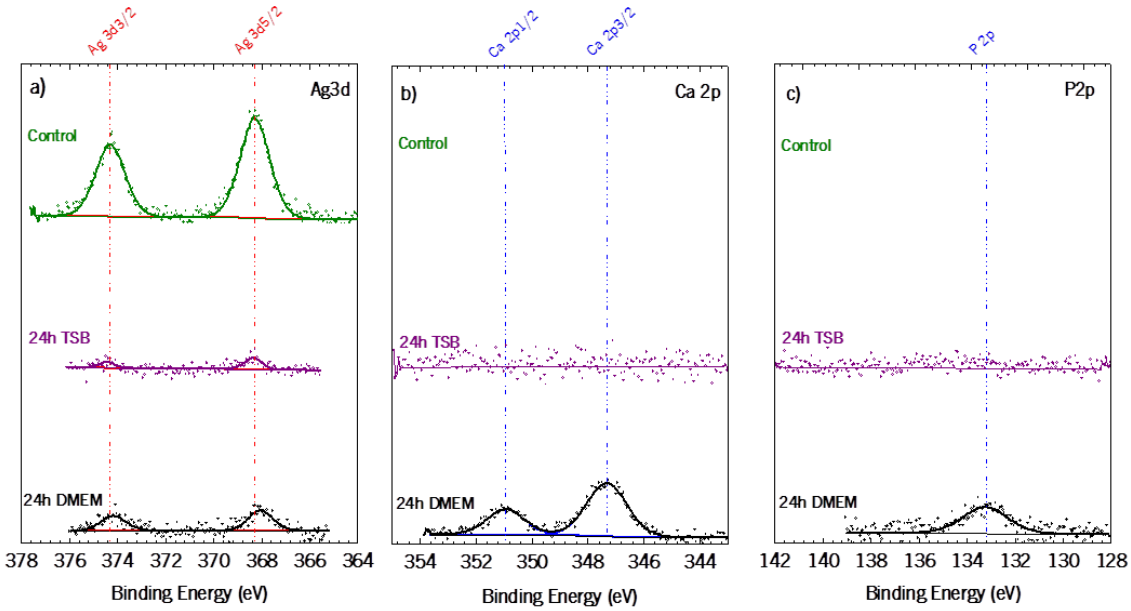

Figure 5.5 XPS spectra of: a) Ag 3d, b) Ca 2p and c) P 2p core levels of Ag/Ti = 0.20 in control samples (top), and samples exposed to 24 h in TSB (middle) and in DMEM (bottom).

Figure 5.5 shows a) the Ag 3d, b) Ca 2p and c) P 2p bands measured for the control sample, the sample treated with TSB, and for the treated with DMEM, respectively. The control sample shows the Ag 3d doublet with the Ag 3d5/2 peak at 367.8 eV which is attributed to Ag-Ag metallic bonds [16], therefore indicating the presence of silver on the coating surface. As it can be observed the intensity of the Ag signal decreases with the immersion of the samples in the culture media, being the decrease more evident for the sample treated with TSB. As pointed out before, these outcomes are in agreement with GDOES and RBS results. In a previous study, where it was evaluated the tribological performance of similar Ag-TiCN coatings with silver content (0 to 8 at. %) against Al_2O_3 counterpart, using a simulated body fluid with bovine serum albumin, it was shown a similar formation of a layer of adsorbed proteins on the surface of coatings to a depth of 500 nm [24]. Additionally, this study showed that this same layer has promoted a reduction in the wear rate, thus demonstrating the influence of albumin in the increase of lubrication coatings. So, proteins seem to prevent somehow the silver ionization and consequently coatings antibacterial inactivity, on the other

hand they have a very important role in lubrication, decreasing debris release and all the negative related consequences.

Figure 5.5 also shows, for the sample immersed in DMEM, the Ca 2p doublet with the Ca 2p3/2 peak 347.3 eV and a broad band P 2p (the doublet is unresolved) at 133.3 eV, already detected in RBS analysis [25]. These peaks can indeed suggest the presence of calcium phosphate thin film on the coating surface that may be preventing or reducing the diffusion of silver to the surface and therefore its ionization.

5.4 Conclusions

GDOES, RBS and XPS analyses were carried out to coatings before and after immersion in different culture media in order to find a possible justification for the antibacterial inactivity of these coatings.

All results obtained by these techniques suggest that the modification of the surface caused by exposure of the sample to the culture media can origin the formation of a layer of proteins in TSB and calcium phosphate in DMEM. Moreover, these layers seem to justify the absence of/low silver ionization, which is related with the absence of antibacterial effect found in these samples and also possibly their non-cytotoxicity.

References

[1] Chekan N M, Beliauski N M, Akulich V V, Pozdniak L V, Sergeeva E K, Chernov A N, Kazbanov V V and Kulchitsky V A 2009 Biological activity of silver-doped DLC films *Diam. Relat. Mater.* **18** 1006–9

[2] Chen W, Oh S, Ong A P, Oh N, Liu Y, Courtney H S, Appleford M and Ong J L 2007 Antibacterial and osteogenic properties of silver-containing hydroxyapatite coatings produced using a sol gel process. *J. Biomed. Mater. Res. A* **82** 899–906

[3] Ewald A, Glückermann S K, Thull R and Gbureck U 2006 Antimicrobial titanium/silver PVD coatings on titanium. *Biomed. Eng. Online* **5** 22

[4] Huang H-L, Chang Y-Y, Lai M-C, Lin C-R, Lai C-H and Shieh T-M 2010 Antibacterial TaN-Ag coatings on titanium dental implants *Surf. Coatings Technol.* **205** 1636–41

[5] Kumar R and Münstedt H 2005 Silver ion release from antimicrobial polyamide/silver composites. *Biomaterials* **26** 2081–8

[6] Lan W-C, Ou S-F, Lin M-H, Ou K-L and Tsai M-Y 2013 Development of silver-containing diamond-like carbon for biomedical applications. Part I: Microstructure characteristics, mechanical properties and antibacterial mechanisms *Ceram. Int.* **39** 4099–104

[7] Sant S B, Gill K S and Burrell R E 2007 Nanostructure, dissolution and morphology characteristics of microcidal silver films deposited by magnetron sputtering. *Acta Biomater.* **3** 341–50

[8] Trujillo N A, Oldinski R A, Ma H, Bryers J D, Williams J D and Popat K C 2012 Antibacterial effects of silver-doped hydroxyapatite thin films sputter deposited on titanium *Mater. Sci. Eng. C* **32** 2135–44

[9] Stanley N R, Britton R A, Grossman A D and Lazazzera B A 2003 Identification of Catabolite Repression as a Physiological Regulator of Biofilm Formation by Bacillus subtilis by Use of DNA Microarrays *J. Bacteriol.* **185** 1951–7

[10] Zhao G, Ye L, Huang Y, Yang D, Li L, Xu G and Lei Y 2011 In vitro model of bacterial biofilm formation on polyvinyl chloride biomaterial. *Cell Biochem. Biophys.* **61** 371–6

[11] Donlan R M 2001 Biofilms and device-associated infections *Emerg. Infect. Dis.* **7** 277–81

[12] Garrett T R, Bhakoo M and Zhang Z 2008 Bacterial adhesion and biofilms on surfaces *Prog. Nat. Sci.* **18** 1049–56

[13] Stobie N, Duffy B, McCormack D E, Colreavy J, Hidalgo M, McHale P and Hinder S J 2008 Prevention of Staphylococcus epidermidis biofilm formation using a low-temperature processed silver-doped phenyltriethoxysilane sol-gel coating. *Biomaterials* **29** 963–9

[14] Escobar Galindo R, Manninen N K, Palacio C and Carvalho S 2013 Advanced surface characterization of silver nanocluster segregation in Ag-TiCN bioactive coatings by RBS, GDOES, and ARXPS. *Anal. Bioanal. Chem.* **405** 6259–69

[15] Calderon V. S, Galindo R E, Oliveira J C, Cavaleiro a. and Carvalho S 2013 Ag+ release and corrosion behavior of zirconium carbonitride coatings with silver nanoparticles for biomedical devices *Surf. Coatings Technol.* **222** 104–11

[16] Manninen N K, Galindo R E, Benito N, Figueiredo N M, Cavaleiro A, Palacio C and Carvalho S 2011 Ag–Ti(C, N)-based coatings for biomedical applications: influence of silver content on the structural properties *J. Phys. D. Appl. Phys.* **44** 375501

[17] Palacio C 1997 Carbon nitride thin films formation implantation by Ni ion 709–13

[18] Riedo E, Comin F, Chevrier J and Bonnot A M 2000 Composition and chemical bonding of pulsed laser deposited carbon nitride thin films *J. Appl. Phys.* **88** 4365

[19] Serro A, Gispert M, Martins M, Brogueira P, Colaço R and Saramago B 2006 Adsorption of albumin on prosthetic materials: Implication for tribological behavior *J. Biomed. Mater. Res. A* **78** 581–9

[20] Vanea E, Magyari K and Simon V 2010 Protein attachment on aluminosilicates surface studied by XPS and FTIR spectroscopy *J. Optoelectron. Adv. Mater.* **12** 1206–12

[21] Advincula M, Fan X, Lemons J and Advincula R 2005 Surface modification of surface sol-gel derived titanium oxide films by self-assembled monolayers (SAMs) and non-specific protein adsorption studies. *Colloids Surf. B. Biointerfaces* **42** 29–43

[22] Lebugle A, Subirade M and Gueguen J 1995 et Biophysica Structural characteristics of a globular protein investigated by X-ray **1248** 107–14

[23] Moulder J F, Stickle W F, E.'Sobol P and Bomben K D 1992 *Handbook of X-ray photoelectron spectroscopy* ed J Chastain (Eden Prairie, Minnesota: Perkin-Elmer Corporation, Physical Electronics Division)

[24] Alves C F A, Oliveira F, Carvalho I, Piedade a. P and Carvalho S 2014 Influence of albumin on the tribological behavior of Ag–Ti (C, N) thin films for orthopedic implants *Mater. Sci. Eng. C* **34** 22–8

[25] Ciobanu C S, Iconaru S L, Pasuk I, Vasile B S, Lupu a. R, Hermenean a., Dinischiotu a. and Predoi D 2013 Structural properties of silver doped hydroxyapatite and their biocompatibility *Mater. Sci. Eng. C* **33** 1395–402

Chapter VI – Final conclusions and work perspectives

Chapter VI – Final conclusions and work perspectives

6.1 Final conclusions

In the present study the multifunctionality of TiCN coatings doped with different Ag contents, combined with the antibacterial effect of silver were studied in order to understand its main limitations and potential for application in joint prostheses.

Consequently, the Ag-TiCN coatings were produced and in a first step, characterized physical and chemically, including the evaluation of thickness, chemical composition, structure and the main chemical bindings. Moreover, given the importance of surface properties for the biomedical field, the roughness of the coatings, which can be related with the morphology, was studied, as well as the tribomechanical propertiestheir hardness and wear rate. Chemical composition obtained by EPMA showed that coatings presented a silver content between 2 and 15 at. %. Moreover, according to XRD and XPS results, the coatings without silver were crystalized in a B1-NaCl crystal structure typical for $TiC_{0.3}N_{0.7}$.With the Ag content increased into the coatings, the appearance of the soft phases (Ag and CN_x phases) became dominant and led a substantial reduction in the grain size of TiC_yN_{1-y}, decreasing the hardness and the wear resistance. The best hardness and wear resistant coatings were obtained for low Ag contents (up to 6 at. % of Ag or Ag/Ti ≤ 0.20) with hardness of 18 GPa and specific wear rate values in the range of 10^{-6} mm^3/Nm.

Since good chemical and mechanical properties were obtained the next step was the determination of coatings' cytotoxicity and antibacterial activity. Moreover, coatings hydrophobicity was also determined in order to investigate its influence on bacterial adhesion.

All coatings have shown to be biocompatible. However, they do not present any antibacterial effect. Additionally, the hydrophobicity of coatings with Ag content was higher than coatings without Ag, probably afforded by higher number of contact zones between the bacteria and the film surface resulting from the softs phases (Ag and CN_x phases), which tend to segregate in the grain boundaries of $TiC_{0.3}N_{0.7}$, leading to less rough and more hydrophobic surfaces, causing a favourable bacterial adhesion.

The absence of antimicrobial properties of these coatings can be related with both surface properties or the media used to culture cells. Regarding the surface properties it was then described that chemical properties, as well as, hydrophobicity and surface tension, could

affect bacterial adhesion and maybe they were the responsible for the increase in the number of viable cells present in coatings with silver.

Moreover, the absence of silver ionization or in very low concentrations, maybe explained by the possible formation of protein layer from culture media that effectively prevents or reduces the ionization of silver and consequently being insufficient to cause the bacteria death. Antagonizing with the failure of the antibacterial action, the presence of the protein layer adsorbed to the coatings surface has proven to be beneficial in tribological terms, reducing the wear rate.

Although without antibacterial activity, the developed coatings presented multifunctionality with only 6 at. % of silver. Thus, these coatings may be an option in industry since they have similar properties to the ceramic materials and have at least two advantages: are not brittle and less expensive.

6.2 Work perspectives

With this study it was concluded that the silver incorporation up to 6 at. % in the TiCN coatings present a favourable mechanical and tribological performance level, combining with the fact that these coatings are biocompatible for use in implants (in this particular case would be to use in the femur head). In addition to the properties assessed, corrosion is a very important issue that should be tested in multifunctionality evaluation. In fact some preliminary studies in the group demonstrated a protective effect of albumin against corrosion in this type of coatings. So, one topic to be assayed in these coatings in future work is to carry out more corrosion tests, since the environment in which the joint prostheses are inserted is naturally corrosive.

The desired antibacterial effect has not been achieved, and it was attributed to the absence of silver ionization or at very low values, in which case concluded to be the layer of proteins adsorbed on the coatings surface. Therefore, another aim for future research on these samples is to understand the mechanism that could cause the silver ionization and improve it by using an oxidizing agent for example.

In addition was also observed a layer of $CaPO_4$ on the coatings surface after having been in contact with the DMEM medium. As a future issue, the $CaPO_4$ layer formed on coatings surface should be analyzed, ascertaining if it could be the bioactive agent hydroxyapatite, which promotes osseointegration not desirable in this specifically application for their adverse effects (increased wear rate). In this sense, their application in the femur stem, for example, where the osseointegration should be verified.